The University of Birmingham

The effect of tempering parameters on the hardness and precipitation characteristics of quenched and tempered RQT701 steel plate.

Jonathan Richard Driscoll

Masters of Science by Research and Dissertation

Student ID: 0950379

Date of Submission: 01/12/2014

Supervisors

Professors Claire Davis and Martin Strangwood

Contents

Abstract

Reheated quenched and tempered 701 steel (RQT701) is a high strength low alloy martensitic grade commonly used in the earth moving and construction industries. A combination of high strength and adequate toughness is required in these applications and this is achieved by tempering the as-quenched martensitic structure. A great deal of literature exists for the tempering response of higher alloyed (2Cr – Mo wt. %) steels, however there is little information on the tempering response of RQT701 steel. The aim of this project was to investigate the tempering response of RQT701 steel over a range of tempering temperatures (580 – 620 °C) and times (up to 100 hours).

Steel plate, of composition 0.17C, 0.29Cr and 0.53Mo (all wt. %) and 15 mm thickness, was supplied in the as-quenched condition. It was found that the as-quenched condition (water cooled from 925 °C at 60 $°C^{-s}$, surface measurement) consisted of autotempered martensite with a hardness of 430 HV. Ice water quenching, with an increased cooling rate, also resulted in an autotempered martensitic structure although with a higher hardness of 460 HV. The different autotempered microstructures did not have any effect on the tempering response past 30 minutes.

Through thickness hardness measurements on samples that had been tempered between 1 and 4 hours at 580 °C, 600 °C and 620 °C showed a secondary hardness peak (increase of approximately 10 HV) between 2 and 3 hours. Particle analysis using SEM images for samples tempered between 1 and 4 hours at 600 °C revealed the average precipitate equivalent circle diameter to increase from 45 to 71 nm, the number density to decrease from 63 to 52 per μm^2, and the volume fraction of precipitates to increase from 0.017 to 0.022 %. Based on Thermo-Calc predictions for the RQT701 composition (suppressing the most stable carbide phases to reveal metastable phases representative of short term tempering) and available literature data, the results suggest that the formation of very fine M_2C, in combination with cementite, cause the secondary hardening peak.

A further hardness increase was seen on longer tempering times (≥27 hours) which is suggested to result from the formation of M_7C_3 phase, based on Thermo-Calc and literature predictions. SEM images from samples tempered at 48 hours for 600 °C and 27 hours for 580 °C show the presence of fine precipitates that were not observed at shorter tempering times, these images correspond to the elevated hardness values and support the suggestion that a new precipitate phase is forming.

1. Introduction

High strength low alloy (HSLA) steels include many standard and proprietary grades specifically engineered with desirable combinations of properties, such as strength, toughness, formability, weldability and atmospheric corrosion resistance. Such demanding combinations of mechanical properties are achieved by the use of small alloy additions and complex processing conditions, yet since HSLA steel production is contrived to achieve a mechanical specification it is not considered part of the alloy steels range; HSLA steel is an independent steel category. This form of steel production has led to a vast area of research and development as suppliers search for advantages either in cost or mechanical properties over their competitors.

Some quenched and tempered (Q&T) steels can be considered to be a type of HSLA steel, an example composition can be seen in Table 1. These steels possess relatively low carbon and low alloy content, yet have a minimum yield strength of 690 MPa ranging up to >1100 MPa depending on the thickness, precise composition and process route. Q&T steels are common within the construction and material handling or earth moving industries, in particular with mining and quarrying equipment. Q&T steels have a balance of high yield and tensile strength with good notch toughness and excellent weldability. They pose significant benefits in extreme working conditions where maximum structural performance is desired with a favourable strength to weight ratio.

Table 1: The composition (all wt. %) of Reheated Quenched and Tempered 701 steel plate with a thickness of 8 – 130 mm. www.brownmac.com/products/quenched-and-tempered-steel-plate/rqt-701

C	Si	Mn	S	P	Cr
0.20	0.50	1.60	0.010	0.025	1.00
Mo	**Nb**	**V**	**Ni**	**Cu**	**B**
0.70	0.060	0.08	1.50	0.40	0.004

To achieve such a challenging balance of mechanical properties, Q&T steels are normalised and cooled rapidly by quenching in water to form martensite, a very hard but brittle microstructure. This provides the high yield strengths necessary for Q&T steels and then toughness and ductility are subsequently improved through sub-critical heating, known as tempering. Although yield strength generally declines with tempering, appropriate use of microalloying additions can help to delay softening and achieve the most advantageous balance of strength and toughness.

Due to the high demand of Q&T steels in a rich and global economic industry, refining the composition and processing to create stronger and tougher steels through cheaper and faster production, can be hugely financially rewarding for steel manufacturers and all of the industries involved (H. Mohrbacher, 2010). Therefore this subject is of great importance and hence the motivation for this review.

Literature Review Contents

2. Background Literature

Q&T steels are generally continuously cast into a slab, bloom or billet, depending on the final application, then hot rolled or controlled rolled to the final shape followed by subsequent heat treatment. Traditionally Q&T steel plate was air cooled after rolling and later reheated, quenched and tempered (RQT, as shown in Figure 1a). This process still exists although some modern steel making facilities allow direct quenching and tempering (DQT, as shown in Figure 1b). In addition to the obvious economic benefit of DQT, advantages to the toughness properties have been noted for some HSLA steels (C. L. Davis and J. E King, 1993). The JFE steel company have advanced this process route to include tempering as part of the same production line, known as heat treatment online process (HOP). HOP production has been demonstrated to produce even higher strength steels (I. Nobuyuki, et al., 2006) and has been commercially recognised and active since 2008.

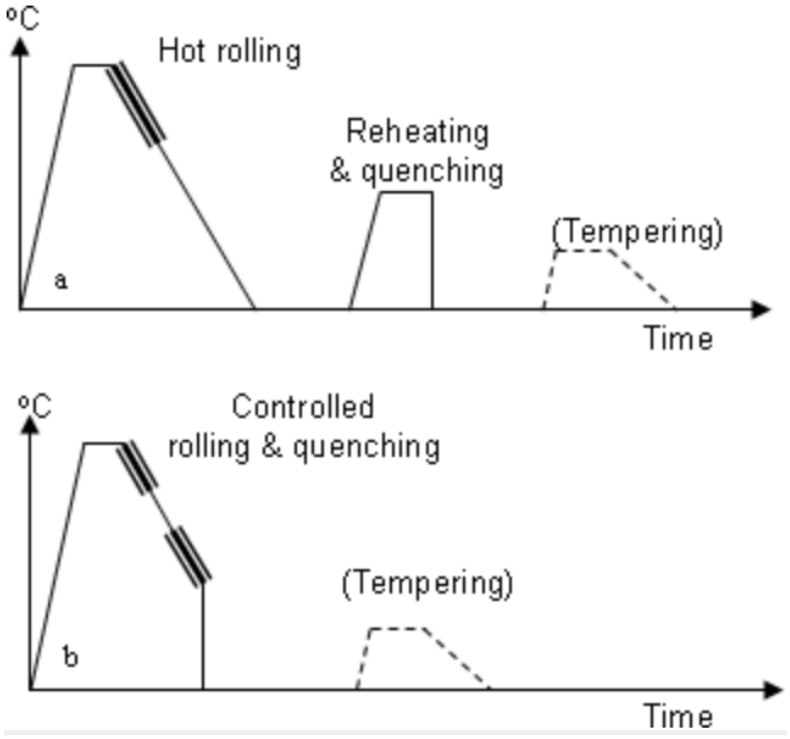

Figure 1: Schematic diagram showing the difference between (a) reheat quenched and tempering and (b) direct quenched and tempering. (D. Porter, 2007)

2.1 Process Conditions

Design criteria such as the plate chemistry and thickness will influence the behaviour of the steel during reheating (normalising), quenching and tempering. Therefore to achieve a precise mechanical specification both the processing conditions and design criteria are altered accordingly. For RQT701 and a tempering temperature between 600 °C and 650 °C, the tempering duration ranges from 1 – 6 hours depending on the plate chemistry and thickness. The relationship between design and process conditions is discussed in detail throughout section 2.1.

The quenching process is ideally used to produce a fully martensitic microstructure thus maximising hardness, whilst tempering is carried out to improve the toughness of the steel without sacrificing too much of the strength. Within the Q&T steel plate industry it is important to understand what happens when tempering martensite, bainite, or a mixed martensitic and bainitic microstructure. This review focuses on tempering martensitic microstructures only.

2.1.1 Normalising Temperature

Normalising is the heat treatment of steel above the eutectoid temperature and fully into the austenite region, and hence is referred to as reaustenitisation. For Q&T steels the primary reason for normalising is to reaustenitise the steel, in order to quench to form martensite. At the ferrite – austenite transformation temperature the steel undergoes a change in crystal structure increasing particle dissolution, which in turn allows for a more uniform chemical distribution. An additional benefit of normalising is that microalloying elements dissolve in austenite, and are therefore available in solution to improve hardenability (discussed in section 2.1.2.1) and affect precipitation during subsequent tempering in order to benefit mechanical properties (discussed in section 2.1.3).

Another consideration during reaustenitisation is the nucleation and coarsening of austenite grains. S. Maropolous, S. Karagiannis and N. Ridley (2008) report that austenite grain size increases from 32 – 35 μm to 60 – 70 μm between 950 $^{\circ}$ C and 1100 $^{\circ}$ C in low alloy steel. Figure 2 however, shows that for a C – Mn steel the austenite grain size is 60 – 70 μm at 925 °C. The precise grain coarsening temperature is dependent on the microalloyed content, nitrogen content and prior thermo-mechanical treatment (M. Maalekian, 2007). One factor that commonly inhibits austenite grain growth is the pinning of grain boundaries controlled by the distance between pinning precipitates formed during or after hot rolling (A. Kundu, 2011) in particular those of vanadium, niobium and titanium.

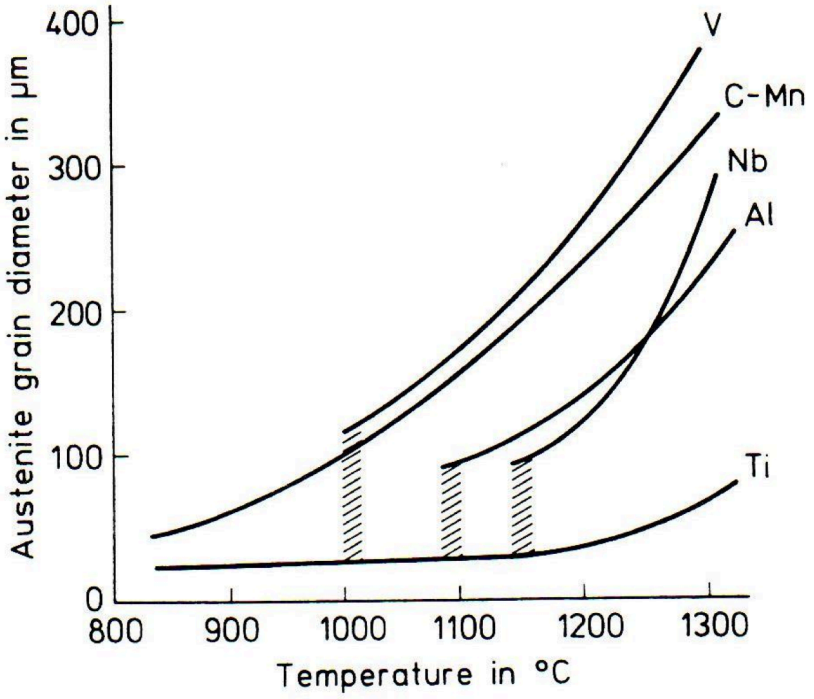

Figure 2: The general effect of microalloy additions on the grain coarsening temperature of austenite in C – Mn steels containing a volume fraction of 0.0005 of alloy carbide or nitride. (A. K. Sinha, 1989 and T. Gladman, 1997)

H. R. Bakhsheshi-Rad, et al. (2011) explain the change in hardness and tensile strength with reaustenitisation temperature for a 3Cr – Mo wt. % steel (Figure 3). At 800 °C hardness remains low as austenite consists of a low percentage of carbon and large amounts of undissolved alloying element. Dissolution increases with temperature up to 880 °C and plateaus until 950 °C giving a higher carbon content in austenite and strengthening the microstructure. Peak hardness was found at 920 °C and tensile strength at 950 °C, above which they both declined with a further increase in dissolution.

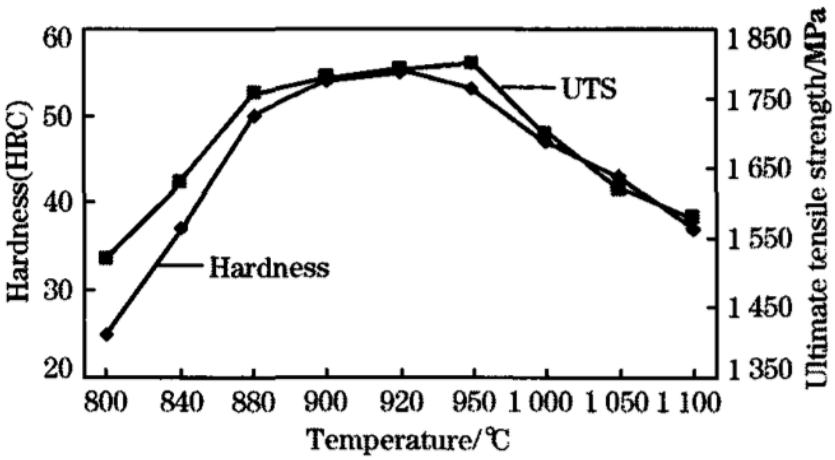

Figure 3: Effect of austenitisation temperature in 3Cr – Mo wt. % low alloy steel, on the hardness and ultimate tensile strength, for a 30 minute holding time. (H. R. Bakhsheshi-Rad et al., 2011)

2.1.2 Quenching to Martensite

Quenching is a rapid cooling process whereby austenitic steels are typically cooled to temperatures below the martensite start temperature. The quenching medium and uniformity of application are integral to the rate of cooling, the degree of distortion and thus the amount of residual stress. In low carbon Q&T steels quenching usually forms martensite, which is the phase of highest hardness for a given composition and therefore a desirable microstructure to obtain before further processing.

Quenching prohibits significant diffusion of interstitial elements (namely carbon) by a diffusionless transformation to martensite, which inherits the composition of the parent austenite phase. Thus the high solubility of carbon in face-centred-cubic (FCC) austenite gives a high supersaturation of carbon in body-centred-tetragonal (BCT) martensite, whereby the solution exceeds the known solubility capacity of carbon in ferrite (0.022 wt. % at 1000 K, D. E. Jiang and E. A. Carter, 2003).

Carbon atoms in the martensite matrix rearrange themselves along one axis of the martensite crystals and in sufficient quantity effectively replace an iron atom, typically causing a shape strain of 20 % and a volume expansion of 3 % (J. K. H. Buschow et al., 2011). These combined effects cause BCT martensite to shear on transformation and a row of dislocations form to accommodate for the discrepancy in alignment of the crystal structure. A typical dislocation density for 0.2 wt. % carbon steel is between 0.3 and 1.0 $\times 10^{12}$ cm^{-3} (R. W. K. Honeycombe & H. K. D. H. Bhadeshia, 1995). As shown in Figure 4 raising the carbon content increases hardness, and this is due to a higher supersaturation of carbon in the matrix giving a larger crystallographic misalignment and thus a higher dislocation density. In low carbon steels (0.1 – 0.2 wt. % carbon) the quenched hardness is expected to fall between 400 and 500 HV (Figure 4).

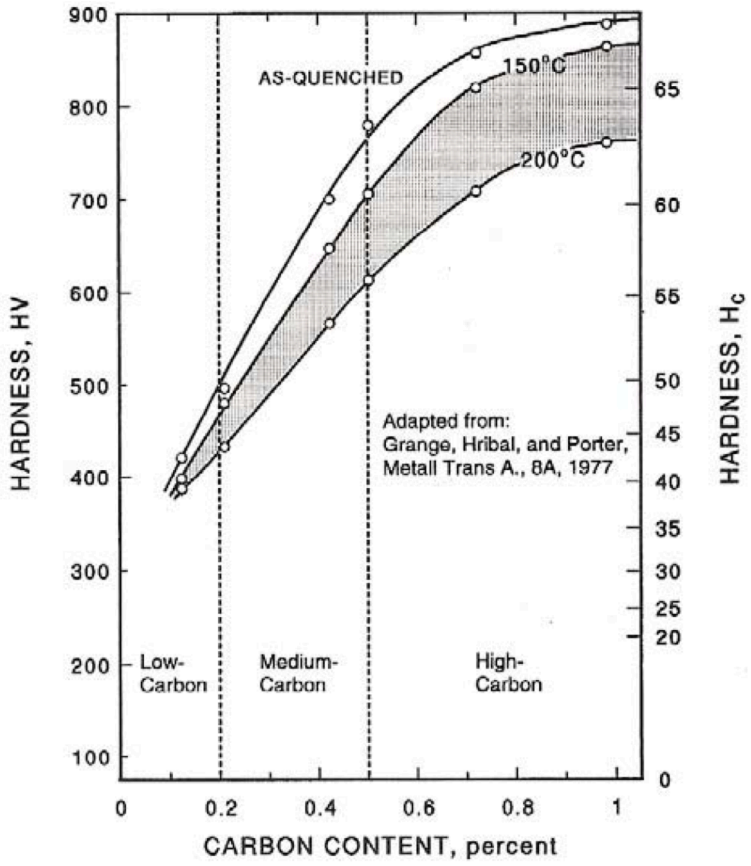

Figure 4: Hardness as a function of carbon content for quenched and low temperature (150 and 200 °C) tempered microstructures. (G. Krauss, 2005; adapted from R. A. Grange, C. R. Hribal and L. F. Porter, 1977)

The result of a diffusionless shear transformation gives a microstructure of incredibly high stored energy; 1714 $Jmol^{-1}$ for martensite of 0.2C – 0.15Mn wt. % steel compared with an equilibrium reference state of ferrite, graphite and cementite at 300 K with zero stored energy (R. W. K. Honeycombe & H. K. D. H. Bhadeshia, 1995). This means martensite is highly thermodynamically unstable and as such is not represented on phase diagrams (H. K. D. H. Bhadeshia, 2001).

If the volume expansion upon transformation cannot be achieved regions of retained austenite can exist within the martensite matrix, and in cases of residual stress at the surfaces, quench cracking can occur (D. R. Askeland and P. P. Phulé, 2002). Therefore despite achieving high levels of hardness and thus tensile strength martensite is brittle even with low carbon steel and is unsuitable for applications that require good toughness.

2.1.2.1 Hardenability effect to quenching

The hardenability of a material is the ease of formation of martensite on quenching. The martensite start (M_s) and finish (M_f) transformation temperatures determine the homogeneity of martensite formed in the final microstructure, and as shown in Figure 5 is inversely related to carbon content. In low carbon steel the elevated M_s and M_f temperatures give a more uniform as quenched microstructure. However in medium to high carbon steels the chance of developing retained austenite or a mixed martensite and bainite microstructure increase as the M_f temperature drops and falls below 0 °C (H. R. Bakhsheshi-Rad et al., 2011). These regions of retained austenite may then destabilise during subsequent tempering and cooling to form untempered martensite with undesirable and unpredictable toughness. (M. C. Payares-Asprino, H. Katsumoto and S. Liu, 2008).

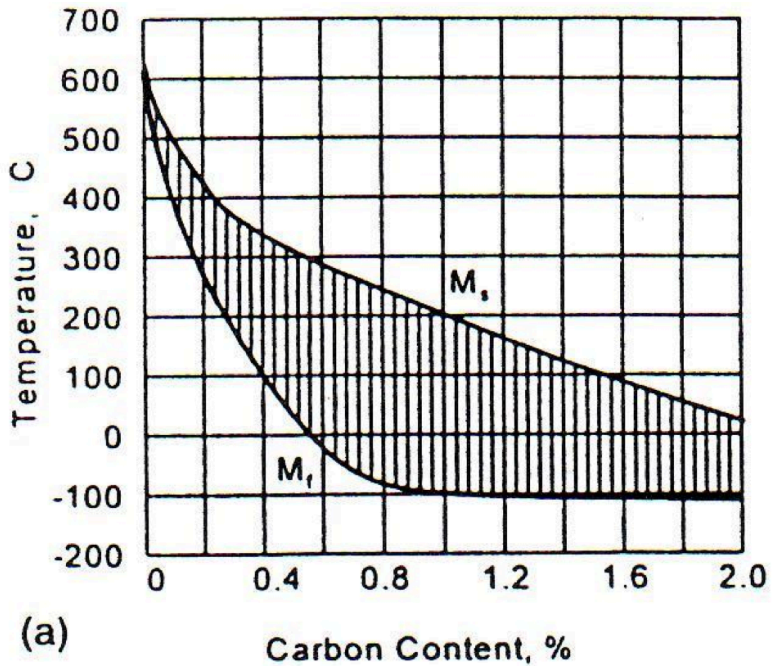

Figure 5: Martensite start (M_s) and finish (M_f) transformation temperatures as a function of carbon content. (M. Maalekian, 2007)

Figure 6 shows a continuous cooling transformation (CCT) diagram for medium carbon steel and the microstructures present during cooling, based on the composition, bar diameter and cooling rate. Figure 7 shows the CCT diagram with cooling curves for the surface and core of hypothetical steel, this diagram indicates that, for a thick section, different cooling rates can occur through the sample thickness and therefore different microstructures can form. In this case the different cooling rates result in martensite forming at the surface and bainite at the core. Therefore thicker plate requires a high hardenability or faster quench to maintain homogeneity, and since a faster quench encourages the accumulation of residual stress by a larger differential cooling rate with depth, hardenability changes are favourable.

(a)

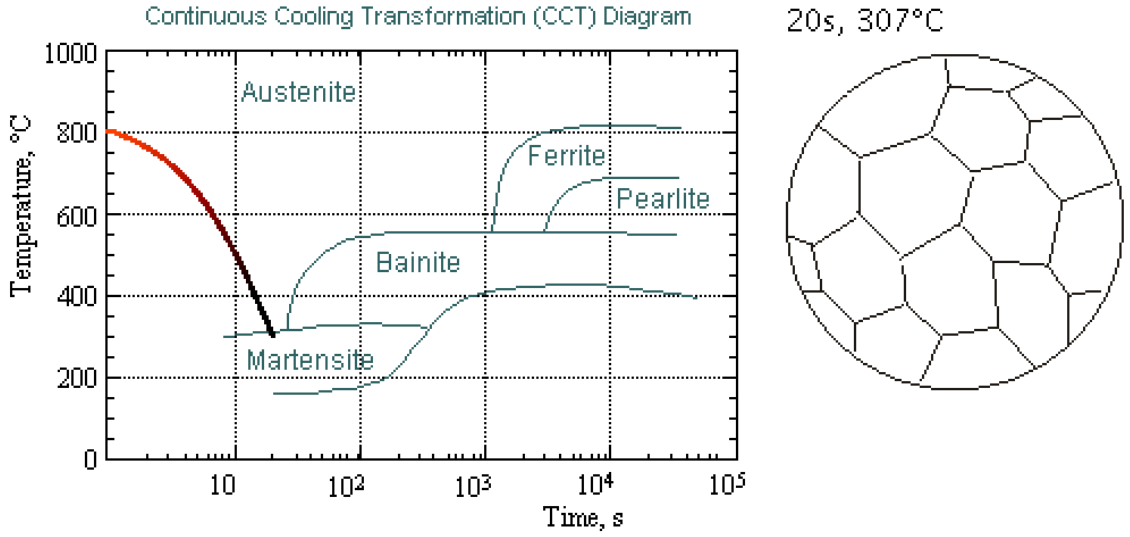

(b)

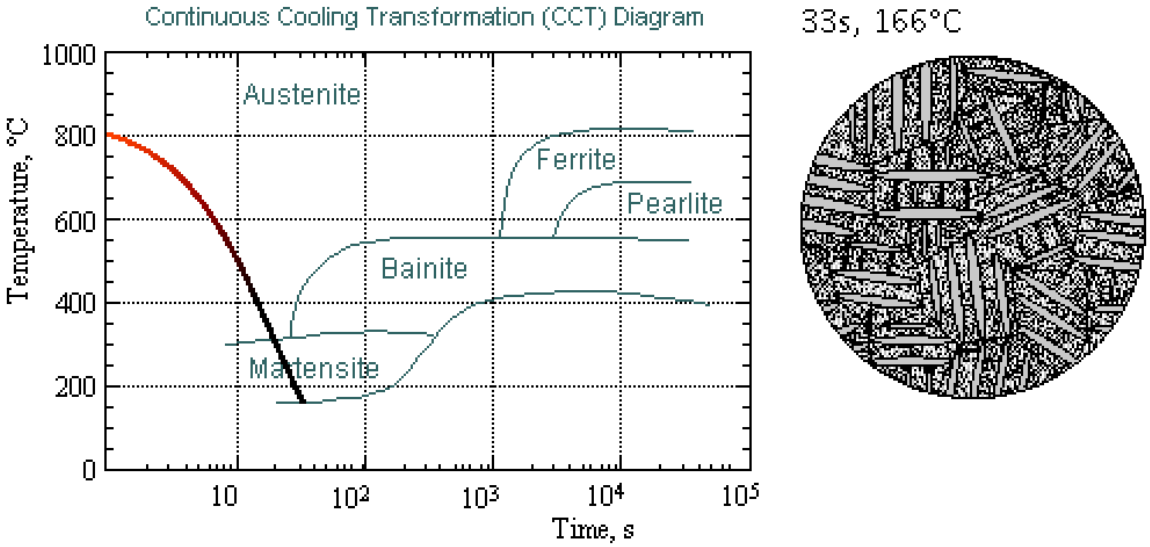

Figure 6: CCT diagram for 0.4C, 1.5Mn and 0.5Mo (all wt. %) steel of 70 mm bar diameter. The microstructures are shown at the M_s and M_f transformation temperatures for the cooling rate used corresponding to (a) 300 °C after 20 seconds and (b) 170 °C after 34 seconds respectively. (www.matter.org.uk/steelmatter/metallurgy, accessed 27/11/13, updated 2000)

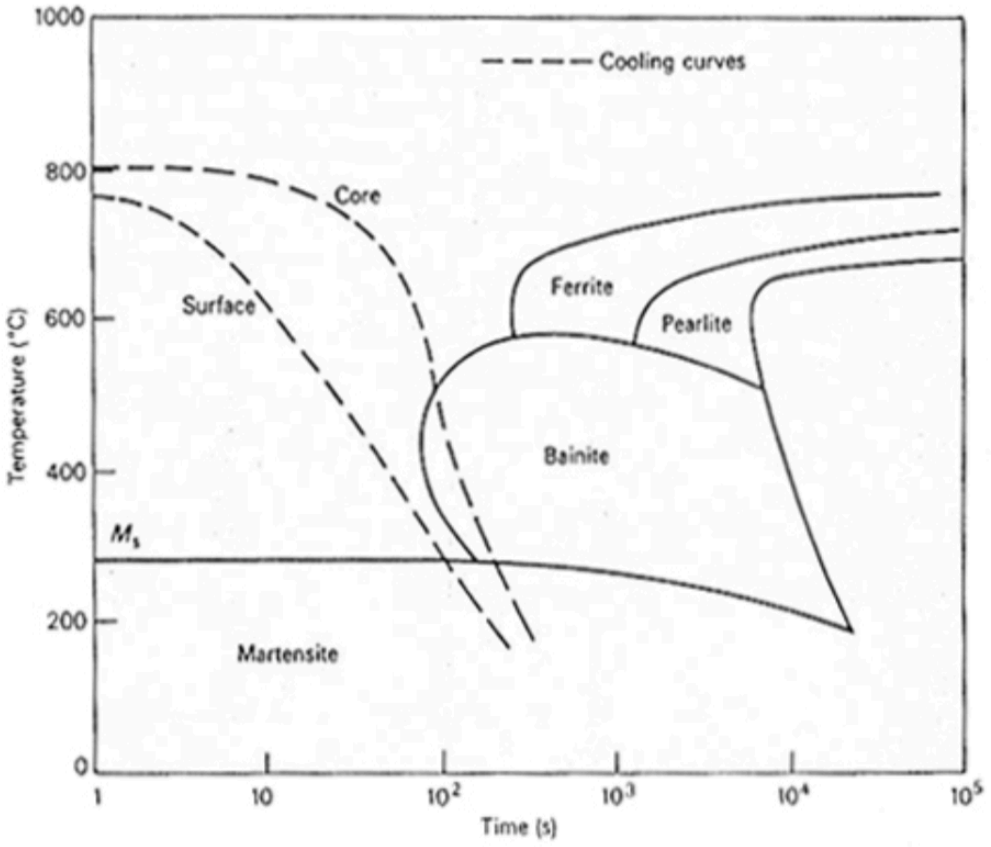

Figure 7: Schematic CCT diagram of the surface and core cooling rates for oil quenched hypothetical steel of 95 mm bar diameter. (www.keytometals.com/Articles/Art146.htm, accessed 27/11/2013, updated 2010)

Martensite that forms close to the M_s transformation temperature can temper throughout the remainder of the quench since the diffusion of carbon is very rapid; even in a short time period

carbon can segregate to lattice defects and precipitate as fine 5 – 10 nm transition carbides (G. R. Speich and W. C. Leslie, 1972). This is shown by the development of very fine black dots in the schematic micrograph illustrations over the duration of 13 seconds from Figure 6a to 6b. This process is known as autotempering and lowers the hardness of quenched martensite. G. R. Speich (1969) reported that for a 0.2 wt. % carbon steel, almost 90 % of the carbon segregates to lattice defects during quenching, although not all of the martensite that forms will autotemper. S. W. Ooi et al. (2009) reported autotempering of (0.15C, 1.54Mn, 0.2Mo, all wt. %) low alloy steel reaustenitised to 945 °C for 5 minutes and quenched in an 80 % water, 20 % polymer mix in excess of 30 $°C^{-s}$ (sufficient to avoid transformation prior to the formation of martensite). The resultant autotempered microstructure (Figure 8a) was 420 HV, carbides were coarsest towards the center of martensite plates and precipitate free zones were seen at the plate edges (Figure 8b). This indicates a competition between carbide precipitation and the partitioning of carbon as the martensite cools below its M_s temperature. Dark field TEM confirmed carbides with two different cementite morphologies. Very fine spherical cementite (5 – 10 nm in size, Figure 8c) and coarser elongated cementite (100 nm in length, Figure 8d) with the latter forming earlier in the quenching process.

(a) 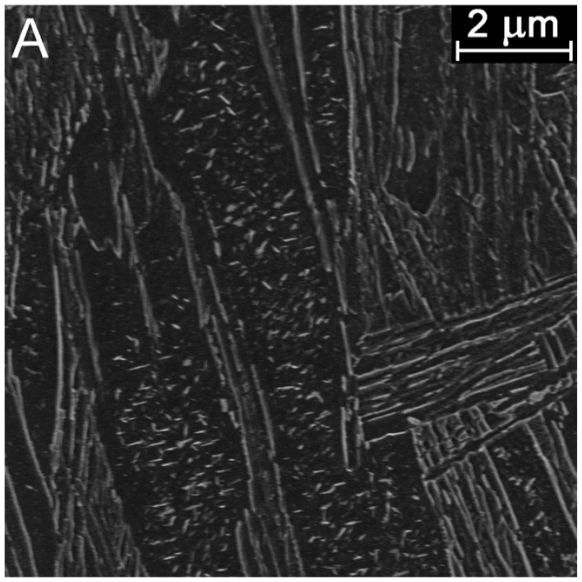

(b) 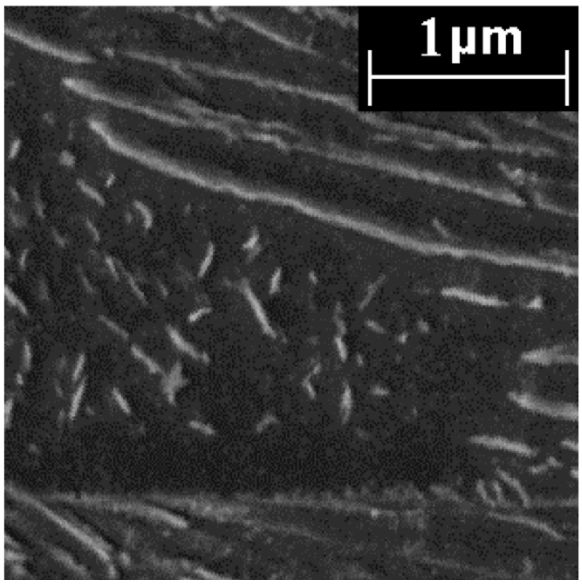

(c) 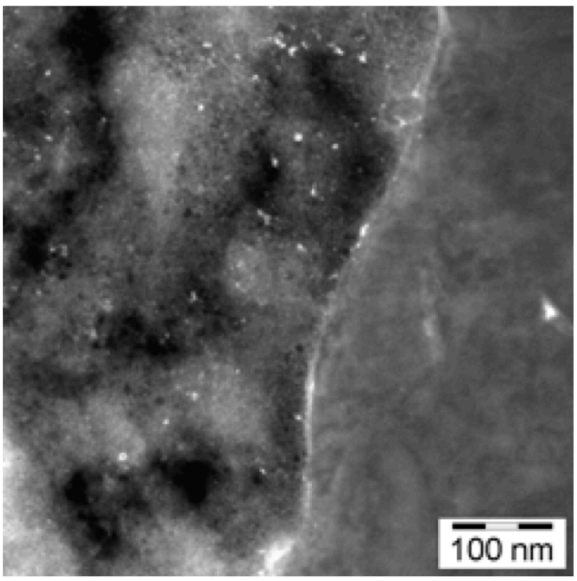

(d) 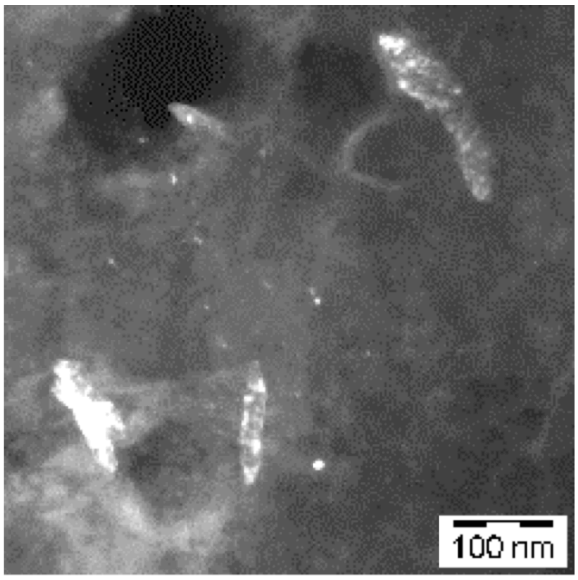

Figure 8: SEM images of low alloy (0.15C, 1.54Mn, 0.2Mo, all wt. %) steel showing (a) autotempered martensite (b) coarser particles towards the centre of the martensite plates with precipitate free zones at the plate edges. Dark field TEM images reveal (c) very fine spherical cementite (d) coarser elongated cementite. (S. W. Ooi et al., 2009)

Hardenability is primarily affected by the steel composition. Increasing the carbon content is the easiest method to increase hardenability and this delays the formation of ferrite, pearlite and bainite by shifting the transformation C curves to the right on a CCT diagram, giving more time during cooling to achieve the martensite transformation. This effect is due to the segregation of carbon to form carbon rich regions at the interface of an advancing transformation boundary, thus retarding the growth of the phase. However, as shown previously (Figure 5) during quenching, carbon in solution increases the chances of retained austenite as the M_f temperature drops below room temperature. Therefore microalloy additions are used in combination with low or medium carbon steels to provide a similar but more effective solute drag force to delay transformation (J. C. McMahon, 1980) alongside numerous other benefits. The influence of individual alloying elements on hardenability is discussed in section 2.2.1. Besides changing the composition, increasing the

austenite grain size reduces grain boundary area giving fewer low energy sites for ferrite, pearlite and bainite to nucleate. Grain coarsening is possible at higher normalising temperatures (S. Maropolous, S. Karagiannis and N. Ridley, 2008) and increases hardenability to favour martensite transformation (R. A. Grange, C. R. Hribal and L. F. Porter, 1977). However a larger austenite grain size tends to produce a larger martensite packet size and can adversely affect toughness (G. Krauss, 1999) and so the optimum austenite grain size is dependent on the required balance between strength (from improved hardenability) and toughness (by limiting the martensite packet size). Overall increasing hardenability by changing the alloy content is the most successful method, and is generally sufficient to achieve a fully martensite microstructure even in thick plate and with deliberately slow cooling rates that minimise residual stress.

2.1.3 Tempering Martensite

Tempering as quenched martensite is the process of sub-critical heating below the eutectoid temperature to allow carbon diffusion, and is fundamentally a thermodynamic evolution from an unstable microstructure with high stored energy towards a more favourable equilibrium condition. Therefore the tendency of a microstructure to temper depends on the deviation of stored energy from equilibrium. Tempering improves toughness and fracture resistance at the expense of hardness, by removing residual stress in the quenched martensite through the diffusion of carbon from interstitial sites and the precipitation of new carbide phases (J. Hufenbach et al., 2012). The tempering temperature, duration, material composition and quenched microstructure affect the rate of removal of micro-residual stresses and thus the change in mechanical properties. The trade-off between strength and toughness that occurs with tempering is carefully balanced to provide optimum mechanical properties, and is especially apparent in alloyed steels where softening can be sufficiently delayed to give a secondary hardness peak.

C. S. Roberts, B. L. Averbach and M. Cohen (1953) and B. S. Lement, B. L. Averbach and M. Cohen (1955) identified three major structural changes that occur during tempering of plain carbon steels. The temperature ranges given below are dependent on the carbon content and tempering time, and with each stage there is a continual evolution of microstructure so some overlap in the temperature ranges between stages 1 – 3 is expected (J. K. H. Buschow et al., 2011).

1. Stage I (100 – 200 °C): Carbon atoms can readily diffuse and are rejected from the supersaturated matrix to form $Fe_{2.4}C$ transition carbides (also known as ε -transition with low activation energy (16000 $calmol^{-1}$, C. S. Roberts, B. L. Averbach and M. Cohen, 1953). Transition carbides are very fine rods (3 – 5 nm) forming in the martensitic laths and

contribute to an improvement in toughness, as evidenced by the initial peak in the toughness curve with tempering temperature (Figure 9). In this para-equilibrium state a proportion of carbon has precipitated out of solution and some tetragonality to the crystal orientation is lost, reducing hardness and the matrix carbon composition. Alloy steels behave identically at 100 – 200 °C since substitutional elements have low diffusivity.

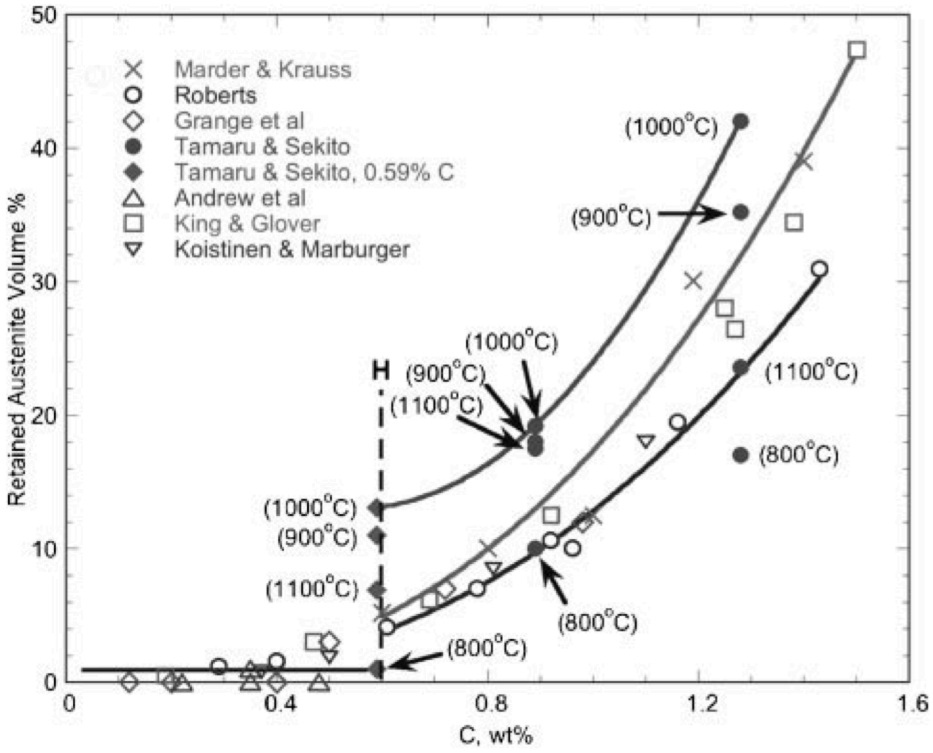

Figure 9: Influence of carbon on the amount of retained austenite in quenched plain carbon steels. The amount of retained austenite is negligible below the H-point. The temperatures given in the graph are the reheat temperatures before quenching (O. D. Sherby et al., 2008)

2. Stage II (200 – 300 °C): Any retained austenite following quenching decomposes to form ferrite and cementite (Fe_3C). O. D. Sherby et al. (2008) reported that plain carbon steels

below 0.6 wt. % carbon contain a negligible amount of retained austenite (Figure 9). In plain carbon steel, cementite forms coarse plate-shaped precipitates predominantly in between martensite laths and prior austenite grain boundaries causing a decrease in toughness by intergranular fracture, this is known as temper embrittlement. The same process occurs in alloyed steels (Figure 10a) with susceptibility to intergranular fracture generally increasing with alloy content, impurity levels and the time held at critical temperatures (I. Olefjord, 1978). The toughness trough at 300 °C (Figure 10a) and the ductility trough at 400 °C (Figure 10b) show that temper embrittlement occurs higher in alloy compared to plain carbon steels. This takes into consideration the delay in cementite precipitation by alloying elements and is discussed in section 2.2.

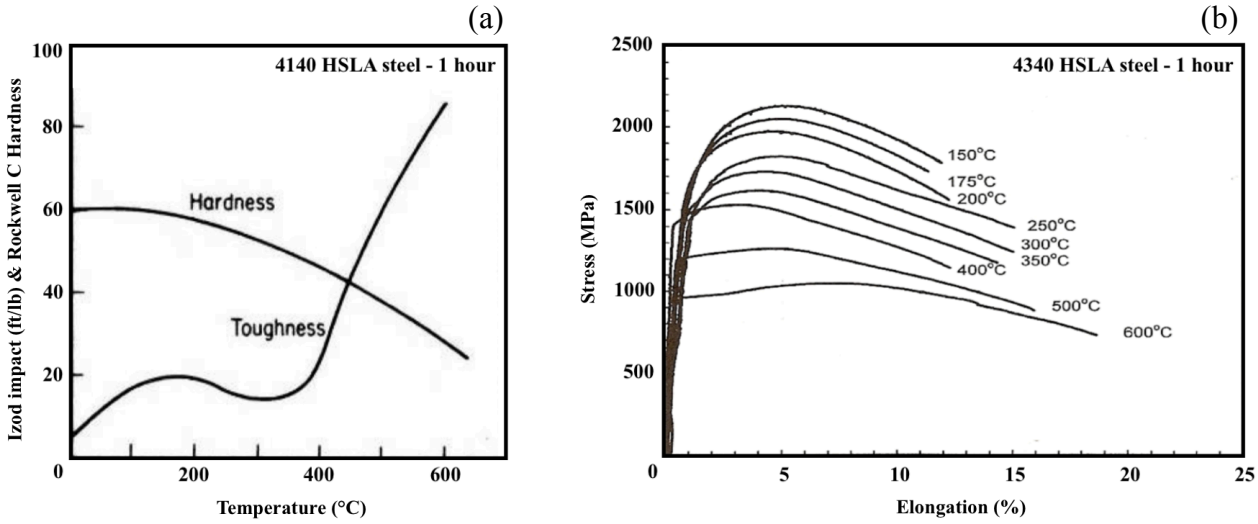

Figure 10: Effect of temping on (a) hardness and toughness with tempering temperature for 4140 HSLA steel (0.41C, 0.3Si, 0.85Mn, Cr, 0.2Mo, all wt. %) and (b) engineering stress versus elongation after tempering 4340 HSLA steel (0.41C, 0.25Si, 0.7Mn, 0.8Cr, 0.25Mo, all wt. %) at different temperatures for one hour and quenching to martensite. (L. Young-Kook, unpublished, 1998; cited in: G. Krauss, 2005)

3. Stage III (250 °C – Eutectoid): Cementite nucleates at the grain boundaries and at the ε he ntite nucleates at the grain boundaries and carbides. Cementite particles coarsen and sweep up the remaining transition carbides to eventually form spheroidite above 350 °C (approximately spherical carbides in a ferrite matrix) due to decreasing surface energy. Preferential carbide growth occurs at the grain boundaries due to increased ease of diffusion. These effects increase ductility as seen at the higher tempering temperatures of HSLA 4340 steel in Figure 10b. Martensite laths/plates also coarsen as low angle boundaries are eliminated and the packet morphology is maintained until high tempering temperatures of 600 °C. The already low carbon solubility in martensite falls to negligible amounts as the crystal structure aligns to form body-centered-cubic (BCC) ferrite; this reduces the dislocation density and hardness drops (Figure 10a). Further tempering causes recrystallisation of the ferrite to form smaller equiaxed grains. If tempering temperatures rise above the eutectoid threshold austenite can reform and later cool to martensite returning the undesirable toughness properties, this is a common problem during welding.

2.1.3.1 Strengthening by secondary hardening

Despite the high driving force that quenched martensite provides for tempering reactions the equilibrium condition may be difficult to attain, and therefore a series of kinetically favoured metastable phases can precipitate (N. Fujita, 2000). Any preferential formation of metastable phases accompanies a reduction in free energy that delays formation of the equilibrium phase; this usually corresponds mechanically to secondary hardness (N. Fujita, 2000). The contribution of a metastable phase to secondary hardness lies in the type, size, distribution and volume fraction of precipitates that form. Figure 11 shows various hardness peaks for tempered alloyed steels compared to that of plain carbon steel.

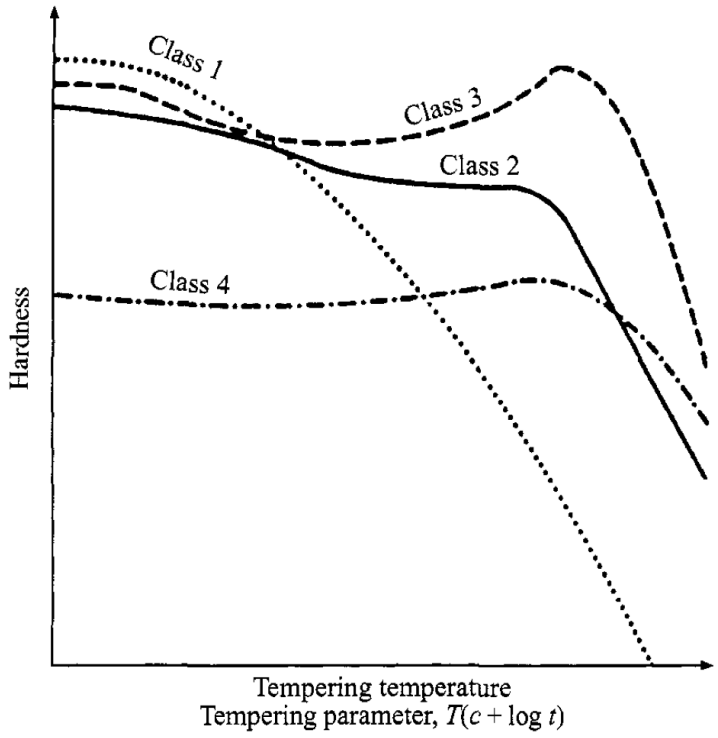

Figure 11: A schematic diagram of hardness as a function of tempering temperature (or as a function of a temperature/time parameter) for plain carbon steel (Class 1), medium alloyed steels (Class 2), high speed tool steels (Class 3) and HSLA steels with lower carbon content (Class 4). (J. K. H. Buschow et al., 2011)

The ability of a precipitate to contribute to the strength of a material lies in its ability to oppose dislocations from passing. The precipitate pinning force [Equation 1] is proportional to the overall precipitate volume fraction and inversely proportional to its radius (M. Gomez, S. F Medina and P. Valles, 2005). Therefore a high volume fraction of fine precipitates will provide the greatest resistance to oppose dislocation movement. The size of a precipitate is governed by its energy barrier for nucleation, as well as its growth rate and is discussed in section 2.3.

Since quenching to martensite is a diffusionless transformation elements with a high solubility in austenite can have a larger effect on the subsequent precipitate formation. Therefore the composition of each carbide phase influences the precipitate pinning force by the solubility of its constituent elements in austenite. D. Delagnes et al. (2012) state that to achieve the highest strength by precipitation the homogeneity of carbide forming element in martensite is crucial in order to develop a uniform distribution of fine precipitates. Different carbide phases and the solubility of important carbide forming elements are discussed in sections 2.3 and 2.2.2 respectively.

[Equation 1] Precipitation Pinning Force $F_p = \frac{f_{vol}}{r^n}$

Where F_p is the pinning force of the precipitates, f_{vol} and r are the volume fraction and radius respectively, and n is a constant exponent suggested as either 1, $^2/_3$ or 2. The value of n varies with the assumed flexibility of grain boundary interaction with precipitates and the assumed existence of precipitates on sub grain boundaries before recrystallisation. (M. Gomez, S. F Medina and P. Valles, 2005)

2.1.3.2 Tempering parameters

In 1945, J. H. Holloman and L. D. Jaffe developed a single tempering parameter [Equation 2] to be used when measuring the extent of tempering for martensitic steels. The *'Holloman and Jaffe parameter'* gives a relationship between time and temperature that allows them to be interchangeable to give a consistent tempered microstructure (measured by hardness). Furthermore since hardness is commonly used as a measure to determine the degree of tempering in steel, and assuming no retained austenite is present after quenching, the parameter can be used to accurately predict mechanical properties (J. H. Holloman and L. D. Jaffe, 1945).

[Equation 2] *Holloman-Jaffe Parameter* $$H = \frac{T(C + \log t)}{1000}$$

Where H is the Hollomon-Jaffe parameter, T is the temperature in Kelvin, C is a constant (19.5 for steels containing 0.15 – 0.45 wt. % carbon), and t is the time in hours for an isothermal condition.

Although the parameter does not relate to the physical properties of the microstructure, it is consistently accurate when relating hardness to the tempering conditions for a range of different microalloyed steels. The effect of these microalloying additions cannot be directly substituted into the original formulae, although the constant *C* can be tailored to varying carbon levels, which is sufficient. Z. Janjušević et al. (2009) demonstrated close agreement of the parameter for HSLA steel (0.3C, 0.9Si, 0.98Mn, Cr, all wt. %) tempered for a range of temperatures and times using a value of 19.5 for *C*.

Since toughness and strength tend to have the opposite response during tempering, there are two critical temperature ranges for obtaining optimum microstructural properties (balance of good strength and toughness) for Q&T steels. The first is a low temperature temper to obtain excellent

tensile strength and relatively good toughness (about 200 °C, below the temperature range that tempering embrittlement occurs) and the second is a high temperature temper (about 600 °C) to obtain excellent toughness with high tensile strength by secondary hardness. The toughness and strength response to the tempering temperature is shown in Figures 10a and 12 respectively.

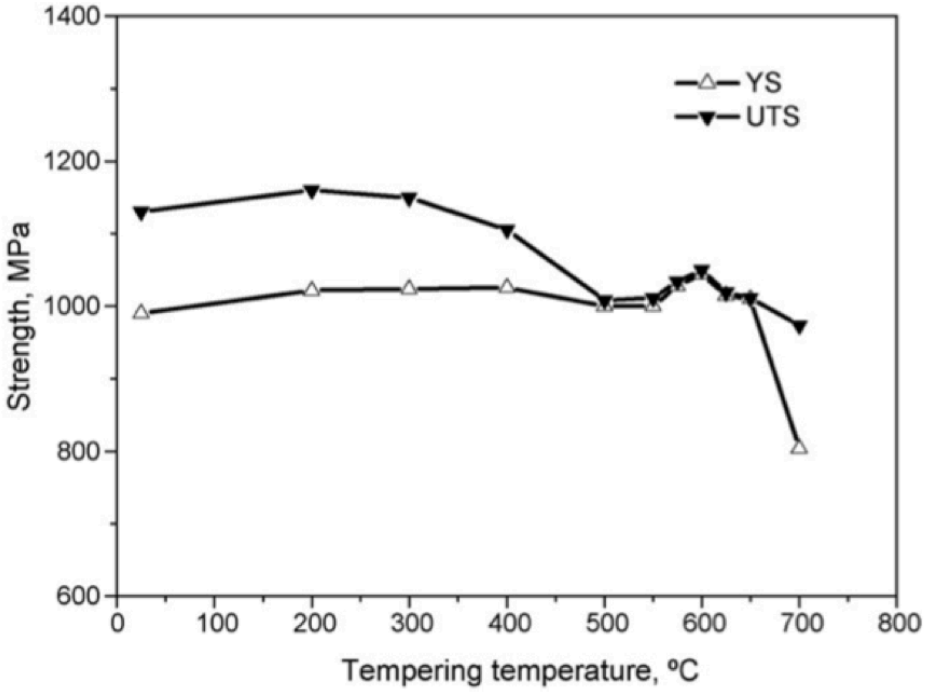

Figure 12: Ultimate tensile strength (UTS) and yield stress (YS) as a function of tempering temperature for an ultra low carbon high strength low alloy steel (0.046C, 0.3Mo, 0.3Cr, 1.77Mn, all wt. %) tempered for 30 minutes. (W. Yan et al., 2009)

2.2 Alloy Composition

The influence of microalloying elements on the behaviour of Q&T steel, during all of the processing stages described above, are ultimately what govern the final mechanical properties. This section explains the influence alloy composition has on the hardenability during the quench process, and also on the tempering response by secondary hardening.

Carbon is fundamental to the production of steel and is the most important hardening element. Alloy elements commonly seen in HSLA Q&T steels, such as that of RQT701 can be divided into two categories; those that can form chemical compounds with carbon and iron in steel (Cr, Mo, V, Ti, and Nb) and those that are present predominantly as solid solutions (Mn, Ni, Si, Co and Cu, although Cu can be an exception). The first group of compounds can form stable carbides, nitrides or carbo-nitrides, or alternatively they can be present in solid solution within the steel matrix.

2.2.1 Influence of Alloy Composition on Hardenability

The steel composition is the most influential way to improve hardenability and generally higher alloyed steels have a higher hardenability than less alloyed or plain carbon steels. However each element has a different level of contribution and cost per unit of increased hardenability. For plain carbon steel, raising the manganese content to 1.4 wt. % is considered to be the most cost effective method to improve hardenability by decreasing the critical cooling rate required to form martensite and providing an easier and more stable quench (www.keytometals.com/Articles/Art146.htm accessed 27/11/13, updated 2010). However above a concentration of 1.7 wt % manganese, R. A. Grange, C. R. Hribal and L. F. Porter (1977) report adverse effects on hardenability by encouraging grain boundary decohesion. Therefore if hardenability needs further improvement other elements are used in addition to manganese, such as chromium, molybdenum and boron, which also have a reasonable cost per unit of increased hardenability.

Boron and phosphorus are regarded as very influential elements to increase hardenability (C. J. McMahon, 1980) although since phosphorus (at the concentrations required to improve hardenability) has adverse effects by toughness embrittlement, boron is favourable. Boron has a very low solubility in austenite (0.001 wt. % at 912 °C and increasing with temperature to a maximum value of 0.005 wt. %, M. Maalekian, 2007) and as such segregates to grain boundaries. Small particles of boron carbide ($Fe_{23}BC_6$) form coherent with the austenite grains providing atomic contact and as such lower surface tension and grain boundary energy. The presence of boron in very small coherent carbides and/or as solute lowers the driving force for ferrite, pearlite and bainite nucleation at grain boundaries thus increasing hardenability. When the steel is quenched the solubility of the matrix becomes even lower, further increasing the concentration of boron at grain boundaries. Boron has an optimum effect at around 0.002 wt. % (M. Maalekian, 2007; Figure 13). However since boron is highly reactive it easily combines with residual nitrogen before cooling, thus coming out of solution and losing all contribution to hardenability; therefore to protect the

boron in solution, titanium and/or aluminium are added in moderation to react more readily with residual nitrogen (H. Mohrbacher, 2010).

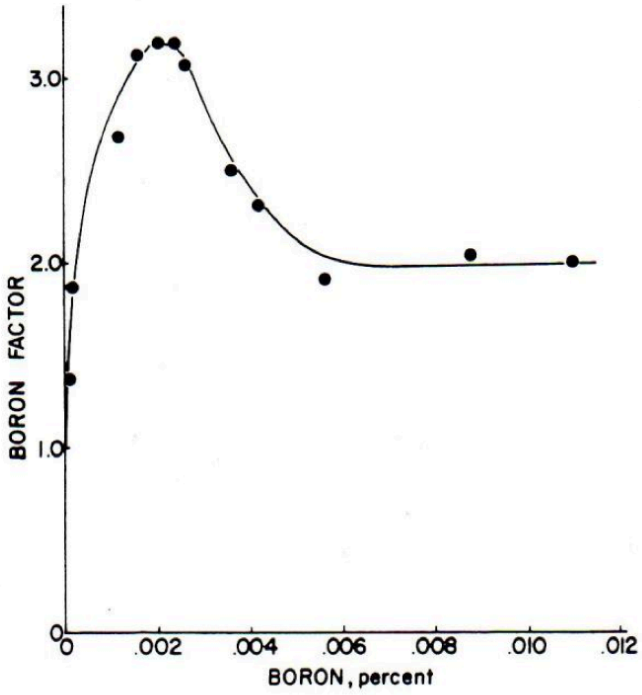

Figure 13: Boron hardenability factor as a function of boron content (in solution) for high strength low alloy steel containing 0.2C, 0.55Mo, 0.65Mn (all wt. %). (M. Maalekian, 2007)

With increasing carbon content (or elevated normalisation temperatures and times) carbon may co-segregate alongside boron to grain boundaries providing a higher driving force for $Fe_{23}CB_6$ formation (H. Mohrbacher, 2010). This coarsens $Fe_{23}CB_6$ particles increasing grain boundary decohesion, which raises the fracture appearance transition temperature and lowers impact toughness in addition to reducing hardenability (H. Mohrbacher, 2010). However in the presence of molybdenum, carbon forms a more uniform distribution of Mo-C clusters (Figure 14) reducing the availability of carbon in solution and causing $Fe_{23}CB_6$ to remain finer (with a high presence of boron in solution) at grain boundaries providing maximum contribution to hardenability. The

clustered and more uniform distribution of carbon in the matrix also reduces softening during tempering by increased secondary hardness as discussed in section 2.2.2.

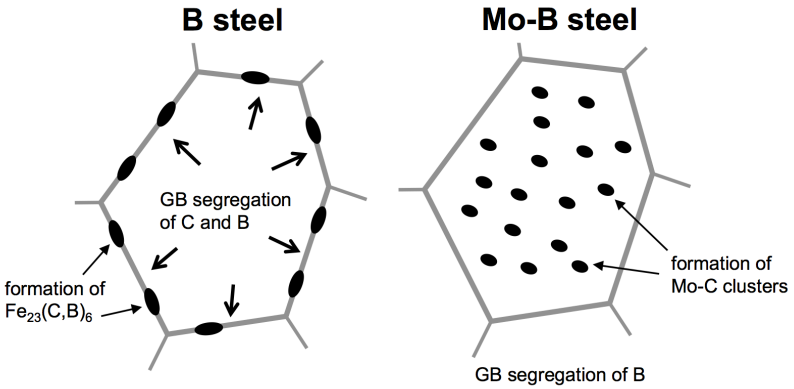

Figure 14: A schematic of boron grain boundary segregation and precipitation in B and Mo-B containing steels. (H. Mohrbacher, 2010)

Molybdenum, and to an extent chromium, also have a direct influence on hardenability. They inhibit ferrite, pearlite and bainite transformation by a solute drag type effect on advancing boundaries during cooling (C. J. McMahon, 1980). This lowers the M_s transformation temperature and promotes a martensitic microstructure throughout the thickness of the cooled plate that gives consistently high strength and toughness (X. Sun, 2010). Figure 15 shows how 0.35 wt. % molybdenum steel increases hardenability, and in the faster cooling rate when martensite can be expected the molybdenum containing steel possesses a higher hardness.

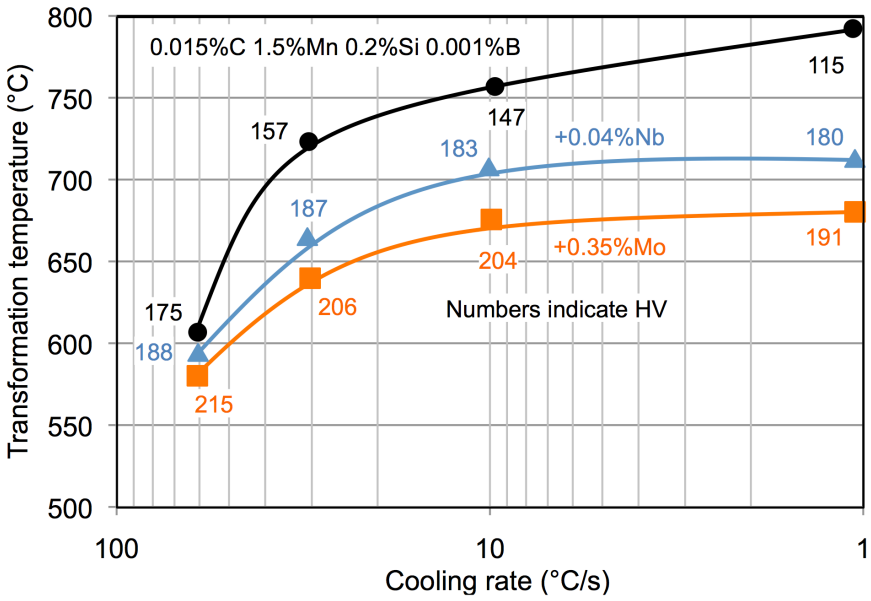

Figure 15: The effect of cooling rate on transformation temperature and hardness in ultra low carbon steel with B, Nb-B and Mo-B alloying. (H. Mohrbacher, 2010)

2.2.2 Influence of Alloy Composition on Secondary Hardening

Alloying elements are fundamental to reduce the softening of martensite during tempering. R. A. Grange, C. R. Hribal and L. F. Porter (1977) noted that elements have a different tempering response and thus contribution to secondary hardening at different times and temperatures, although this review focuses on high temperature tempering (~600 °C). Figure 16 shows the benefit that microalloying elements chromium and molybdenum provide to reduce softening at 600 °C compared to plain carbon steels; both alloyed steels generally show a shallower decline in hardness by stabilising features such as lath boundaries and pinning dislocation movement (J. D. Robson and H. K. D. H. Bhadeshia, 1997a and J. D. Robson and H. K. D. H. Bhadeshia, 1997b) and specifically a secondary hardening peak due to the formation of alloy carbides after one hour.

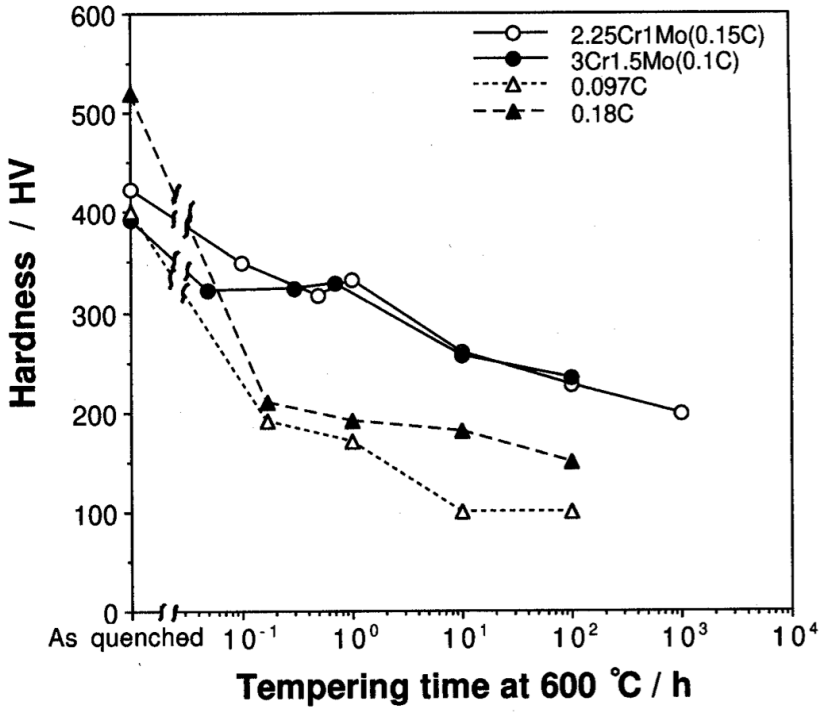

Figure 16: Change in Vickers Hardness as a function of tempering time at 600 °C for $2^1/_4$Cr – Mo and 3Cr – 1.5Mo steel (N. Fujita, 2000) compared with plain carbon 0.097 and 0.18 steel. (G. R. Speich, 1969)

In 1949, E. C. Rollason demonstrated the effect of varying molybdenum content on hardness during tempering and found that above compositions of 1 wt. % molybdenum, a pronounced secondary hardening peak appears after one hour of tempering at 600 °C (Figure 17). The effect of chromium on secondary hardness is less strong and about 9 wt. % chromium is required to give a secondary hardness peak (Figure 18) for tempering of a 0.35 wt. % carbon steel. Molybdenum carbides are generally finer than chromium carbides, due to a lower diffusivity, and therefore give greater secondary hardening in alloyed steels (M. Cohen, 1962). Both steels have a high solubility in austenite (Figure 19) and in equal solute concentration after normalising and quenching, should subsequently precipitate with a high volume fraction and even distribution upon tempering. However the faster diffusion of chromium in comparison to molybdenum allows a higher volume fraction to form before cementite coarsens too much.

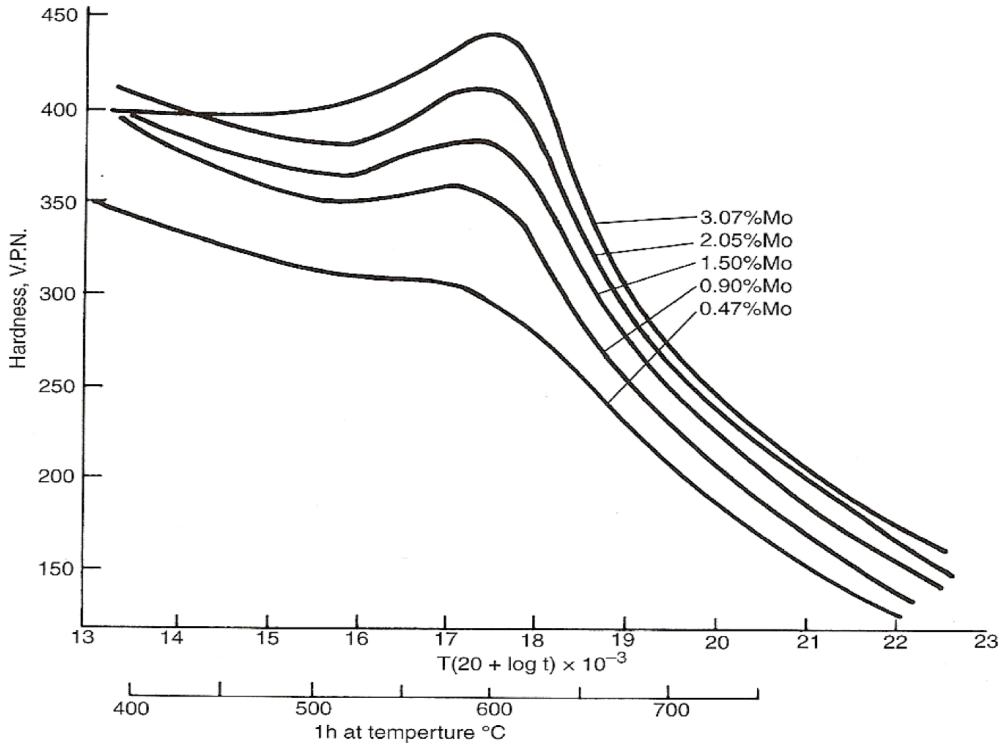

Figure 17: Effect of molybdenum content on the hardness change in 0.1 wt. % carbon steel for high temperature tempering. (E. C. Rollanson, 1949)

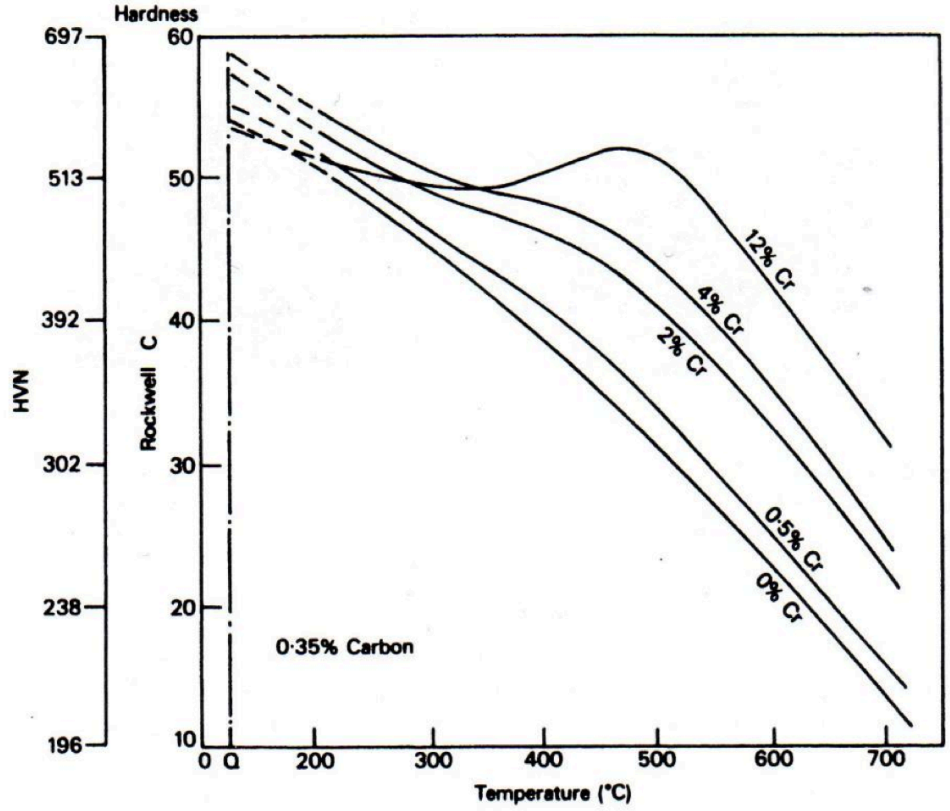

Figure 18: Effect of chromium on secondary hardness as a function of tempering temperature for a 0.35 wt. % carbon steel tempered for 1 hour. (M. Maalekian, 2007)

A. Kundu (2011) stated that in commercial steels with many alloying elements, a synergistic affect between the constituent elements of a complex microalloyed system, influences the solubility of the individual elements in austenite. For example in 1970, the solubility of molybdenum in austenite was shown to increase when acting in synergy with other alloying elements (D. J. Abson and J. A. Whiteman, 1970). Furthermore, ultra low carbon steel with 0.3 wt. % molybdenum (W. Yan et al., 2009) recorded a secondary hardness peak at 600 °C with less molybdenum than the steels tested by E. C. Rollanson (1949); therefore a synergistic affect of the complex microalloyed system must have occurred in order to produce the secondary hardening effect (Figure 12).

R. G. Nooning, (1999) also demonstrated that the stability of certain carbide phases improve in multi-component systems. Since molybdenum is an expensive element, and yet also the primary cause of secondary hardness in HSLA steels, steelmakers may search for synergistic advantages to reduce material and production costs.

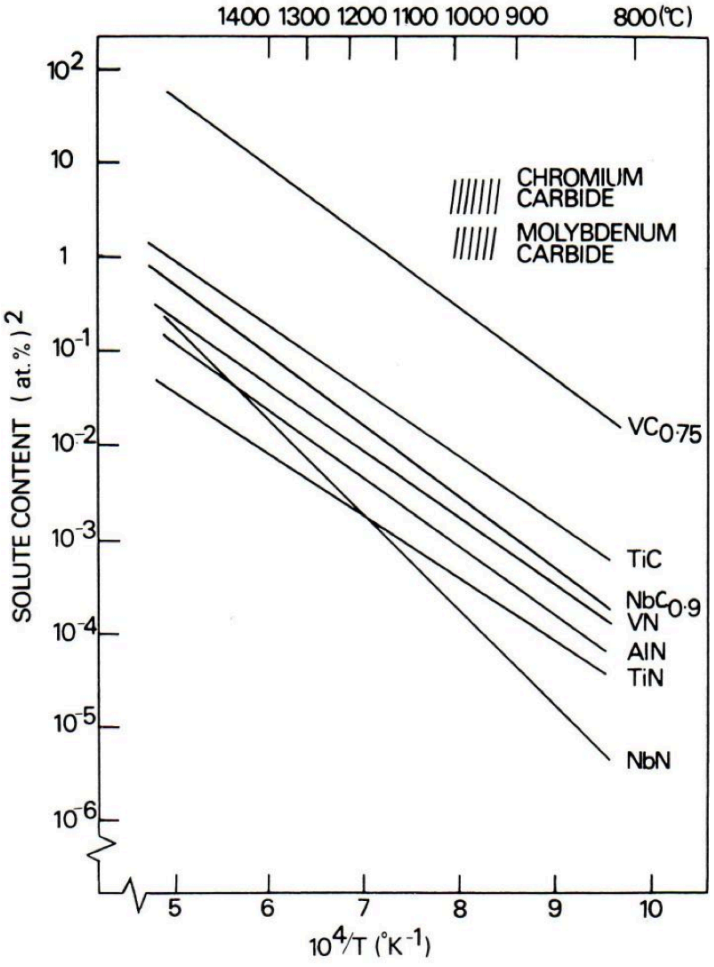

Figure 19: The solubility product of carbides and nitrides in austenite as a function of temperature. (D. A. Porter and K. E. Easterling, 2004)

2.3 Precipitation Characteristics

The heavily dislocated martensite laths provide many nucleation sites for ε-carbide formation. This process only requires the diffusion of carbon and is very rapid, sometimes by autotempering as described earlier. The formation of ε-carbide ($Fe_{2.4}C$) is unstable and so is classed as a transition phase. Following the brief occurrence of transition carbides, cementite similarly requires only the diffusion of carbon, and combined with a low enthalpy of formation (Figure 20) it is the first stable phase to nucleate during the tempering of martensite (A. Hultgren, 1947). Cementite (Fe_3C) is likely to precipitate at existing leate during the tempr at grain boundaries by heterogeneous nucleation (R. G. Nooning, 1999).

Later in the process alloy carbides will nucleate from existing cementite or by solute diffusion to grain boundaries. Nucleation occurs by reduced strain and surface energy at lath or grain boundaries or by the segregation of carbon (and other alloying elements) to grain boundaries. Nucleation and growth take place until all of the solute carbon has precipitated, at which point coarsening of larger carbides occurs by the consumption of smaller less stable carbides known as Ostwald ripening. The loss in surface area between the particles and the matrix acts as the driving force for ripening. In low alloy steels the formation of new phases are dependent on the tempering temperature and time characteristics that in turn influence diffusivity. In comparison, nucleation and growth depend on both the diffusion of solute and on the misfit and the interfacial energies (M. Maalekian, 2007).

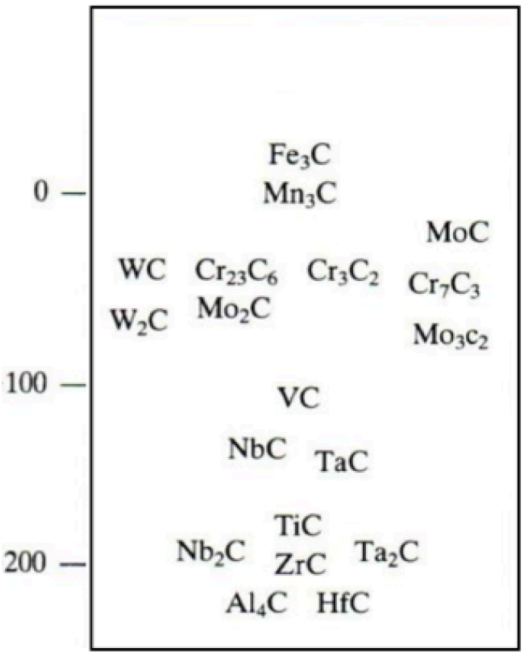

Figure 20: The enthalpy of formation (in Δ_f / KJ mol^{-1}) of carbides at 298.15 K. (adapted from M. Maalekian, 2007)

In alloy steels there are six stable carbide phases that can be found on tempering steels, these are listed in Table 2. The composition of the steel will determine the sequence of metastable phases to form after cementite and it will determine the equilibrium condition. Group one carbides have a more complex crystal structure compared with group two carbides, and with the exception of cementite (Fe_3C) produce relatively coarse carbides.

Table 2: Possible variants of carbide formation in steel, 'M' represents an intermetallic particle (M. Maalekian, 2007)

Carbides of group I	Carbides of group II
M_3C	MC
$M_{23}C_6$	M_2C
M_7C_3	
M_6C	

Table 3 summarises the size and morphology of cementite for 0.18C, 0.2Si, 1.2Mn, Cr, (all wt. %) steel, tempered for one hour at 200 °C, 400 °C and 600 °C. At 600 °C there appears to be two types of morphologies, Widmanstätten 0.08 x 0.25 μm and Spheroidal 0.3 μm. (F. H. Samuel, 1985)

Table 3: Quantitative TEM metallography of cementite tempered for 1 hour at 200 °C, 400 °C and 600 °C in 0.18C, 0.2Si, 1.2Mn, Cr (all wt. %) steel. (F. H. Samuel, 1985)

Specimen designation	*Tempering temperature* (°C)	*Carbide in the martensite phase*			*Cementite in the ferrite phase*	
		Type	*Morphology*	*Size* (μm)	*Morphology*	*Size* (μm)
Q	200	Cementite	Widmanstätten	0.015 x 0.125	—	—
Q	400	Cementite	Fragments	0.10 x 0.40	—	—
Q	600	Cementite	Widmanstätten	0.08 x 0.25	—	—
			Spheroidal	0.30		

2.3.1 Carbide Evolution

The precipitation of cementite happens almost instantaneously in comparison to that of alloy carbides that require substitutional solute diffusion (N. Fujita, 2000). Cementite forms at around 200 – 350 °C and is commonly found along lath or grain boundaries; when present as a fine dispersion it inhibits the reorganisation of dislocations from the martensite sub structures to delay softening (A. A. Gorni, 2011). However due to the high diffusivity of carbon, cementite coarsens rapidly and has low stability at high temperature.

The presence of alloying elements (e.g. Si, Mo and Cr) can delay the coarsening of cementite and stabilise it to higher temperatures between 400 – 700 °C (R. W. K. Honeycombe and H. K. D. H. Bhadeshia, 2006). Silicon is commonly added between 1 – 2 wt. % for this purpose and is known to enter the crystal structure and retard precipitation and coarsening. Molybdenum and chromium also stabilise cementite, although at a slower rate by substitutional solute diffusion. M. Cohen (1962) reported that with sufficient chromium in solution, the composition of cementite changes so that chromium displaces some of the iron atoms. N. Fujita (2000) demonstrated similar results for two HSLA steels tempered at 600 °C. The metal atoms in cementite at equilibrium were predominantly chromium while at para-equilibrium they were iron (Figure 21) thus allowing cementite to resist coarsening by increased stability. Furthermore the amount of chromium in the cementite increases with the concentration of chromium in the steel as shown by comparing Figure 21a (3 wt. % chromium steel) and Figure 21b (2.25 wt. % chromium steel).

A similar comparison can be seen for the concentration of molybdenum in M_2C precipitates when increasing the molybdenum content of the steel. It should also be noted that the increased concentration of molybdenum in M_2C precipitates occurred at the expense of chromium despite that chromium increased more than molybdenum in the bulk composition. This suggests that M_2C

precipitates favour the presence of molybdenum; thus according to section 2.2.2, molybdenum carbides (Mo_2C) are the primary influence of secondary hardening in HSLA steels.

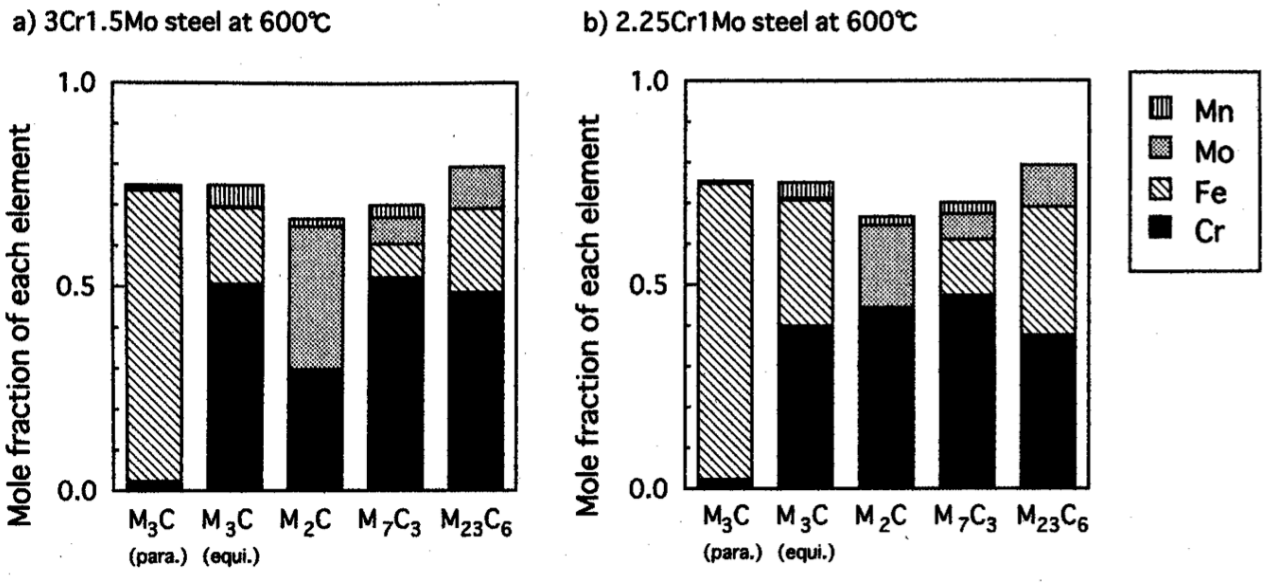

Figure 21: The predicted equilibrium composition for each carbide phase at 600 °C for two HSLA steels. Calculations were performed using MTDATA (S. M. Hodoson, 1989) and SGTE database, allowing the existence of ferrite and all the carbides in each case. (N. Fujita, 2000)

After paraequilibrium cementite precipitation, dissolution occurs naturally when the mean concentration of cementite in the matrix falls below its equilibrium and drives cementite particles to subsequent carbide phases (J. D. Robson and H. K. D. H. Bhadeshia, 1997a). Phase evolution can occur through a change in composition, or by nucleation of a new phase. In molybdenum containing steels Mo_2C precipitates are needle shaped and usually the next type of carbide to form after cementite; they can nucleate at the cementite interface, the martensite lath boundaries or at dislocations. M. Maalekia (2007) stated that Mo_2C precipitates that nucleate at dislocations, are the primary carbide to contribute to secondary hardening by a uniform distribution of fine precipitates.

Mo_2C forms in the temperature region of 500 – 700 °C and is very resistant to coarsening since

substitutional solute diffusion of molybdenum is slow. N. Fujita (2000) calculated that coarsening will primarily occur within the first hour of tempering at 600 °C (Figure 22a) although experimental data by M. G. Hall (1976) shows coarsening with a 50 hour temper at 600 °C (Figure 22b).

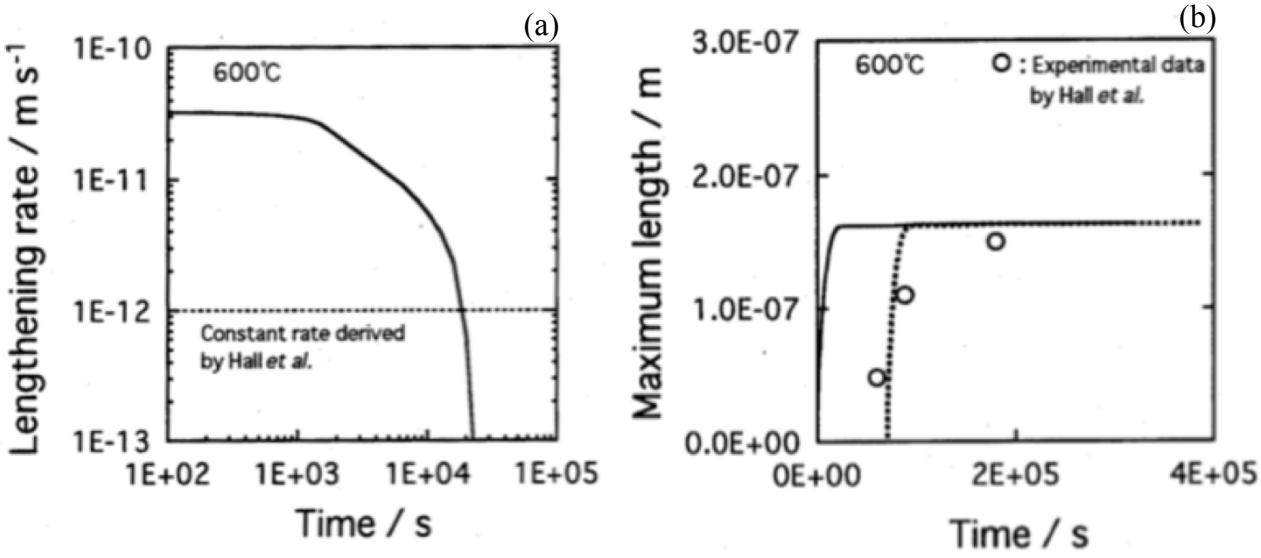

Figure 22: (a) Calculated lengthening rate of M_2C and (b) calculated and experimental length, for 2Mo – 0.1C wt. % steel as a function of time at 600°C. (N. Fujita, 2000)

$M_{23}C_6$ and M_7C_3 are found between temperatures of 500 – 700 °C and are complex carbides that usually precipitate after M_2C and by direct transformation from Fe_3C, although they can nucleate independently. Since chromium diffuses more rapidly than most carbide forming elements, $Cr_{23}C_6$ and Cr_7C_3 are more common at the lower tempering temperatures and shorter times. $Cr_{23}C_6$ and Cr_7C_3 were observed when chromium exceeded 1 wt. % in 0.2 wt. % carbon steel (D. W. Hetzner and W. V. Geertuyden, 2008). If the tempering temperature or duration increases, molybdenum can enter the phase and stabilise it from coarsening. Steels with higher molybdenum content can form $M_{23}C_6$ without the presence of M_7C_3.

There are two sequences (Sq1 and Sq2) reported for carbide precipitation based on literature surrounding HSLA Cr – Mo steels (A. M. El-Rakayby, 1986 and N. Fujita, 2000). The two sequences nucleate independent from one another with the solute chromium content generally driving Sq1 and the solute molybdenum content Sq2.

Sq1) $Fe_{2.4}C - Fe_3C - M_7C_3 - M_{23}C_6 - M_6C$

Sq2) $M_2C - M_{23}C_6 - M_6C$

The composition and temperature will determine the equilibrium phase, however when considering shorter than equilibrium tempering times, the parameters of temperature and time heavily influence the sequence order and the amount of each phase to occur. N. Fujita (2000) experimentally characterised the precipitation sequence in both $2^1/_4$Cr – Mo wt. % steel (Sq3) and 3C – 1.5Mo wt. % steel (Sq4) at 600 °C; it was calculated that there exists continual overlap within each phase and a simultaneous existence of sequences 1 and 2. It is also evident that the higher chromium and molybdenum content (used in Sq4) gives an earlier formation of M_7C_3 compared to M_2C. Therefore Q&T steels such as RQT701 with lower alloy content may have a delayed M_7C_3 precipitation compared to M_2C.

Sq3) $M_3C - M_3C+M_2C - M_3C+M_2C+M_7C_3 - M_3C+M_2C+M_7C_3+M_{23}C_6$

Sq4) $M_3C - M_3C+M_7C_3 - M_3C+ M_7C_3 +M_2C+M_{23}C_6 - M_7C_3+M_2C+M_{23}C_6$

Figure 23 is a schematic diagram of the precipitation sequence for $2^1/_4$Cr – Mo wt. % HSLA steel T22, at an isothermal holding temperature of 565 °C relative to the amount of occurrence of the different carbide phases (P. Kiattisaksri et al., 2001). The observation agrees with the experimental findings of Sq3 for the same composition.

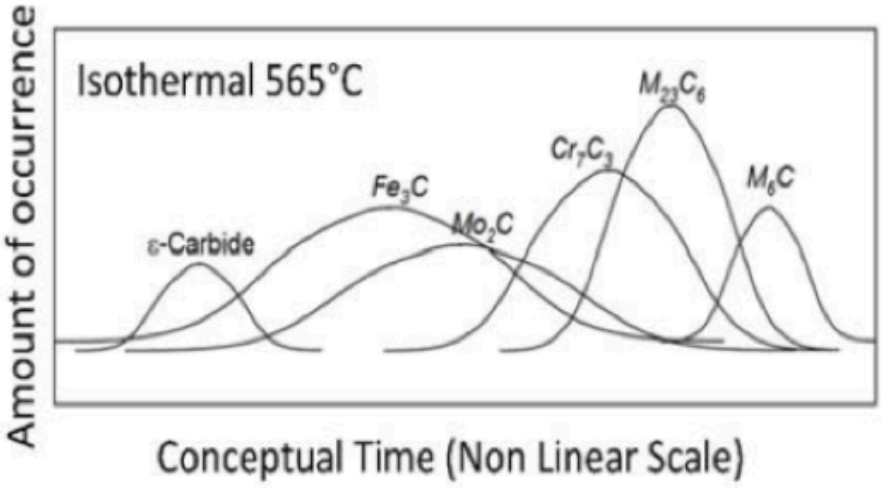

Figure 23: Nucleation and dissolution schematic diagram for HSLA T22 steel (2Cr, Mo, 0.5Si, 0.5Mn, 0.15C, all wt. %) indicating the evolution of carbide phases and their relative amount. The diagram was based on experimental results for an isothermal holding of 750 °C at short term tempering durations using a comparative C value as a function of the Larson-Miller parameter to simulate long term aging at 565 °C. (P. Kiattisaksri et al., 2001)

A. Kroupa et al. (1998) and V. Ayrostkova et al. (1998) performed considerable experimental work on precipitation sequences for long term aging of 2Cr – Mo wt. % HSLA steels (Figure 24). Figure 24a and 24b generally agree with Sq4 that exhibits a delayed formation of M_7C_3 compared with M_2C, which is surprising as their compositions are closer to matching that of the steel used in Sq3.

In steel two the bulk vanadium content is higher compared with steel one and is responsible for stabilising the alloy phases (R. Lagneborg et al., 1999) to longer tempering times as in Figure 24b. The higher vanadium content is also shown to form VC carbides at equilibrium. With one hour of tempering at 580 °C steel one (Table 4) reports cementite and $M_{23}C_6$. Under the same temperature and 15 hours of tempering M_2C and M_7C_3 are reported. The equivalent experimental data is not available for steel two, although theoretical results suggest that M_2C takes closer to 100 hours to appear, hence the retardation to Mo_2C nucleation by increased vanadium.

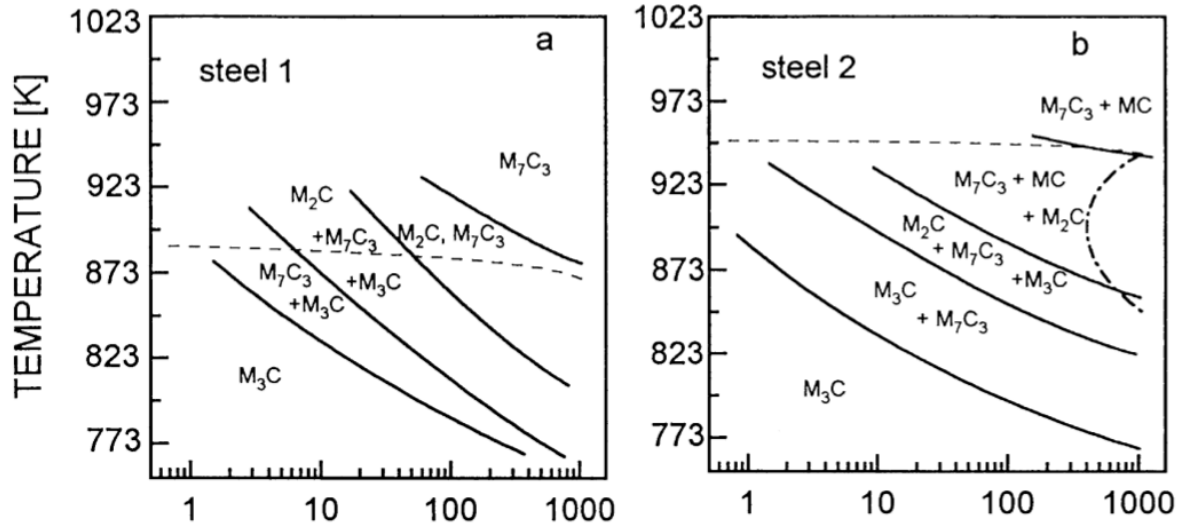

Figure 24: 'Baker-Nutting' style diagrams showing carbide precipitation as a function of time and temperature. The area under the black dashed and dotted and dashed line represents $M_{23}C_6$ and M_6C appearance respectively. The compositions are listed in Table 4. (A. Kroupa et al., 1998)

Table 4: Chemical compositions of investigated steels for Figure 24. (A. Kroupa et al., 1998).

	Composition (wt%)							
Steel	C	Cr	Mo	V	Mn	Si	S	P
1	0.09	2.40	0.70	0.02	0.66	0.32	0.006	0.011
2	0.10	2.55	0.73	0.12	0.66	0.35	0.005	0.015

N. Fujita (2000) predicted Mo_2C precipitation in 2Cr – Mo wt. % steel after about 70 – 80 minutes of tempering at 600 °C using a model proposed by J. D. Robson and H. K. D. H. Bhadeshia (1996). Figure 25 compares these calculations to the work of R. G. Baker and J. Nutting (1959) where M_2X is observed after 90 minutes of tempering at 600 °C. As shown in Figures 12, 16 and 17, this is often the temperature and time whereby a hardness peak is recorded. Looking at Figure 26 however it appears that a tempering duration of 1 – 2 hours at 600 °C is very early on in the development of M_2C and therefore its contribution to mechanical properties may be less than optimum.

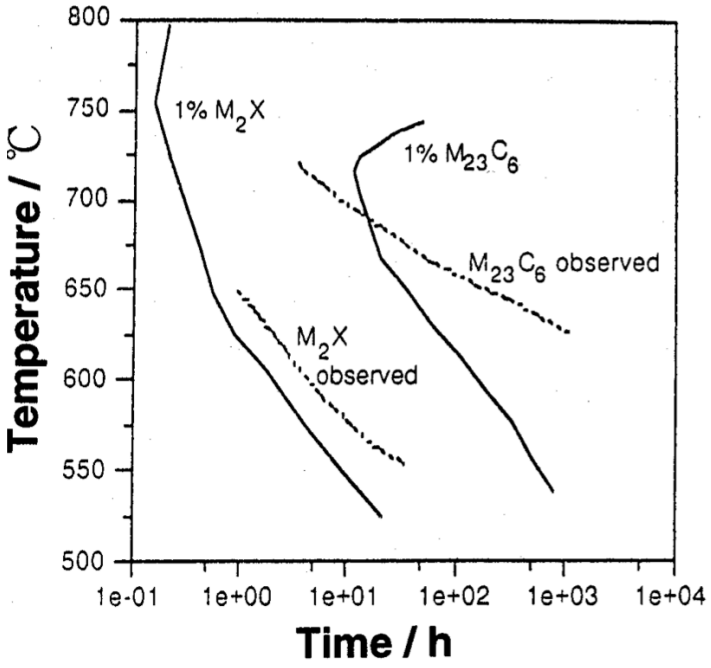

Figure 25: The precipitation sequence relative to tempering temperatures for 2Cr – Mo wt. % steel tempered at 600 °C along with experimental data using the J. D. Robson and H. K. D. H. Bhadeshia (1996) model. (N. Fujita, 2000)

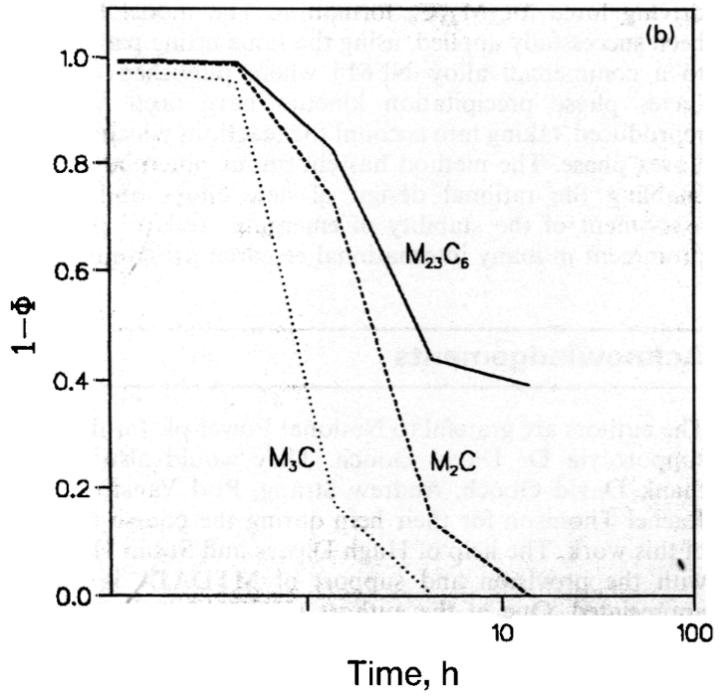

Figure 26: Plot of the extent of reaction Φ as a function of tempering time at 600 °C for 2.25Cr – Mo wt. % steel. (J. D. Robson, 1996)

N. Fujita (2000) calculated the volume fraction of the carbides expected to form with tempering time, for a 2Cr – Mo wt. % steel at 600 °C (Figure 27). Mo_2C is predicted to be the predominant phase after one hour of tempering, however experimental observations found only the existence of cementite. This indicates that either the theoretical calculations using the model of J. D. Robson and H. K. D. H. Bhadesha (1996) are not accurate with respect to time, or the Mo_2C precipitates are too small to be detected in the experimental observations.

Since the experiment by E. C. Rollanson (1949) demonstrated that the effect of secondary hardening varies with molybdenum content (Figure 17) and that after one hour of tempering at 600 °C for a 2Cr – Mo wt. % steel (the same used by N. Fujita, 2000, in Figure 27) a secondary hardening effect occurs, it is reasonable to suggest that Mo_2C is occurring but due to the low extent of reaction (as in Figure 26) the experimental observations were too superficial to be detected. Furthermore Mo_2C is the first carbide to form that contains molybdenum and therefore the experiment by E. C. Rollinson (1949) suggests that Mo_2C is precipitating and causing the secondary hardness peak, unless the effects are due to synergy between the increased molybdenum content and that of carbon or chromium; in which case perhaps the modelling system discussed is too primitive.

Another explanation for the discrepancy between the theoretical and experimental results could be the presence of segregated alloy content. If non-equilibrium solidification occurs and normalisation times and temperatures are reduced to minimise retained austenite, an inhomogeneous microstructure may exist. D. W. Hetzner and W. V. Geertruyden (2008) suggest that this may lead to the evolution of precipitation sequences in a different order to that predicted by the bulk composition. Scientists such as P. Kiatisaksri et al. (2001) use tempering parameters to simulate aging since the time and cost of extracting primary data is so high. Therefore the complex effects of synergy and segregated alloy content are often overlooked in theoretical calculations.

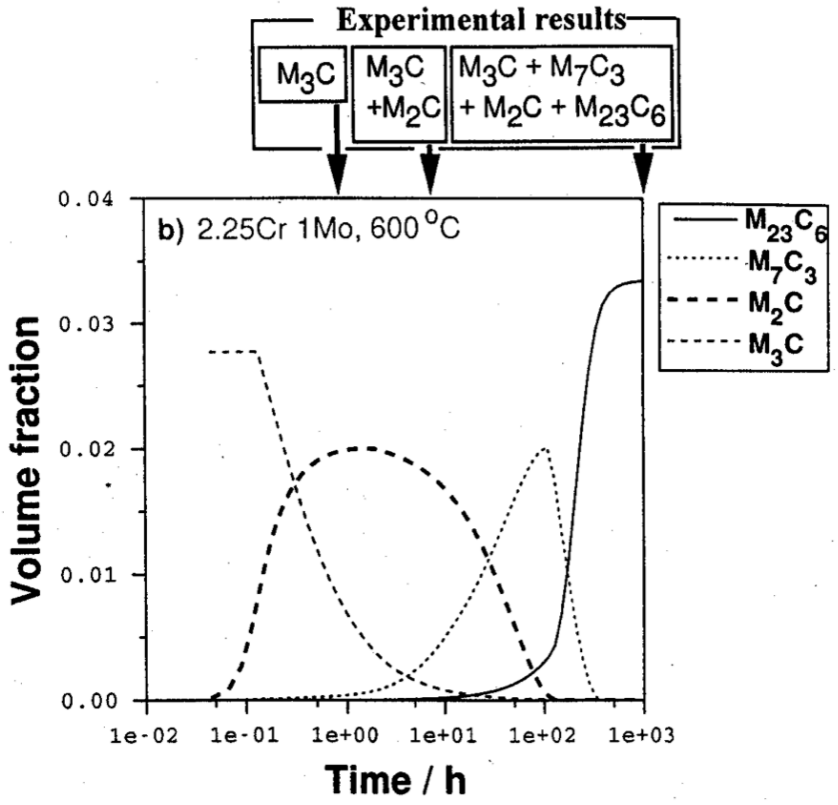

Figure 27: The precipitation sequence predicted using the model by J. D. Robson and H. K. D. H. Bhadeshia (1996) as the volume fraction formed for 2Cr – Mo wt. % steel tempered at 600 °C *compared to experimental observations of the carbides present. (N. Fujita, 2000)*

In addition to modeling difficulties with an inhomogeneous matrix composition, or a less than perfect processing route, N. Fujita (2000) stated that modeling the characteristics of cementite is particularly difficult since its thickness varies depending on its location. Cementite formed on lath boundaries is reported to have a thickness of about twice that of cementite formed within laths, with much more experimental variability in the measurements (Figure 28). D. W. Hetzner and W. V. Geertruyden (2008) also state that carbides to have nucleated on larger inclusions form in the liquid, may grow significantly more than isolated carbides and thus affect the average precipitate characteristics and therefore the modeling data. A. Kroupa et al. (1998) reported significant difficulty when modeling the behavior of molybdenum precipitation in $M_{23}C_6$ and M_2C.

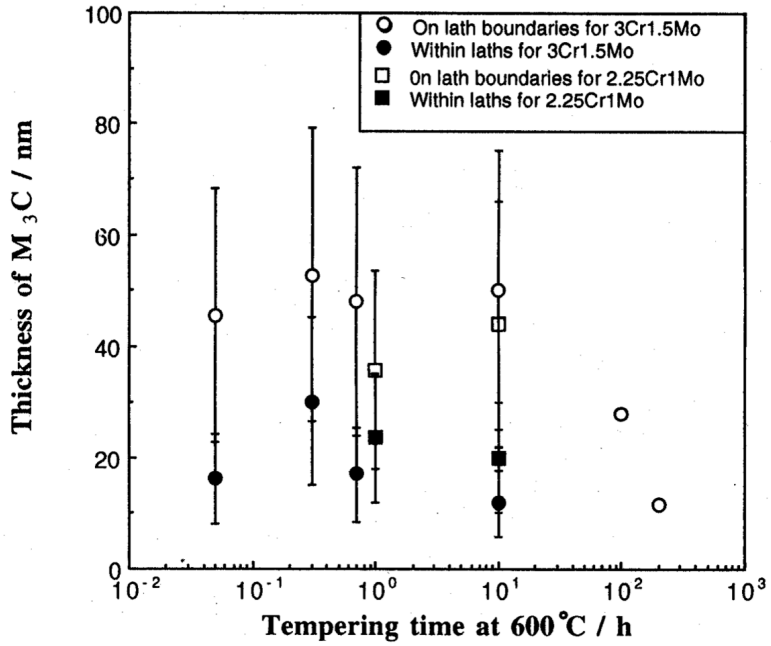

Figure 28: Thickness of cementite on lath boundaries and within laths as a function of tempering time at 600 °C for two steel compositions. (N. Fujita, 2000)

2.4 Summary of Literature Review

In summary it has been suggested that tempering 2Cr – Mo wt. % martensitic steel at 600 °C for one or several hours is ideal to produce a secondary hardening peak, and therefore a desirable balance of strength and toughness. When tempering under these conditions, chromium produces a larger volume fraction of carbides than molybdenum helping to stabilise cementite from coarsening while maintaining good mechanical properties. Meanwhile although slower to diffuse, molybdenum provides the bulk of the strength by a fine carbide distribution despite the smaller volume fraction in comparison to chromium. However despite the global production of 2Cr – Mo wt. % steels in industry and the considerable literature produced around the subject, theoretical calculations give different results to the experimental work, and different experimental works vary even with similar compositions. It is still apparent today the statement by N. Fujita (2000) when she wrote that the precipitation characteristics are not fully understood.

Regarding RQT701 or other low carbon low alloy Q&T steels under similar tempering conditions there is significantly less information available. It can be presumed that the result of using less alloy content may contribute to a smaller secondary hardening effect, perhaps more appropriately referred to as a delay in softening rather than secondary hardening. However there is no experimental evidence to validate such a presumption. The closest compositional match from the literature to RQT701 is the 2009 study by S. W. Ooi et al., which exhibits autotempered martensite with a quenched hardness of 420HV. However the steels tested by S. W. Ooi et al. (2009) were to be used in the quenched condition, which explains their requirement to obtain an autotempered microstructure and so the researchers did not report the effects of tempering.

3. Aim

The aim of this investigation is to determine the tempering response of RQT701 15 mm steel plate over a range of tempering temperatures (580 – 620 °C) and times (up to 100 hours) with a specific focus around the tempering duration of 1 – 4 hours, which is typical of industry conditions.

4. Materials and Experimental Methodology

HSLA RQT701 steel plate, with composition as given in Table 5, was supplied by Tata Steel Europe as 15 mm thick plate that had been laboratory cast and hot rolled, followed by normalising at 925 °C for one hour and water quenching to room temperature using multi-directional jet sprays giving a cooling rate of 60 $°Cs^{-1}$ measured at the surface.

Table 5: The composition of RQT701 lab cast to 15 mm plate as supplied by Tata Steel Europe.

Element	B	C	N	Al	Si	P	V	Cr	Mn	Nb	Mo
Quantity wt%	0.0024	0.17	0.006	0.061	0.32	0.01	0.034	0.29	1.3	0.041	0.53

4.1 Heat Treatments

Samples measuring approximately 20 x 20 x 15 mm were cut from the as-received plate, and tempered at varying times and temperatures from 30 minutes to 48 hours and at 580 °C, 600 °C, 620 °C and 640 °C. A thermocouple was used to ensure the accuracy and consistency of the furnace temperature during the first tempering experiment Figure 29; room temperature samples were added after 60 minutes when the furnace was at the appropriate temperature. The samples were immediately quenched after tempering by immersing in a large bucket of water at room temperature and continuously stirred.

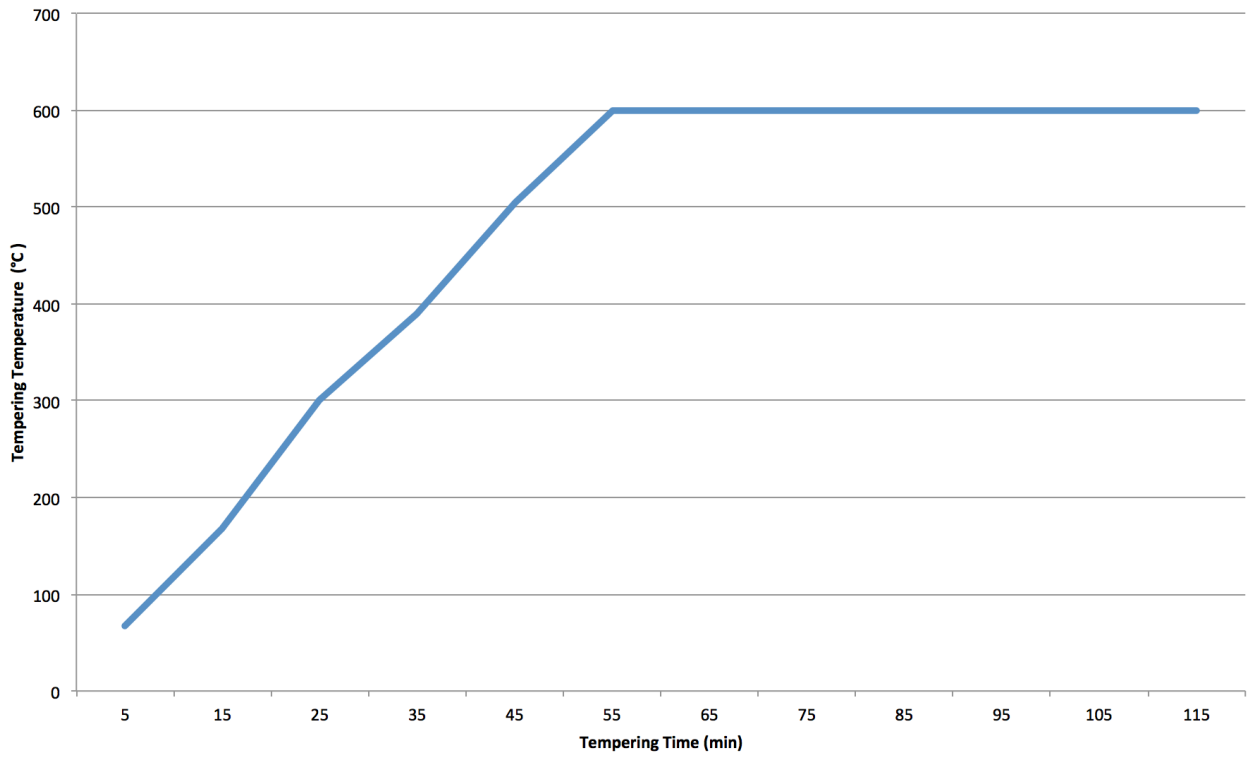

Figure 29: Thermal Profile during the first tempering experiment. A furnace (with a thermocouple inside) was programmed to increase by 10 °C per minute until 600 °C. A room temperature sample was then placed in the furnace for one hour. When the sample was inside, the thermocouple rested on top of the sample. The thermocouple temperature was recorded every 10 minutes.

4.2 Metallography and Microstructural Characterisation

The heat-treated samples were cut in half using an Accutom-5 and the transverse face (with respect to the original rolling direction) was mounted in Bakelite and polished to a 0.5 μm finish. Each polished sample was etched in 2 % nital to reveal the microstructure. The samples were then examined using a JOEL 7000 SEM.

4.3 Hardness Testing

Samples were tested for hardness using a Vickers Hardness machine and micro indenter set with a 200 g load. Eight indents were made across each sample. To avoid interference from any decarburisation regions and from free surfaces, spacing was maintained to a minimum of three indents apart, or from the sample edge.

4.4 Electro-Magnetic Testing

Electromagnetic (EM) sensor signals have been shown to be sensitive to microstructural changes in steels, due to the associated changes in magnetic permeability of the material (J. Liu et al., 2013). Previous work carried out at the University of Birmingham found that the microstructural changes associated with tempering 4330V steel could be measured in situ (X. Hao, unpublished; Figure 30). EM sensor testing has been carried out on RQT701 (which has a lower carbon content than 4330V steel) to determine if the effects of in-situ tempering could be detected.

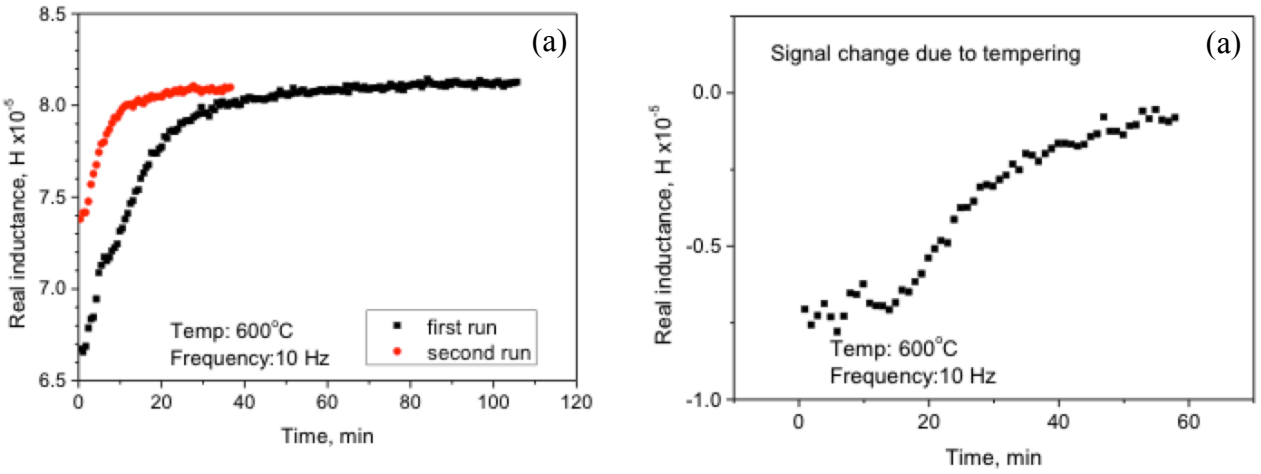

Figure 30: Two consecutive in situ electromagnetic sensor tests of a 4330V steel at 600 °C. (a) shows the signal measured during both tempering runs, (b) shows the resultant signal based on microstructural changes after the influence of temperature changes has been removed. (X. Hao unpublished)

A cylindrical EM sensor and analyser used to collect the signals (Solartron 1260) was used to measure initially as-quenched RQT701 cylindrical samples while tempering at 580 °C, 600 °C and 640 °C. The cylinders were machined to 12 mm diameters (Figure 31) and placed inside the EM sensor within a pre-heated furnace. The samples were double tempered with the duration of the first run long enough (roughly 50 – 100 hours) to assume microstructural stability. The EM signal

results of the first run include the microstructural response to tempering, while the results of the second run that assume microstructural stability, should only show the effect of temperature changes on the sensor and magnetic permeability. Therefore the thermal influence on the EM signal (the value of which is calculated by isolating its effect in the second run) is deducted from the thermal and microstructural influence on EM signal in the first run. This leaves the resultant change in EM signal from the first run to represent the microstructural response to tempering, as shown in figure 30 for the 4330V steel. The cylinder was cut, prepared for optical metallography and examined along the cross-section after the heat treatments (Figure 31).

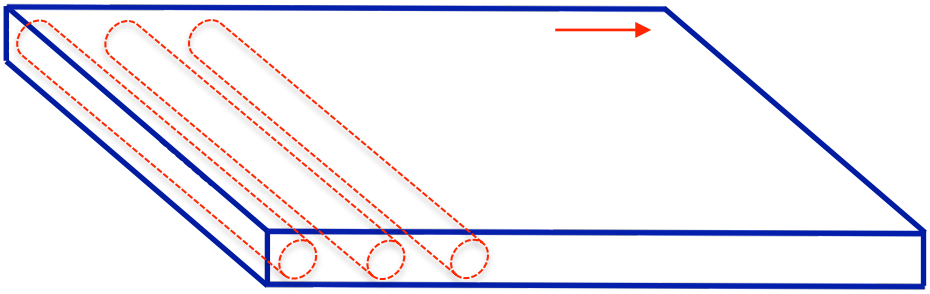

Figure 31: Schematic diagram of the cutting process for 12 mm diameter RQT701 cylinders. The rolling direction has been arrowed.

4.5 Thermodynamic Calculations

Thermo-Calc software Version 7 was used to assess the stable and metastable phase equilibria (by supressing the prior-most stable phase) to derive a precipitation sequence from ε-carbide through to M_6C.

5. Results

5.1 Microscopy & Hardness of as-Quenched RQT701, up to 30 Minutes Tempering

The as-received (quenched state) RQT701 material has a microstructure of autotempered martensite with numerous visible rod-shaped precipitates of approximately 50 – 120 nm in length (based on the minimum size resolvable), Figure 32. The precipitates appear through thickness and are mostly present within the martensite laths with depleted zones around the lath edges. There also appears to be a significant number of smaller circular precipitates that are only barely visible in the SEM (Figure 33); this could be a sectioning effect for rod shaped precipitates, or a separate distribution of very fine precipitates at the limit of resolution in the SEM.

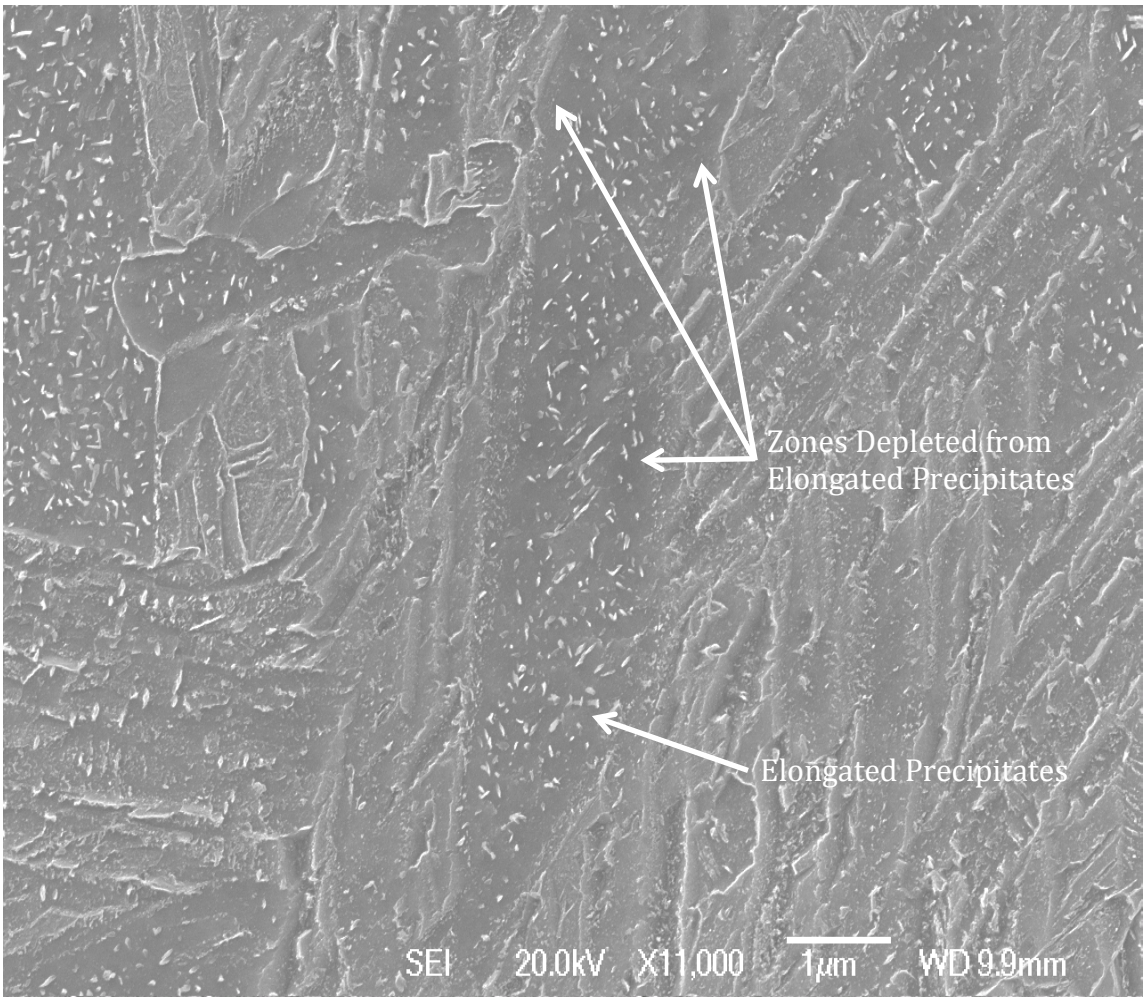

Figure 32: Micrograph of the as-received material RQT701.

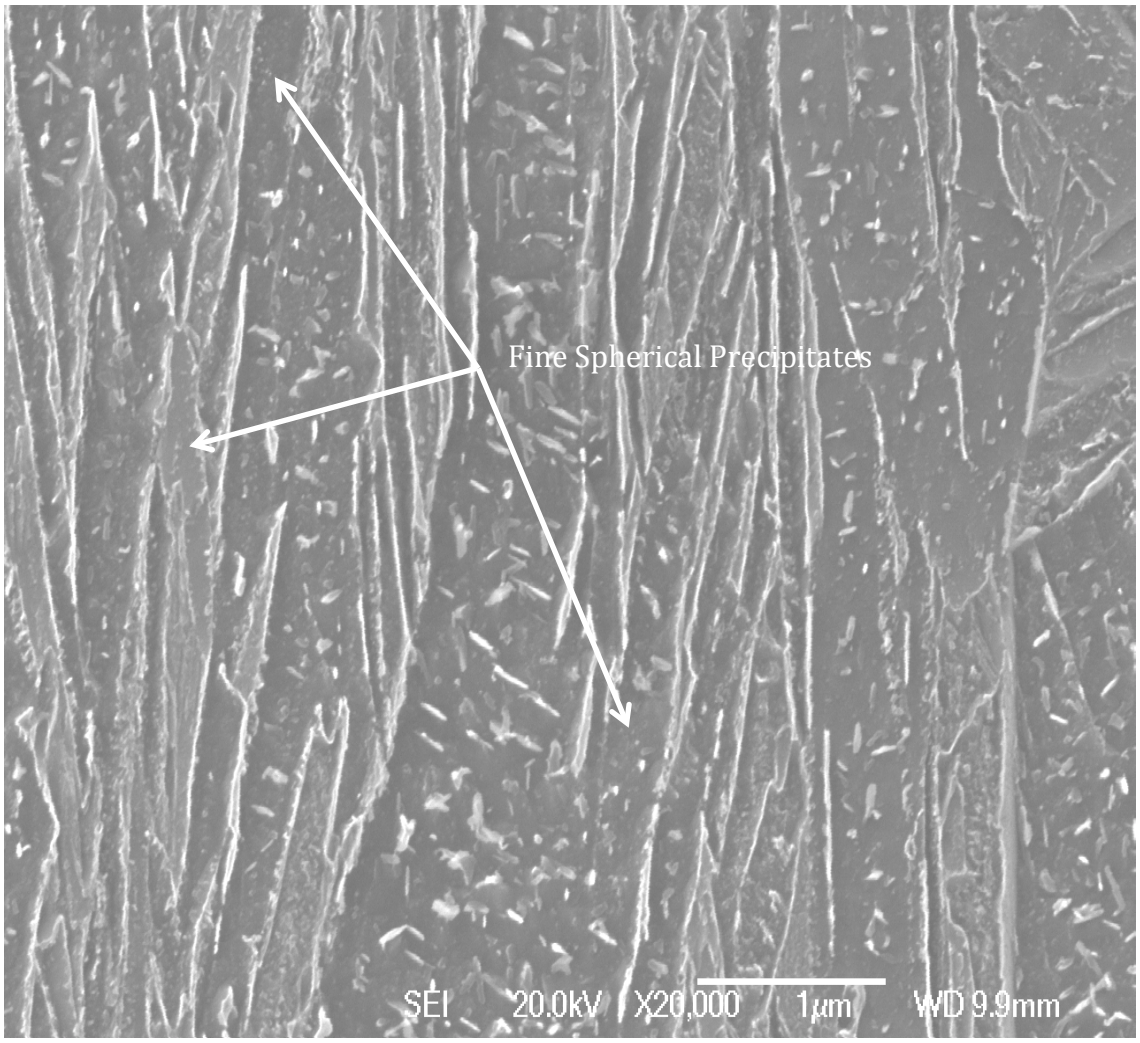

Figure 33: Micrograph of the as-received material RQT701.

These observations are consistent with research by S. W. Ooi et al. (2009) described previously where autotempered martensite was formed on quenching sheets of 180 x 40 x 3 mm low alloy steel (0.15C, 1.54Mn, 0.2Mo, all wt. %) into 80 % water, 20 % polymer solution (Figure 8). Using TEM S. W. Ooi et al. (2009) reported two types of cementite morphologies in the autotempered samples both of Bagaryatski orientation; elongated precipitates 100 nm in length and globule shape precipitates 5 – 10 nm in diameter. Since chromium is known to delay the tempering process and generally slow carbide precipitation (T. Peng et al., 2010) while molybdenum and silicon more specifically slow the formation of iron-rich precipitates such as ε-carbide and cementite (R. W. K. Honeycombe and H. K. D. H. Bhadeshia, 2006) it can be suggested that the autotempered

precipitates in RQT701, which contains more chromium and molybdenum but less silicon than the steel examined by S. W. Ooi et al. (2009) Figure 34, are iron-rich ε-carbide or cementite although confirmation with TEM would be needed. The effect of manganese to slow the rate of cementite coarsening is only observed at longer tempering times or higher temperatures (G. Miyamoto 2007).

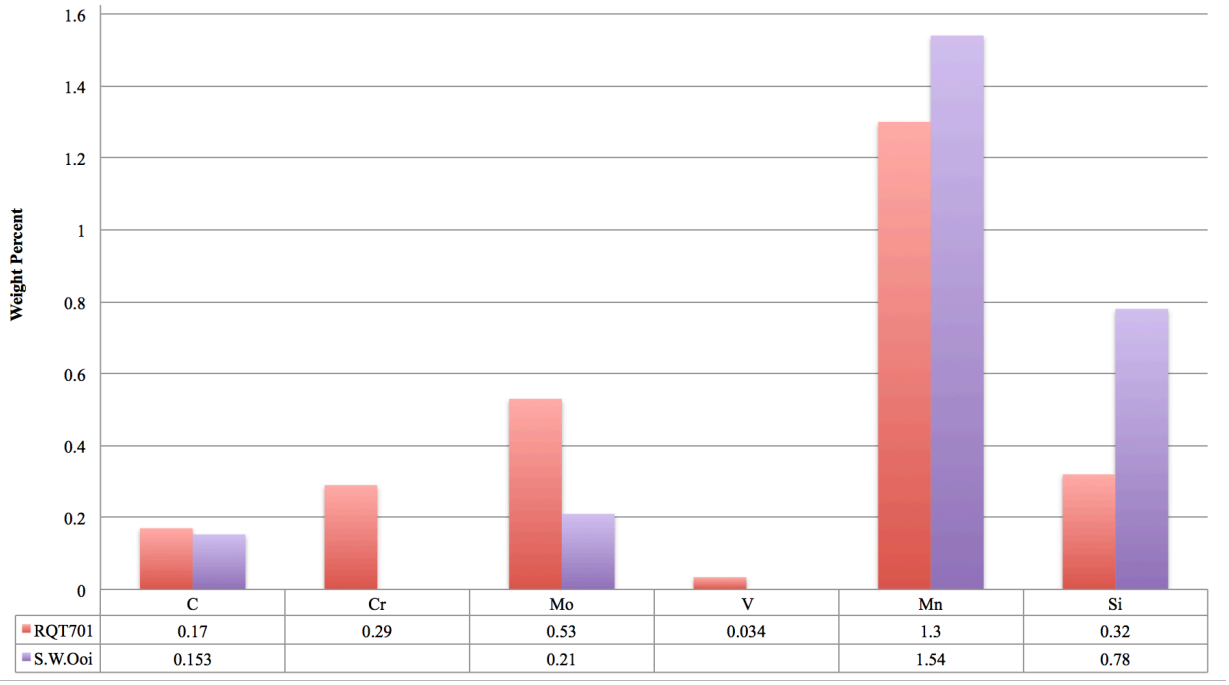

	C	Cr	Mo	V	Mn	Si
RQT701	0.17	0.29	0.53	0.034	1.3	0.32
S.W.Ooi	0.153		0.21		1.54	0.78

Figure 34: Comparison of the composition for RQT701 and the steel from S. W. Ooi et al. (2009).

To test the sensitivity of RQT701 to autotemper given different cooling rates, and to understand if the degree of autotempering has subsequent short term tempering consequences, a 20 x 20 x 15 mm sample of RQT701 as-received plate was reaustenitised at 925 °C for one hour and then quenched into a large bucket of agitated ice water. The presence of fine carbides in both the as-received sample (of cooling rate 60 $°Cs^{-1}$) and the ice water quenched sample (of cooling rate >60 $°Cs^{-1}$) (Figures 32 and 35 respectively) indicates that autotempering still occurs at cooling rates >60 $°Cs^{-1}$ albeit a finer precipitate size is seen through thickness in ice water quenched RQT701. Therefore due to a slower cooling rate, autotempering is expected in water quenched RQT701 plates through thickness also. The cooling rate range to achieve autotempering of RQT701 is over double that

reported by S. W. Ooi et al. (2009) (30 °Cs^{-1} Figure 36) and suggests a much faster process of autotempering presumably due to the lower silicon content.

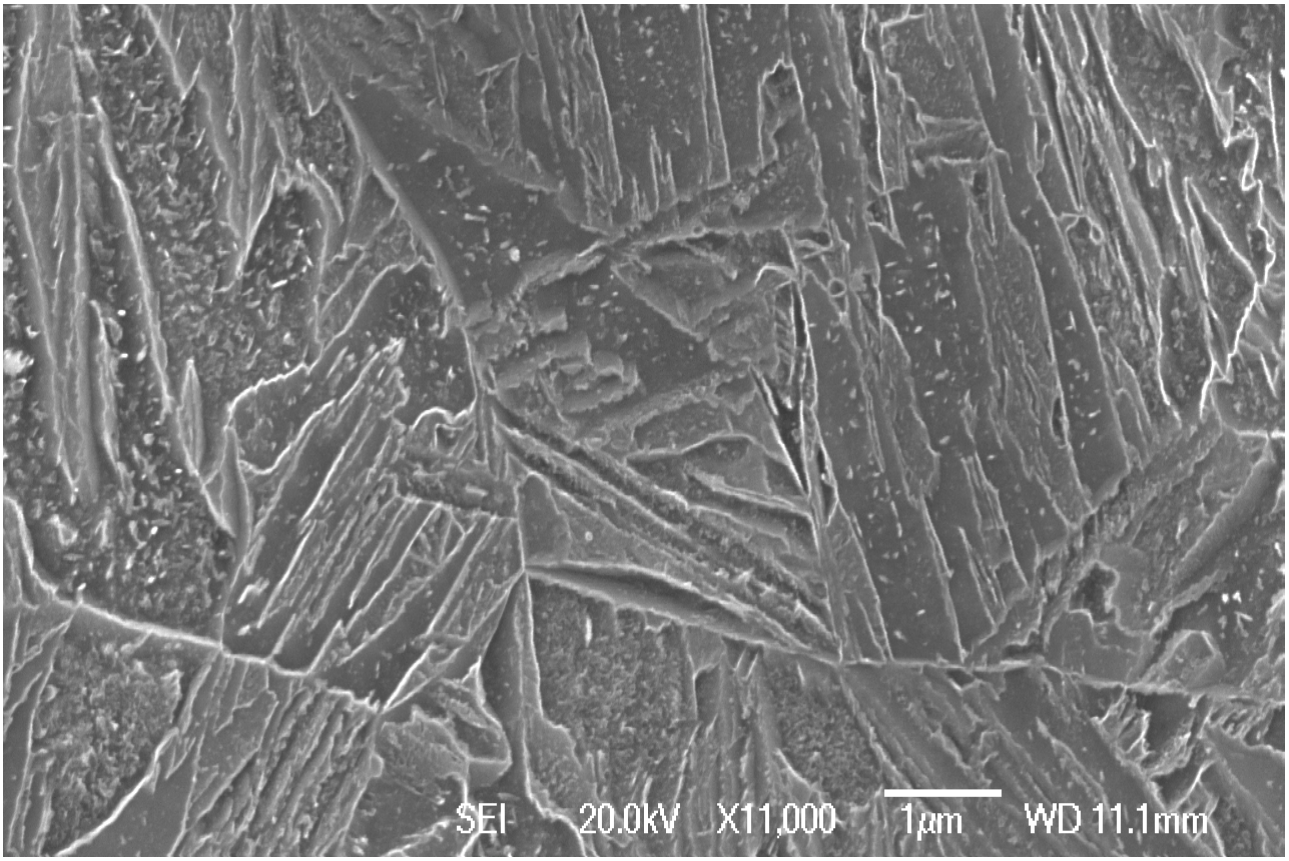

Figure 35: Micrograph of RQT701 reaustenitised at 925 °C for one hour and ice-quenched.

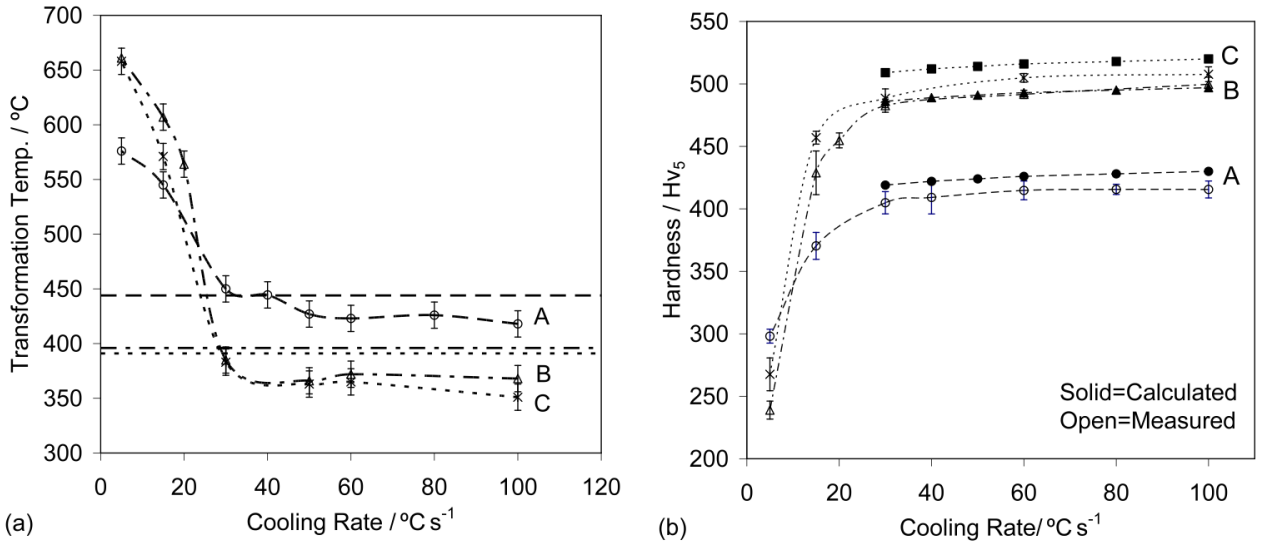

Figure 36: Measured transformation temperature and hardness as a function of the cooling rate. The horizontal lines in (a) show the calculated martensite-start temperature at 444 °C for steel A, and the calculated martensite hardness of steel A is also presented in (b). Steels C and B represent compositions of higher carbon content and are not relevant to the discussion. (S. W. Ooi et al. 2009)

Vickers Hardness results for the room temperature water quenched and ice water quenched samples (430 HV and 460 HV respectively) vary by 30 HV (Figure 37) and confirm that microstructural change by autotempering takes place at cooling rates >60 $°Cs^{-1}$; furthermore the higher hardness obtained from the ice water quenched sample agrees with the observation of a finer precipitate distribution in comparison to the water quenched sample. After tempering for 30 and 120 minutes at 600 °C, both the room temperature water quenched and ice water quenched samples show similar Vickers Hardness values (Figure 37). The statistically insignificant difference between the two quenching mediums after short term tempering suggests that room temperature water quenching (being easier and cheaper) is sufficient to achieve an appropriate microstructure for subsequent tempering heat treatment.

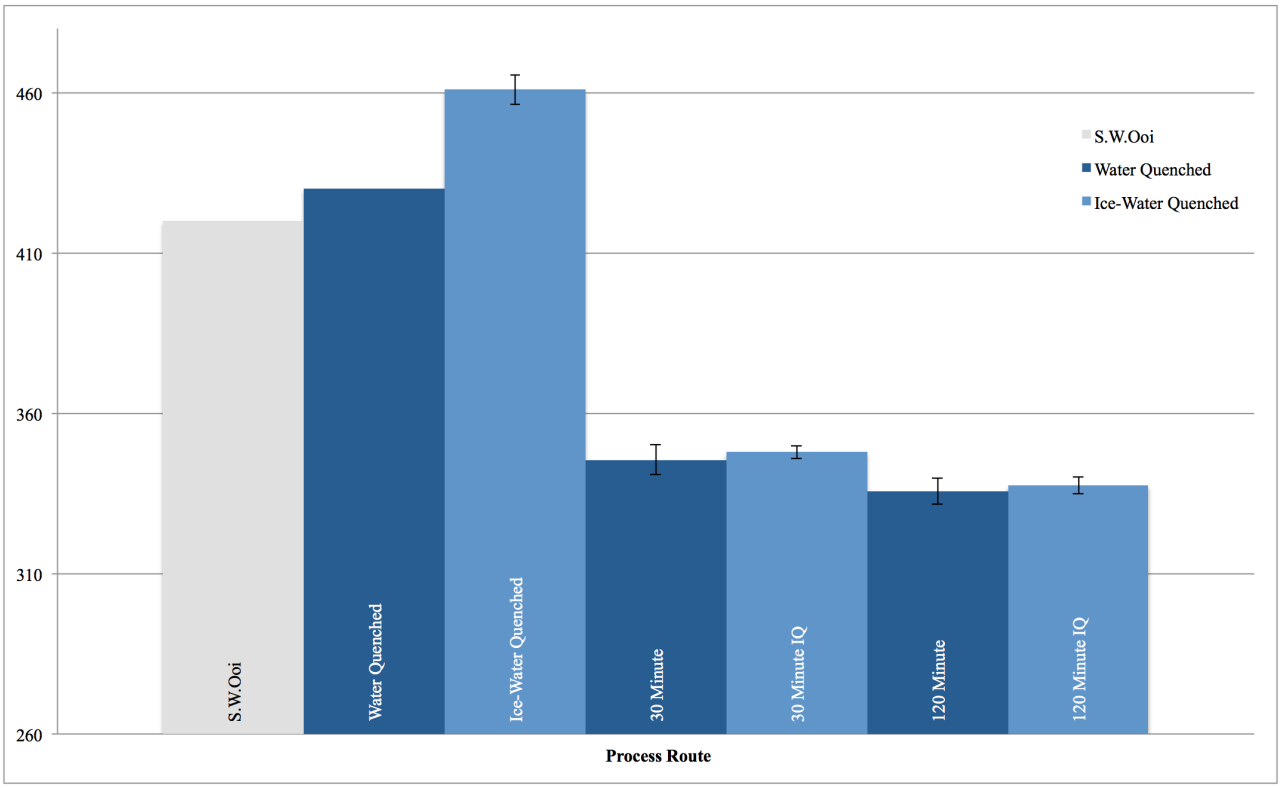

Figure 37: Hardness comparison between room temperature water quenched and ice water quenched samples both in the as-received or quenched state and after short term tempering at 600 °C for 30 and 120 minutes. The hardness value obtained by S. W. Ooi et al. (2009) for quenched low alloy steel of similar composition (shown in grey) has been plotted for reference.

A typical tempered martensite microstructure forms after tempering for 30 minutes at 600 °C (Figure 38) as laths coarsen and lath boundaries become harder to see (although this could be due to variations in etching). Additionally, in comparison to the as-received microstructure precipitates appear larger and fewer in number, predominantly at lath boundaries due to easier diffusion. These observations along with the removal of dislocations explain the significant drop in hardness of the room temperature water quenched sample from 430 HV to 346 HV (after 30 minutes at 600 °C).

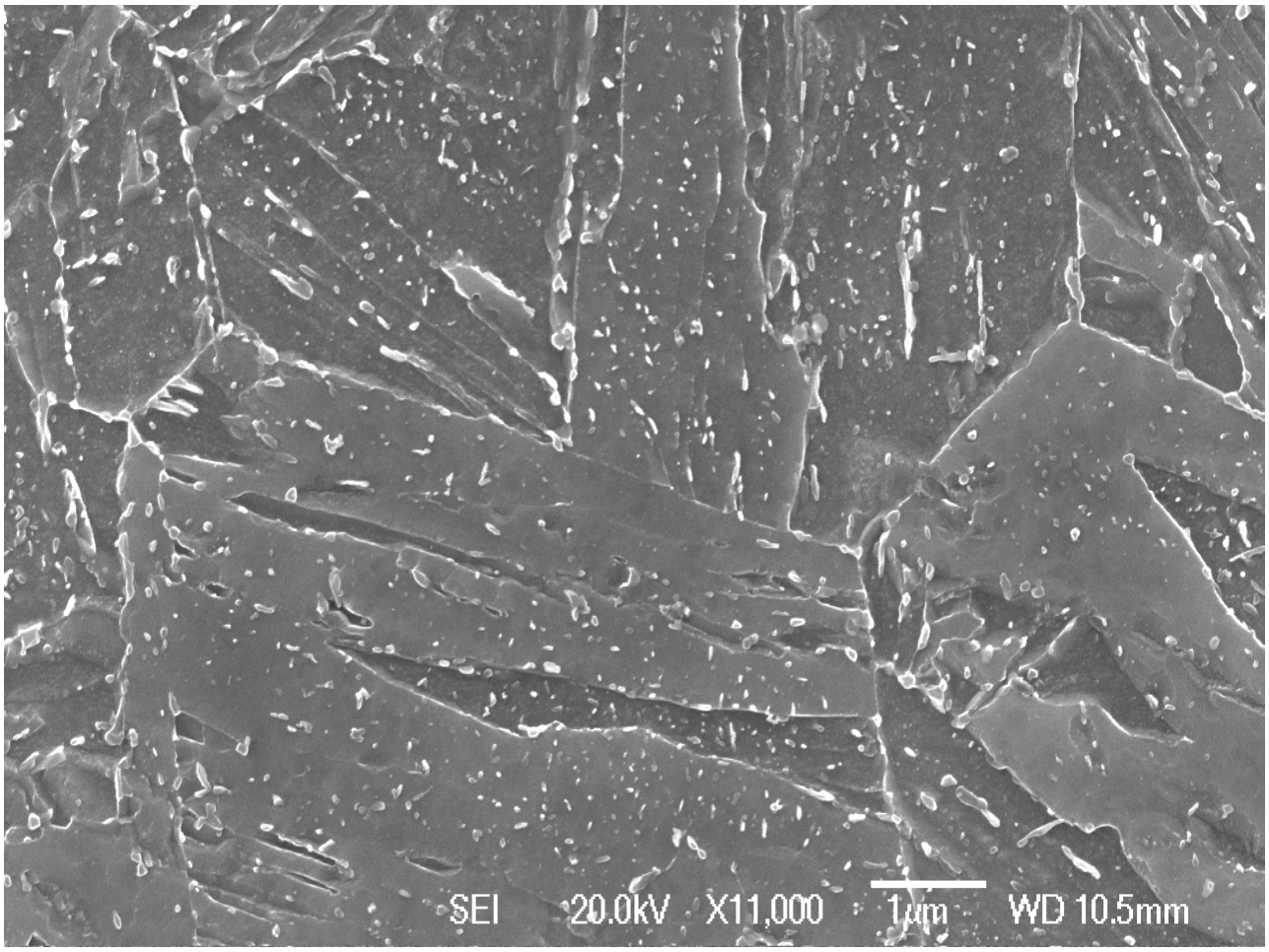

Figure 38: Micrograph of RQT701 tempered for 30 minutes at 600 °C and water quenched.

For this tempering time and temperature it is expected that existing carbides from the autotempered microstructure will coarsen at the expense of smaller neighbouring carbides and any remaining temperature it is expected that existing carbides from the autotempered microstructure will coarsen at the expense of smaller carbides (N. Fujita, 2000).

5.2 Microscopy & Hardness of Tempered RQT701 for 30 Minutes to 4 Hours

Figure 39 shows the hardness values for water quenched RQT701 tempered between 30 minutes and 4 hours at 600 ° C. Tempering between 30 and 60 minutes has a smaller influence on softening than the initial 30 minutes previously since the majority of tetragonality and dislocations are lost/removed (respectively), hardness only deviates (i.e. changes more than the standard deviation) between 45 and 60 minutes (Figure 39). However upon tempering between 1 and 4 hours, the hardness gradually increases and peaks between 2 and 3 hours. The standard deviation shown by the y-error bars suggests a statistical increase between the 1 and 2 hour results by 6 HV and a statistical decrease between the 3 and 4 hour results by 9 HV.

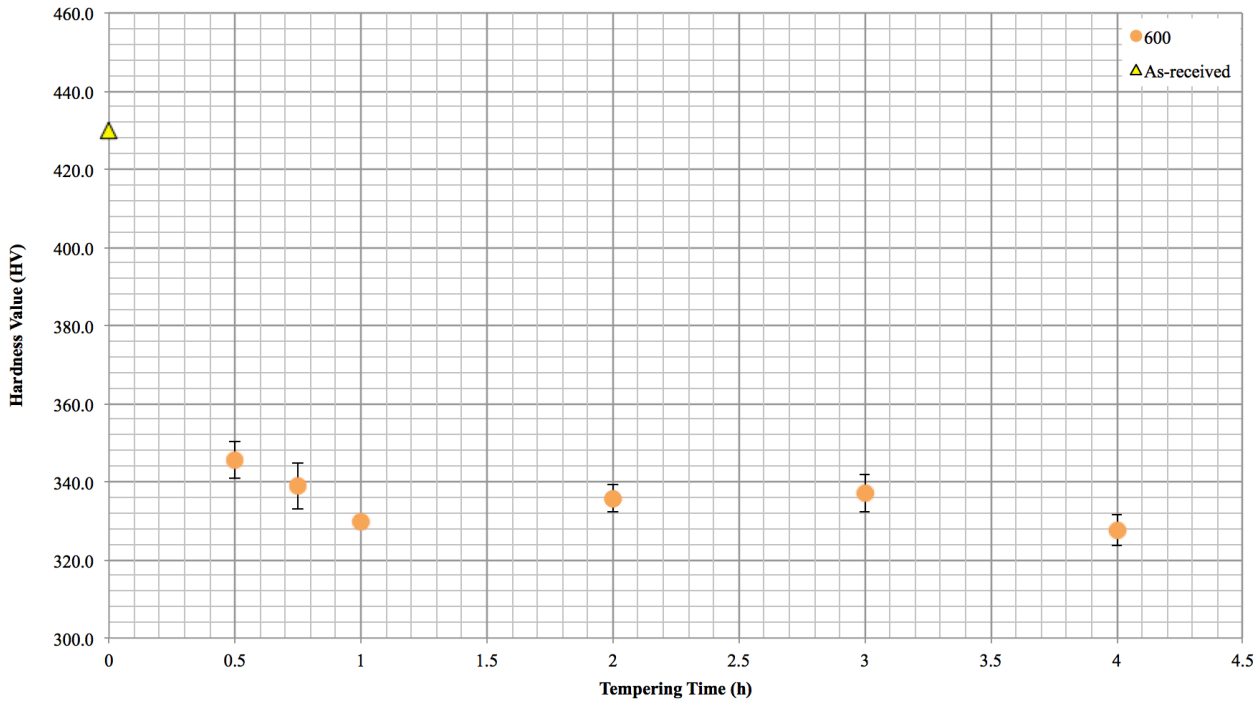

Figure 39: Vickers Hardness with standard deviation results tempered at 600 °C from 30 minutes to 4 hours using a 20 kg load. (The y-error bars for the one hour sample are very small and do not protrude out from behind the circle.)

SEM image analysis of RQT701 tempered for one hour at 600 °C (Figure 40) shows second phase

precipitation. Literature by A. Vyrostkova et al. (1998) and A. Kroupa et al. (1998) found cementite precipitates after tempering of 2.5Cr, 0.7Mo, 0.1C (all wt. %) steel for 1 and 2 hours at 600 °C, with some $M_{23}C_6$ also being observed. The rough size and elongated appearance (43 nm Table 6) suggest that Figure 40 shows cementite precipitation.

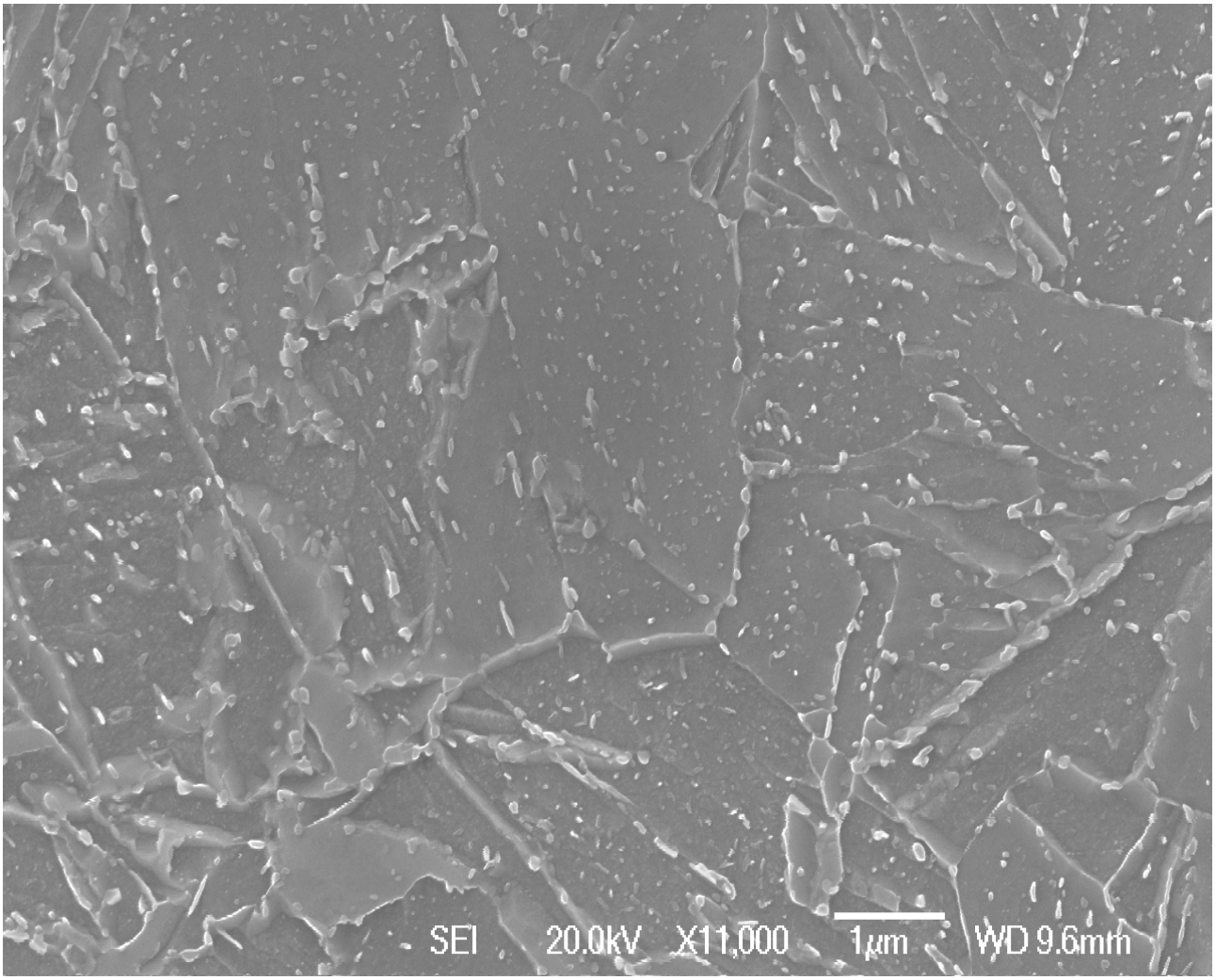

Figure 40: Micrograph of water quenched RQT701 tempered for one hour at 600 °C.

Particle analysis of SEM images for RQT701 tempered at 1, 2 and 4 hours at 600 °C (Figure 41) revealed a 39 % increase in the equivalent circle diameter (ECD) of the cementite due to coarsening and a decrease in number density (Table 6). The overall volume fraction increases by 23 %, which may be due to further precipitation of cementite from carbon in solution and/or the coarsening of

very fine carbides formerly undetectable by SEM, to become detectable. Whilst the volume fraction increases the number density decreases and this may explain the small change in hardness of just 10 HV (Figure 39).

Table 6: Particle analysis of second phase precipitates for tempering at 1, 2 and 4 hours at 600 °C.

Second Phase Precipitate	1 Hour	2 Hour	4 Hour
Number Density (μm^2)	*63*	*55*	*52*
Average ECD (nm)	*43*	*60*	*71*
Volume Fraction (%)	*0.017*	*0.020*	*0.022*

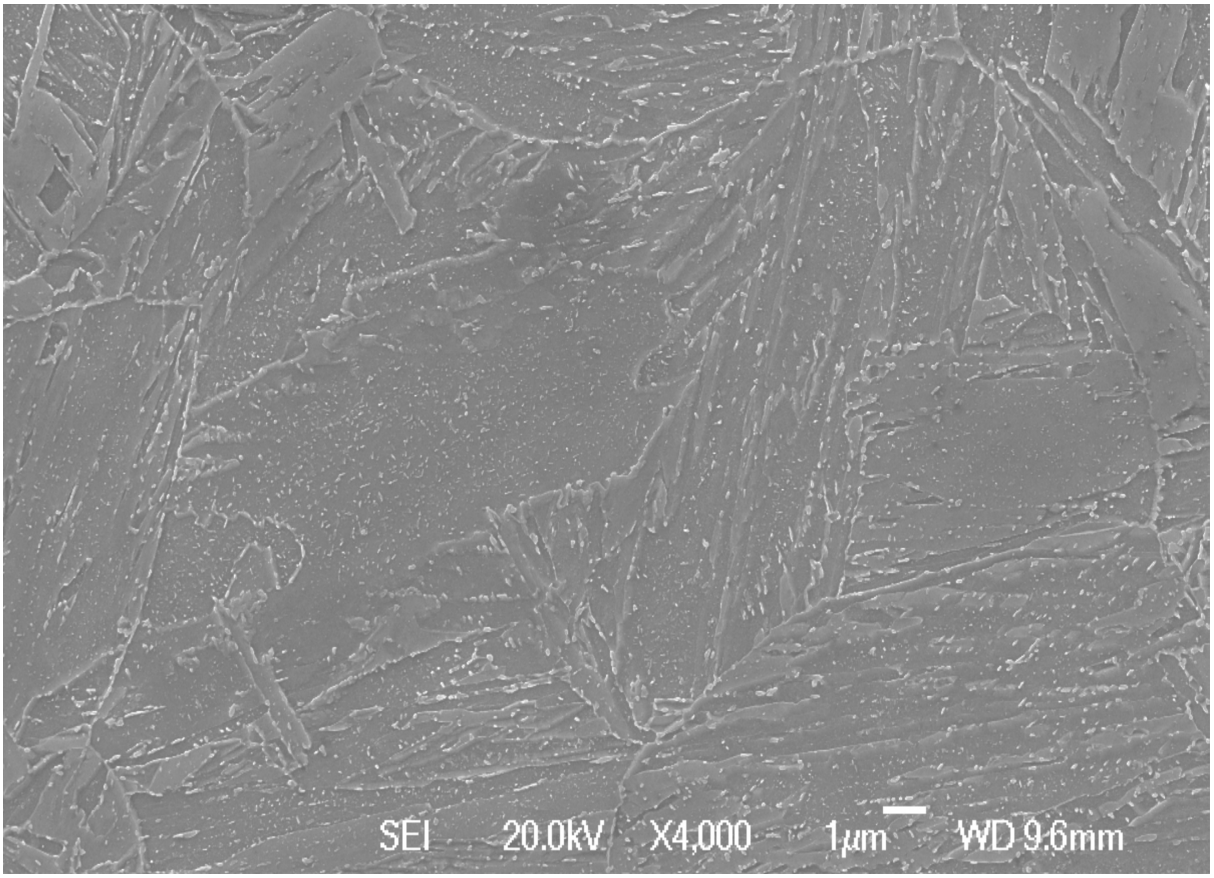

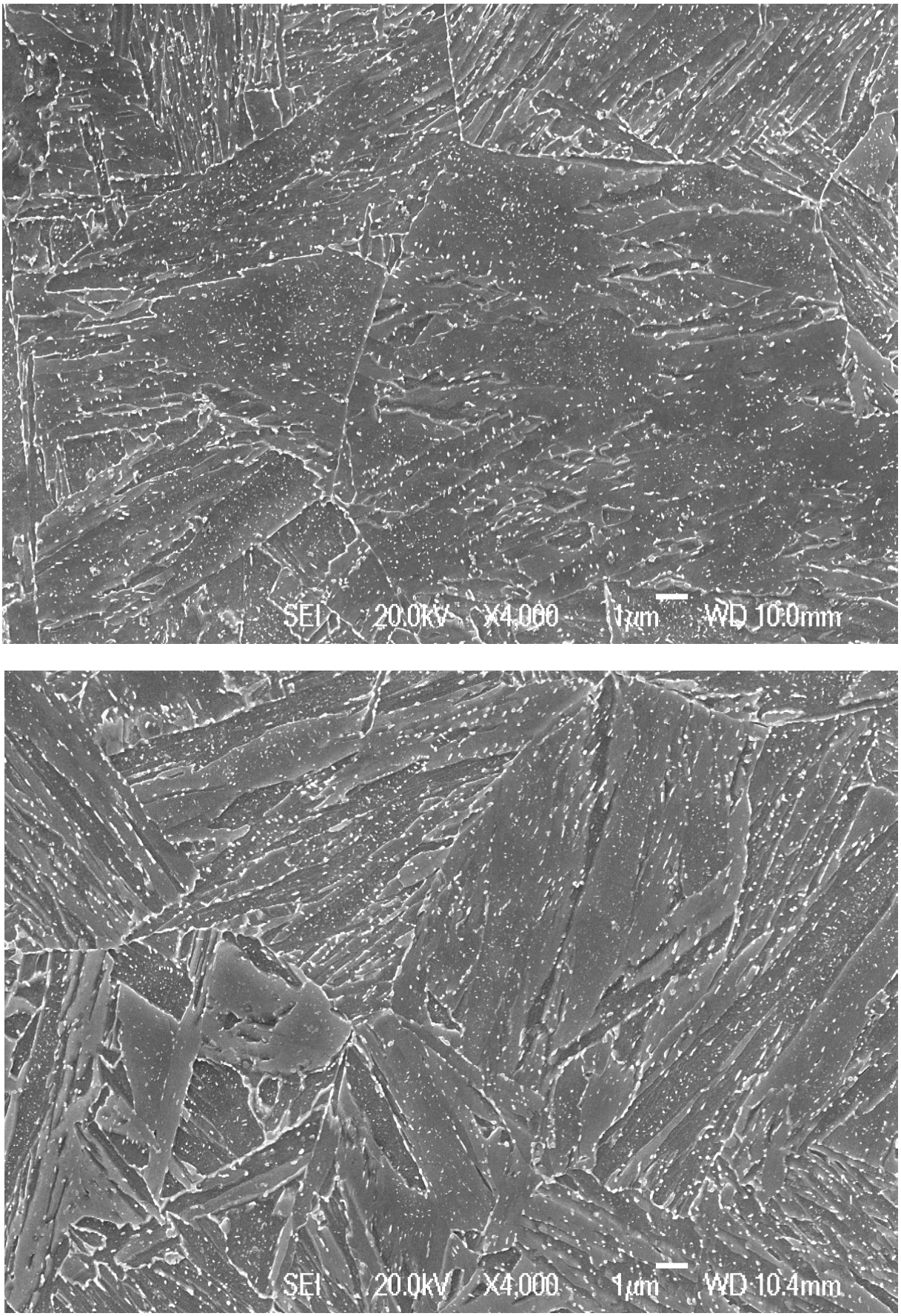

Figure 41: Micrograph of RQT701 tempered for (a) 1 (b) 2 and (c) 4 hours at 600 °C and water quenched.

The hardness increase that occurs between 2 and 3 hours of tempering RQT701 at 600 °C is consistent with the average hardness results for tempering at 580 °C and 620 °C (Figure 42) and as suggested by Figures 40 and 41 is due to an increased number of existing precipitates or the formation (or coarsening) of secondary precipitates that delay softening and even marginally strengthen the microstructure giving a peak hardness between 2 and 3 hours of tempering. Although it should be noted that at 620 °C, despite the average results showing a hardness peak between 2 and 3 hours of tempering, the standard deviation values are larger than the hardness increase. Whilst it might be expected that secondary hardening occurs faster at a higher tempering temperature, the results in Figure 42 either do not show this or reiterate that the peak is due to an increased number of existing precipitates. Perhaps this is due to the relatively small difference in temperature used for tempering and the small differences in hardness values being measured.

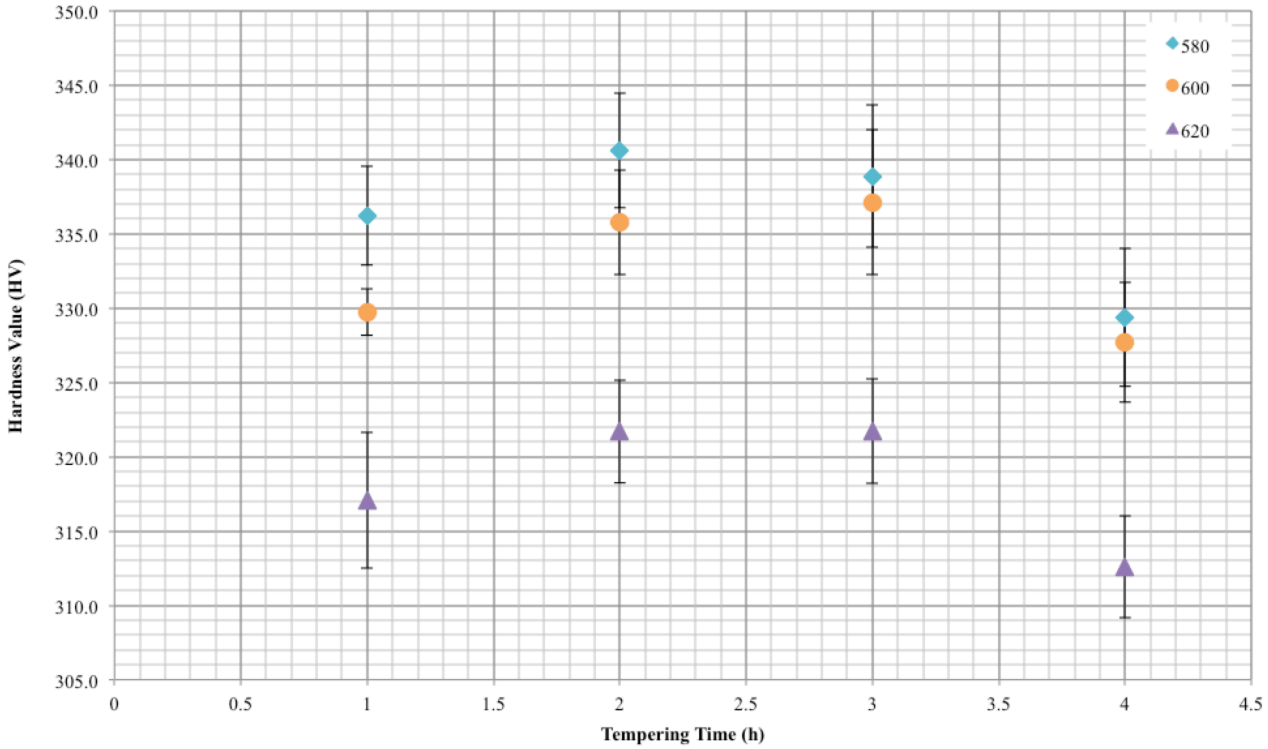

Figure 42: Vickers Hardness with standard deviation tempered at 580 °C, 600 °C and 620 °C between 1 and 4 hours using a 20 kg load.

Experimental hardness data by E. C. Rollason (1949) showing the effect of molybdenum content on hardness when tempering at 600 °C (Figure 17) suggests that a secondary peak by Mo_2C precipitation occurs in compositions containing between 0.47 – 0.9 wt. % molybdenum after tempering for an hour at approximately 600 °C. Therefore the 0.53 wt. % molybdenum found in RQT701 may explain the elevation in hardness between 2 and 3 hours at 600 °C, it also suggests that hardness is controlled by the presence of molybdenum content.

G. R. Speich (1969) reported a similar hardness profile for (2.25Cr, Mo, 0.15C, all wt. %) HSLA steel tempered at 600 °C (Figure 16) whereby in the as quenched condition hardness is roughly 420 HV and drops to around 310 HV after 30 – 40 minutes of tempering, before rising to a secondary peak of 340 HV after one hour. The shape of the graph is similar to that of RQT701 in Figure 39, although the secondary peak from G. R. Speich (1969) occurs earlier and is sharper and may be a result of the higher alloy content increasing the driving force for precipitation.

Research by N. Fujita (2000) and J. D. Robson and H. K. D. H. Bhadeshia (1996) for HSLA steel (2Mo, 0.1C and 2Cr, Mo, 0.1C respectively, all wt. %) state that the initial effects of these alloying elements (Mo and Cr) are to reduce the coarsening of lath boundaries and to pin dislocation movement, both of which delay softening. They also predict that M_2C precipitates between 1 and 2 hours at 600 °C. However despite various literatures predicting that Mo_2C will precipitate after 1 – 2 hours, TEM analysis by R. G. Baker and J. Nutting (1959) for a similar 2.25Cr, Mo, 0.15C (all wt. %) steel confirmed M_2X precipitates after 4 – 5 hours at 600 °C with a slower approach to equilibrium (Figure 27). This slower development may also explain the little evidence of secondary precipitation by SEM microscopy.

Furthermore although RQT701 has a higher carbon content (0.17 wt. %) than the steel tested by R.

G. Baker and J. Nutting (1959), which should theoretically increase the precipitation kinetics; research by G. R. Speich (1969) demonstrated that carbon content has less influence on tempering kinetics than alloy content. Therefore since RQT701 has a lower alloy content (and in particular of molybdenum, which is known for its potent contribution secondary hardening) compared with the steels examined by N. Fujita (2000), J. D. Robson and H. K. D. H. Bhadeshia (1996) and R. G. Speich (1969) the driving force for precipitation is lower. This leads to a delayed effect by second phase precipitates and also a reduction in magnitude of the contribution to secondary hardening.

5.3 Microscopy & Hardness of Long Term Tempering of RQT701 (8-100 Hours)

Plotting hardness against the Holloman-Jaffe parameter for times and temperatures between 1 and 100 hours and 580 °C and 620 °C combines the time and temperature variables into a single tempering parameter; therefore providing that the parameter is near equal, differing tempering conditions should give an equivalent hardness. However looking at Figure 43, comparable hardness values (such as 580 °C for one hour with 600 °C at two hours, and with 580 °C at four hours and 600°C for one hour) do not share a consistent Holloman-Jaffe parameter; equally similar Holloman-Jaffe parameters give a wide spread in hardness beyond the standard deviation values.

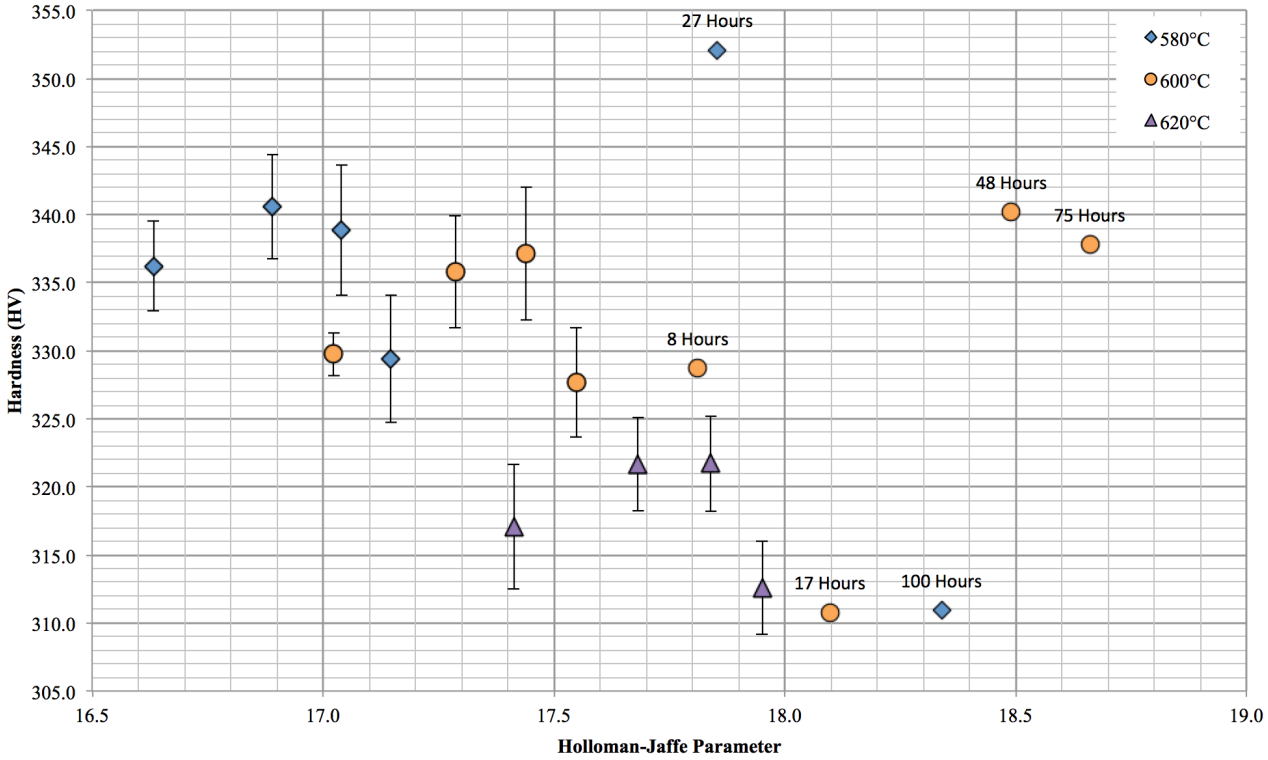

Figure 43: Vickers Hardness with standard deviation plotted against the Holloman-Jaffe parameter for RQT701 (using a C value of 19.5) tempered at 580 °C, 600 °C and 620 °C between 1 and 100 hours. The unlabelled samples were tempered for 1, 2, 3 and 4 hours and follow an inverted U pattern for each temperature range.

Hardness results for the longer tempering durations up to 100 hours (Figure 44) show a second peak at 27 hours for 580 °C and at 50 hours for 600 °C; although more hardness measurements are needed to refine the trend. The significant drop in hardness at 16 hours (for 600 °C) followed by the peak suggests that a new precipitate phase has formed to provide additional strengthening. N. Fujita (2000) and A. Vyrostkova et al. (1998) and A. Kroupa et al. (1998) predict that M_2C, $M_{23}C_6$ and M_7C_3 form under these tempering conditions and the microstructure for 27 hours of tempering at 580 °C shows a high density of smaller precipitates (Figure 45a and 45b) compared with that RQT701 tempered at 600 °C for four hours (Figure 45b). Despite the increase in lath width at 27 hours, the increased number of smaller precipitates indicates that the higher hardness is caused by the formation of a new phase. However this could be a sectioning effect and TEM is needed to confirm the precipitate phase and characteristics.

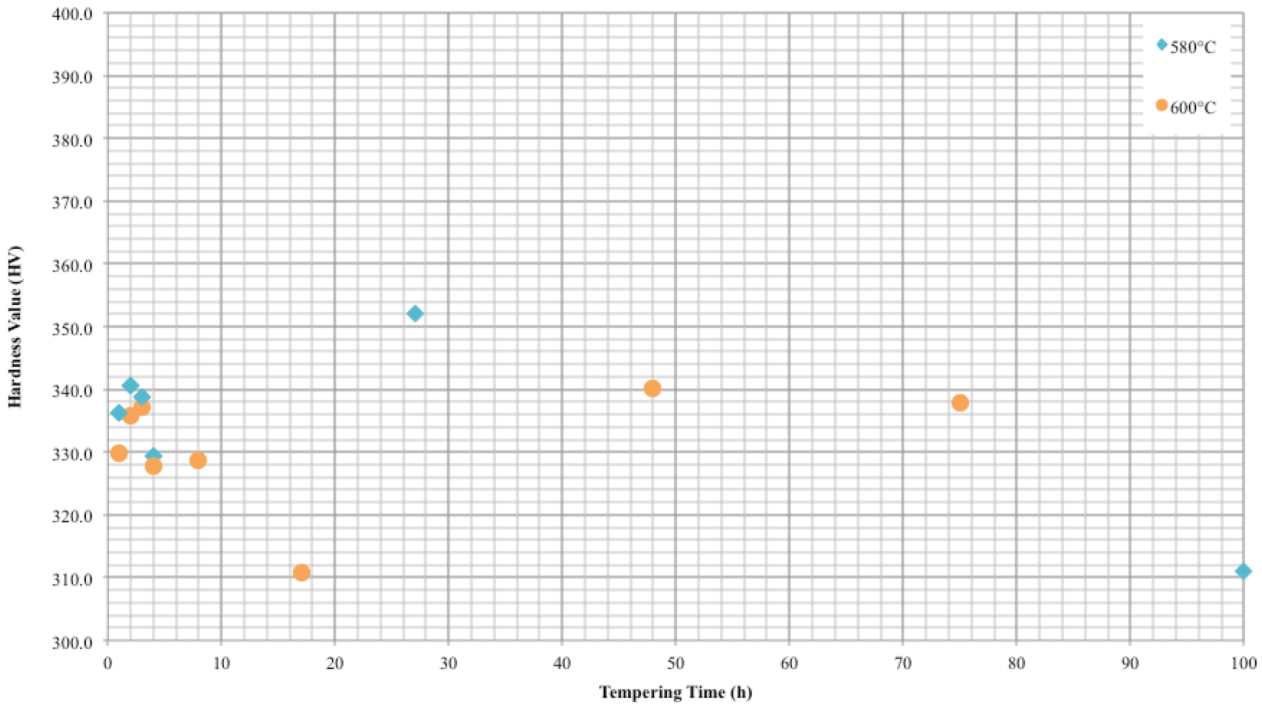

Figure 44: Vickers Hardness tempered at 580 °C and 600 °C between 1 and 100 hours using a 20 kg load.

(a)

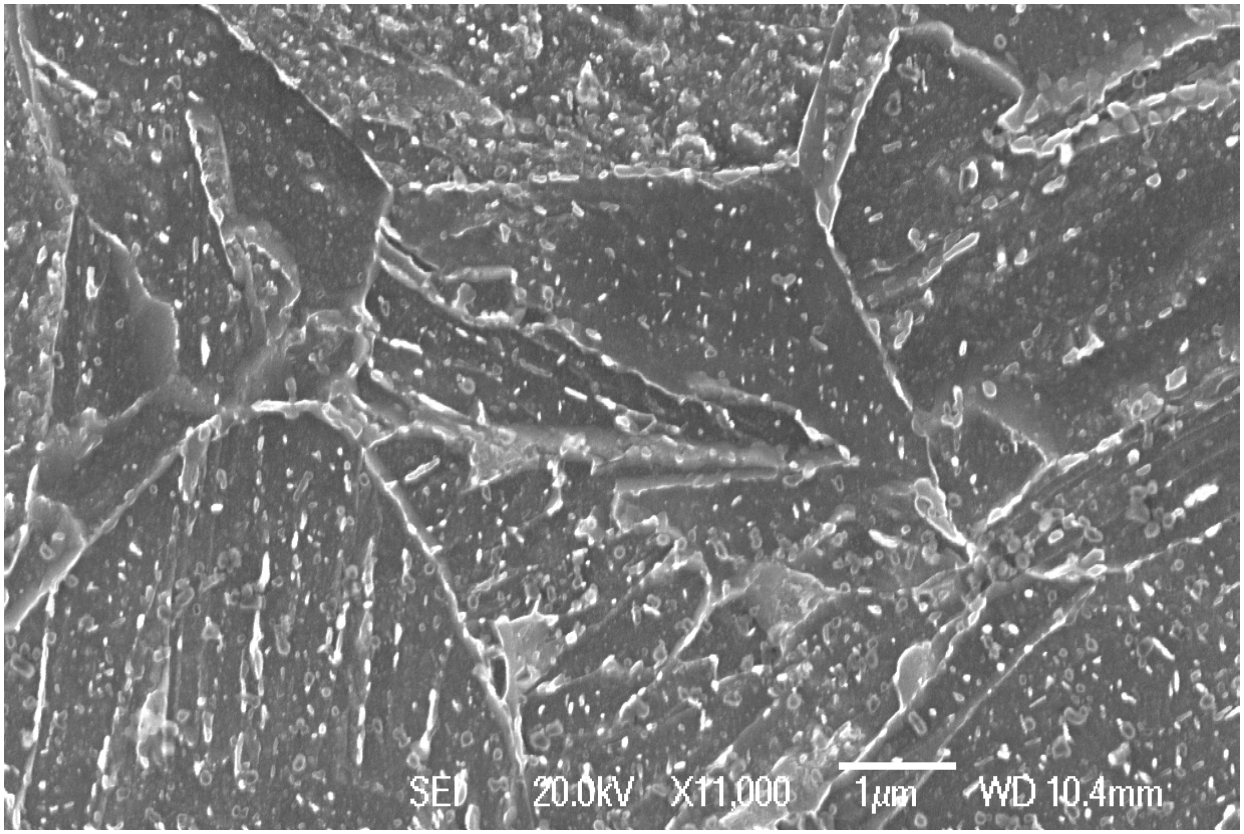

(b)

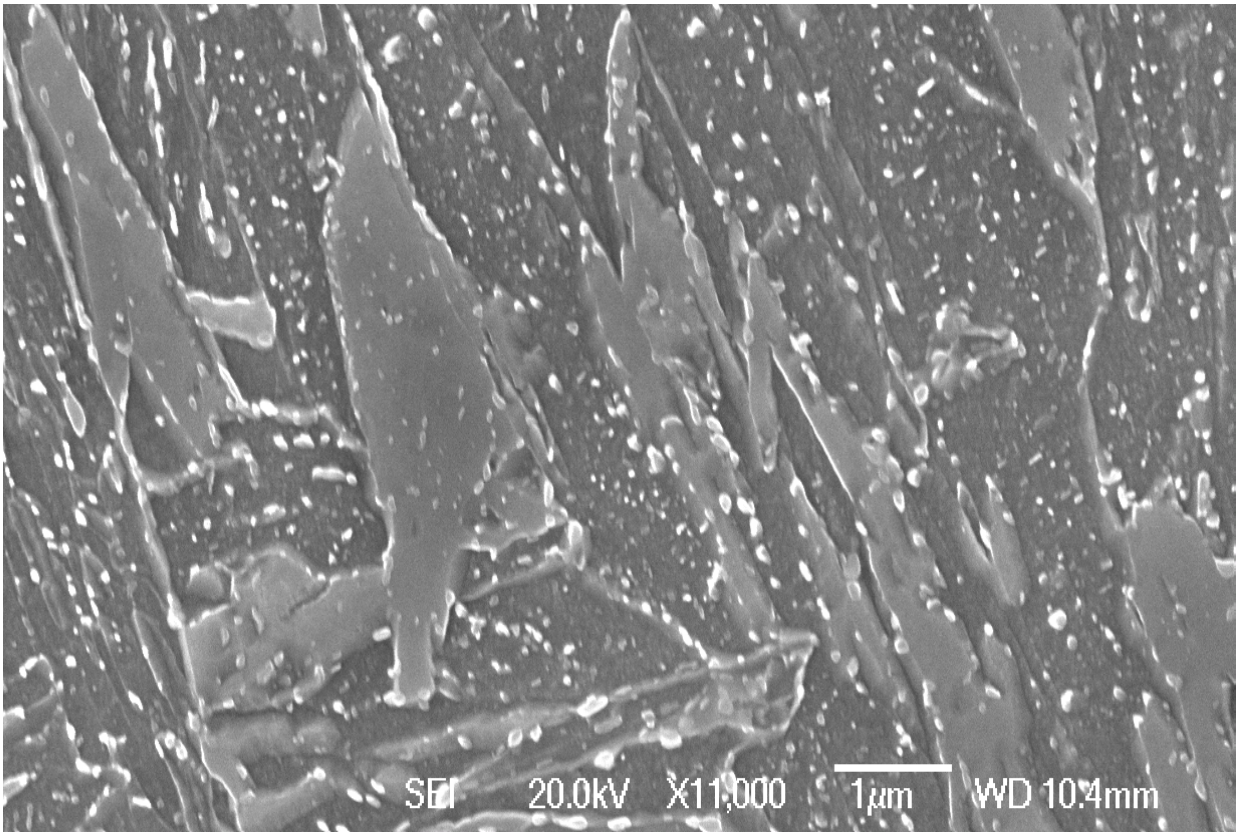

Figure 45: Micrograph of RQT701 tempered for (a) 27 hours at 580 °C and (b) 4 hours at 600 °C, both water quenched.

5.4 Thermodynamic Predictions

Thermo-Calc predicts the volume fractions of each phase at equilibrium for different temperatures based on the input composition and choice of phases allowed to form. Typical Cr – Mo HSLA steel have been reported to show two different precipitation sequences, 1 and 2 (A. M. El-Rakayby, 1986 and N. Fujita, 2000) depending on the composition, as discussed in section 2.3.1 and consists of:

Sq1) $Fe_{2.4}C - Fe_3C - M_7C_3 - M_{23}C_6 - M_6C$

Sq2) $M_2C - M_{23}C_6 - M_6C$

Considering that M_6C is slow to precipitate, taking >2000 hours to begin at 600 °C for 0.9C, 2.4Cr, 0.7Mo (all wt. %) steel (J. Janovec et al. 2005) it has been removed from Thermo-Calc calculations to provide information on the non-equilibrium tempering condition. Furthermore M_7C_3 is predicted by Thermo-Calc to be more stable than $M_{23}C_6$ (scenario four of Table 7) which contradicts Sq1; therefore although J. Janovec et al. (2005) predicts M_7C_3 to precipitate after two hours at 600 °C (Figure 24) the extent of reaction can be expected to be minimal since it forms slower than Fe_3C, $M_{23}C_6$ and M_2C (Figure 46). Therefore M_7C_3 was also removed from the Thermo-Calc calculations as this allows a more realistic prediction of volume fraction for M_2C as expected for the shorter tempering durations used in industrial practice for RQT701.

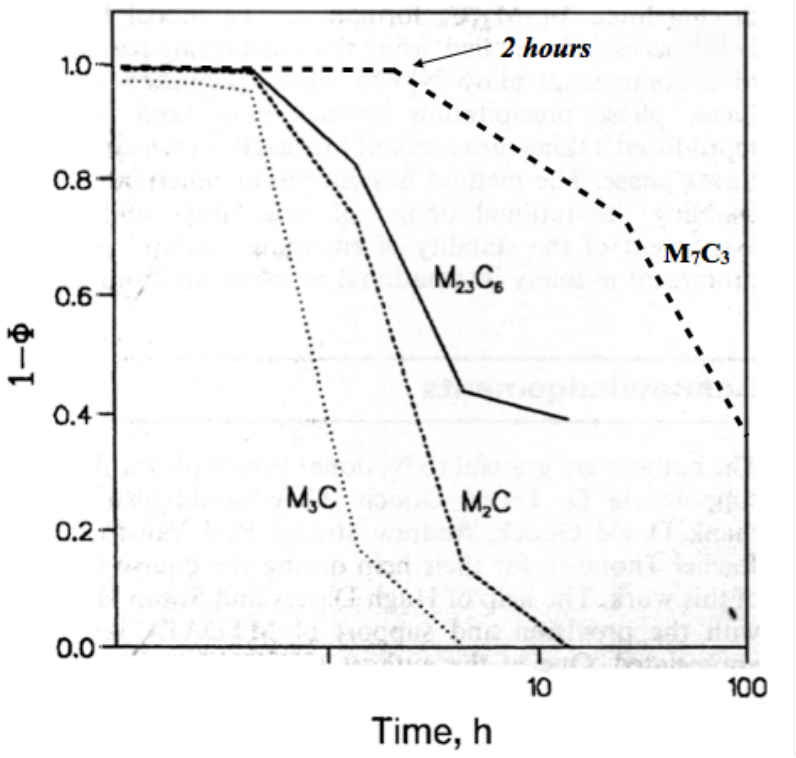

Figure 46: Plot of the extent of reaction Φ as a function of tempering time at 600 °C for 2.25Cr – Mo wt. % steel. (Adapted from Figure 26 by C. S. Robson, 1996)

Figure 47 shows the Thermo-Calc thermodynamic calculation with M_6C and M_7C_3 suppressed. In the temperature region of most interest, between 580 °C and 620 °C, it shows that Fe_3C (labeled cementite) and two different formations of M_2C (labeled HCP_A3#1 and HCP_A3#2) are predicted to form, as highlighted in scenario 2a in Table 7. Cementite is predicted to have a final volume fraction of 0.020 % equal to that determined by SEM for two hours tempering in Table 6; therefore a volume fraction >0.020 % (e.g. 0.022 % after four hours as in Table 6) may be due to an additional precipitate phase forming and Figure 46 and 47 support the formation of M_2C, although experimental error is also possible (overestimation of volume fraction due to etching effect where carbides are proud of the surface).

Nevertheless the extent of reaction for M_2C precipitates after four hours at 600 °C (Figure 46) is predicted to have nearly completed and yet the difference in volume fraction of second phase measured to that predicted for cementite (0.002 %) is less than half that predicted by Thermo-Calc for Mo_2C in scenario 2a Table 7 (0.0047 %); this suggests that either a complex synergy of the alloy system has delayed formation of M_2C precipitates that is overlooked by Thermo-Calc, or that a proportion of perhaps the latter forming M_2C are too small to be resolved by SEM. An alternative explanation for a volume fraction >0.020 % can be identified in scenario 1 of Table 7; the unique presence of cementite at equilibrium gives a volume fraction of 0.025 % and is higher than SEM results after four hours at 600 °C (Table 6) and can be explained as near maximum cementite precipitation in (at that time and temperature) an effectively plain carbon system.

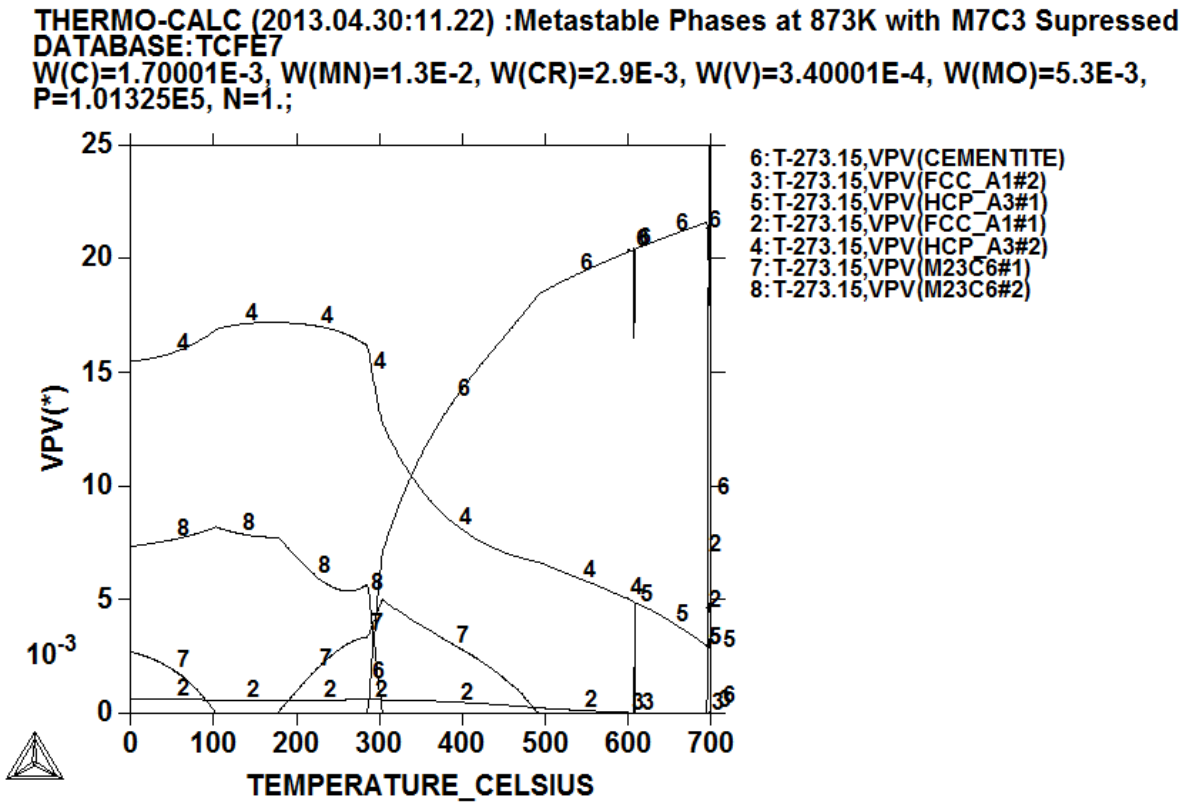

Figure 47: Thermodynamic calculation using Thermo-Calc software with TCFE7 database for RQT701 allowing cementite, $M_{23}C_6$ and M_2C to exist while suppressing M_7C_3 and M_6C formation.

Literature by D. Delagnes et al. (2012) for 0.2C, 2.3Cr, 1.5Mo, 0.9Al, 10Co (all wt. %) shows that M_2C precipitates are 20 nm in length after 10 hours of tempering at 500 °C. Therefore despite an increase in temperature to 580 °C, 600 °C and 620 °C it is likely that if M_2C does form in RQT701 after just 2 – 3 hours, its presence will be too small to detect yet contribute nevertheless to the mechanical properties. However TEM is required to confirm its presence.

Considering that literature for HSLA steel generally suggests that cementite precipitation causes a delay in softening after roughly one hour of tempering at 600 °C (N. Fujita, 2000) the delayed hardness peak between 2 and 3 hours seen for RQT701 is possibly the cause of a complex alloy system that retards the precipitation of cementite and/or is influenced by the presence of fine M_2C precipitates that remain undetected by SEM.

In Figure 47 there is also a brief spike in the Thermo-Calc predictions between 600 °C and 620 °C that represents formation of MC (vanadium and molybdenum rich) carbides (labeled FCC_A3＃2) although research by A. Kroupa et al. (1998) and A. Vyrostková et al. (1998) and J. Janovec et al. (2005) suggest that MC takes 100 hours at 600 °C to form for 0.12C, 0.7Mo, 2.57Cr, 0.34V (all wt. %) steel.

Table 7: Calculated volume fractions of the expected phases during tempering RQT701 at 580 °C, 600 °C and 620 °C using Thermo-Calc software with TCFE7 database. Suppressing the stable phases revealed metastable phases, scenario 2a is most likely to occur during short term tempering.

	Accepted phases in addition to ferrite and austenite	Supressed phases	Existing Phases	Stability	580°C	600°C	620°C
1	**Cementite**	**$M_{23}C_6$, M_2C, M_7C_3, M_6C**	Cementite	*Stable*	2.20E-02	2.25E-02	2.30E-02
2	**Cementite, $M_{23}C_6$**	**M_2C, M_7C_3, M_6C**	Cementite	*Stable*	1.76E-02	1.36E-02	6.22E-03
			$M_{23}C_6$	*Unstable*			1.14E-03
2a	**Cementite, M_2C**	**M_7C_3, $M_{23}C_6$, M_6C**	Cementite	*Stable*	2.00E-02	2.03E-02	2.06E-02
			M_2C	*Unstable*	5.34E-03	5.02E-03	4.67E-03
3	**Cementite, $M_{23}C_6$, M_2C**	**M_7C_3, M_6C**	Cementite	*Stable*	2.00E-02	2.03E-02	2.23E-02
			M_2C	*Unstable*	5.34E-03	5.02E-03	
4	**Cementite, $M_{23}C_6$, M_2C, M_7C_3**	**M_6C**	Cementite	*Stable*		2.35E-03	1.17E-02
			M_2C	*Unstable*	1.51E-03	1.55E-03	2.98E-03
			M_7C_3	*Stable*	1.93E-02	1.73E-02	8.49E-03

Research by A. Kroupa et al. (1998) and A. Vyrostkova et al. (1998) on 2.5Cr – 0.7Mo wt. % HSLA steel, suggests $M_{23}C_6$ precipitation is most probably the phase to form simultaneously with cementite for tempering <2 hours between 580 °C and 620 °C. However Thermo-Calc results for RQT701 reveal that $M_{23}C_6$ does not form in a system that contains M_2C above 500 °C (seen in Figure 47 and scenario 3 in Table 7) although it must be remembered that Thermo-Calc gives equilibrium results where M_2C has completed precipitation. Therefore a more realistic outcome for tempering between 1 and 4 hours at 600°C may be a combination of M_2C, $M_{23}C_6$ and cementite.

Figure 48 shows a Thermo-Calc thermodynamic calculation with M_6C suppressed. In the temperature region of most interest, between 580 °C and 620 °C, Fe_3C (labelled cementite) M_2C (labelled HCP_A3＃1) and M_7C_3 (labelled M7C3＃1) are predicted to form. The graph shows that there is a change in predominant precipitate phase from M_7C_3 to cementite at roughly 610 – 620 °C and the final volume fraction of M_2C in comparison to Figure 47 is significantly less with the inclusion of M_7C_3.

J. Janovec (2005) suggest that M_7C_3 starts to precipitate after two hours although it is slow to form and therefore the development of M_2C should not be affected until M_7C_3 reaches a significant volume fraction, which Figure 46 suggests is minimal before 10 hours. Therefore the fact that Figure 42 does not show a hardness increase between 3 and 27 hours and suggests that either M_2C reaches an optimum contribution to mechanical properties between 2 and 3 hours where its precipitates are just too small to detect by SEM, or it has a minimal contribution entirely. The steady hardness between 27 and 100 hours is likely to be a result of the more stable M_7C_3 carbide.

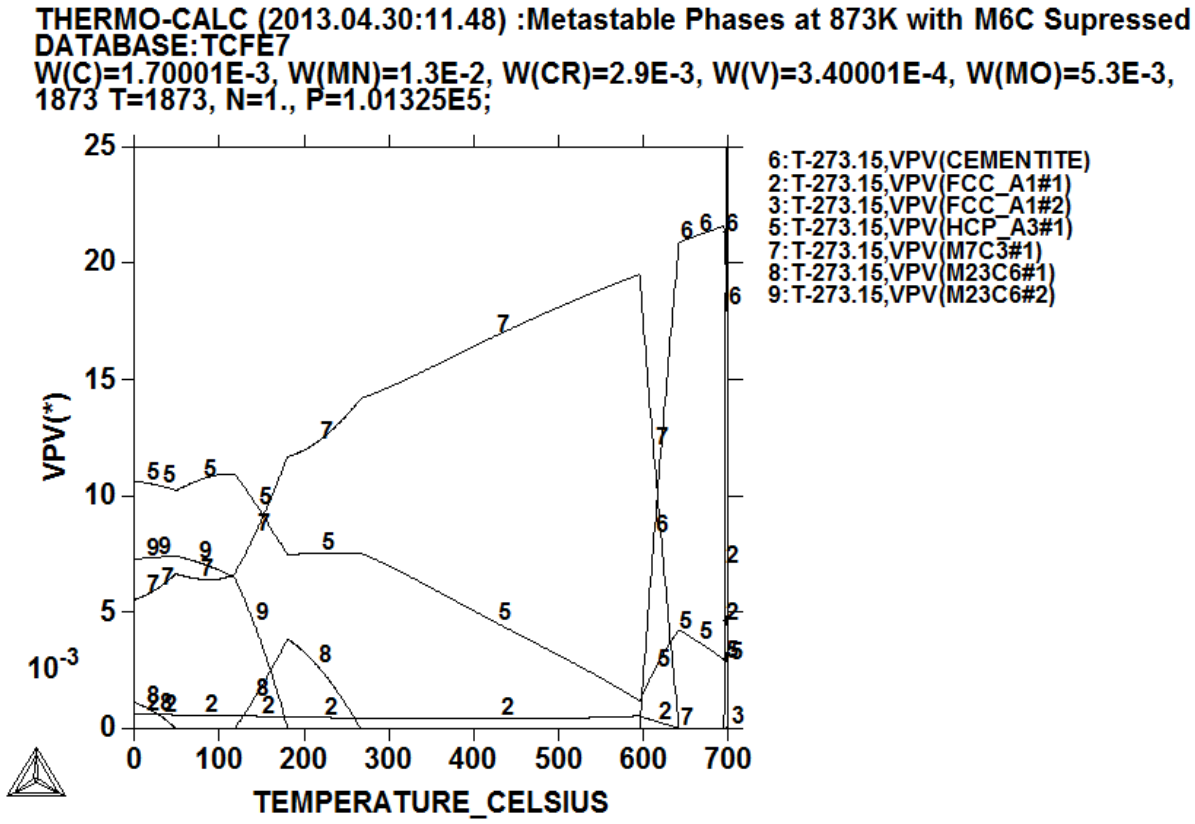

Figure 48: Thermodynamic calculation using Thermo-Calc software with TCFE7 database for RQT701 allowing cementite, $M_{23}C_6$, M_2C and M_7C_3 to exist while suppressing M_6C formation.

In summary, RQT701 has an autotempered martensitic microstructure with a hardness of 430 HV in the as-quenched (water quench) condition. This high hardness reduces on initial tempering at 580 – 620 °C with a small secondary hardness peak being observed between 2 and 3 hours. This is believed to be due to M_2C formation, although it is possible that it reflects an optimum volume fraction and size range of cementite forming with traces of $M_{23}C_6$. The hardness then continues to drop upon further tempering, presumably as the secondary precipitate phase (or phases) coarsen until a further increase in hardness is observed, corresponding to 27 hours for 580 °C and 50 hours at 600 °C, although these times are very approximate as further tempering trials would be required to provide more data points for different tempering times. It is suggested that a new phase dominates the contribution to increased hardness at these longer tempering times, possibly M_7C_3.

6. Conclusions

The aim of the project was to determine the response of RQT701 steel (a martensitic grade containing 1 wt. % chromium and 0.7 wt. % molybdenum) to quenching and tempering in the range 580 – 620 °C for up to 100 hours. Hardness testing and SEM analysis of heat-treated samples was carried out along with Thermo-Calc software predictions of carbide precipitation. The following conclusions were made:

1. Quenching RQT701 from 925 °C (fully austenitic structure) at 60 $°Cs^{-1}$ (measured at the steel surface), using multidirectional jet water sprays representative of industrial practice, results in an autotempered martensite microstructure with a hardness of 430 HV and a uniform distribution of precipitates (presumed to be cementite based on shape and literature results) of 50 – 120 nm in length. A second precipitate type was identified (and presumed as ε-carbide at 5 – 10 nm in length) although due to the resolution of the SEM this was not confirmed and may be a sectioning effect from the needle shaped cementite. The autotempered microstructure was observed through thickness in the 15 mm thick plate. Furthermore a faster quench rate (>60 $°C^{-s}$) into agitated ice water resulted in fewer smaller precipitates in the autotempered microstructure and an increased hardness from 430 HV to 460 HV.

2. After short term tempering between 30 and 120 minutes at 600 °C, the microstructures of room temperature water quenched and ice water quenched RQT701 samples appear the same in terms of precipitates (size and number) and show an equivalent hardness value (346 HV +/- 1 HV for 30 minutes and 336 HV +/- 1 HV for 120 minutes). This suggests that RQT701 may be quenched in room temperature water using multidirectional jet water sprays, which is cheaper and more efficient than immersion into agitated ice water, without influencing its subsequent tempering characteristics.

3. Upon tempering RQT701 between 1 and 4 hours at 600 °C there was a small secondary hardness peak observed between 2 and 3 hours based on a rise in hardness of 6 HV between 1 and 2 hours (greater than the average standard deviation of +/- 2.5 HV), and fall in hardness of 9 HV between 3 and 4 hours (greater than the average standard deviation of +/- 4.4 HV) indicating that the trend is

statistically significant. This slight peak in hardness is suggested to be due to the formation of M_2C, based on the literature, with the small hardness increase being due to the lower molybdenum content of RQT701 (0.7 wt. %) in comparison to the literature results for 2Cr – Mo wt. % HSLA steels, where a hardness increase of 20 – 30 HV is commonly reported.

4. SEM particle analysis on samples tempered at 600 °C for 1, 2 and 4 hours confirmed precipitate coarsening due to a simultaneous reduction in number density with increase in precipitate size. Cementite coarsens significantly faster than M_2C and will dominate the particle analysis results. The reduction in number density may also be influenced by the precipitation of $M_{23}C_6$ that occurs at the expense of cementite and M_2C, and hence why hardness may drop off at four hours despite M_2C being resistant to coarsening. The volume fraction of precipitates increases between 1 and 4 hours presumably due to previously unresolved carbides that coarsen to become detectable (such as remaining ε-carbide transformation to cementite and M_2C diffuse zones precipitating to form M_2C). A similar secondary hardness increase between 2 and 3 hours of tempering was also observed for samples tempered at 580 °C and 620 °C.

5. A further hardness increase after tempering at 580 – 620 °C occurred between 8 and 100 hours indicating the precipitation of a new phase, for example the hardness increased from 311 HV after 16 hours of tempering at 600 °C to 340 HV after 48 hours, and from 330 HV after 4 hours to 352 HV after 27 hours at 580°C. SEM analysis shows a dense presence of fine precipitates in the higher hardness samples that were not previously visible at shorter tempering times. TEM would be required to confirm the size and type of precipitate (although it is presumably M_7C_3 based on literature reports for similar steel compositions). This second peak is the hardest microstructure of RQT701 after the onset of tempering.

6. At 600 °C Thermo-Calc, using non-equilibrium predictions through suppressing phases that are not expected to occur during short term tempering (based on the literature for similar composition steels) predicts the combined presence of cementite and M_2C. $M_{23}C_6$ is also predicted to be present using Thermo-Calc, with literature evidence suggesting possible formation after one hour tempering. For

longer durations of >10 hours M_2C is expected to complete precipitation, and a combination of cementite, M_2C and M_7C_3 is predicted to be present in the steel.

7. Future Work

The project has characterised the hardness and microstructure (focusing on the precipitates using SEM) for RQT701 steel following quenching and tempering at 580 – 620 °C for up to 100 hours. From the results obtained the following areas of further work are suggested:

1. A more continuous series of Vickers Hardness experiments could be carried out between 4 and 100 hours at 600 °C to determine an accurate hardness profile of RQT701 with time, in particular the position and hardness increase associated with the secondary hardening events. Furthermore around the critical tempering time of 1 – 4 hours it would be useful to perform hardness tests after every 30 minutes of tempering time to more clearly define the shape of the secondary hardness peak.

2. The possibility of using electromagnetic (EM) sensor testing to monitor the tempering process was considered during the project. Some initial trials were carried out but inconclusive results were obtained (see Appendix). The EM sensor has been shown to be sensitive to tempering in power generation steel grades: 9, 91 and 22 (J. Liu et al, 2013) where grade 22 has a similar composition to RQT701. This method is potentially a very efficient way to summarise the behaviour of steels during tempering and is worth further experimentation.

3. DICTRA software can be used to predict the development of carbide populations (size and type) during tempering, although some assumptions on the initial carbide distribution are required. These predictions can be compared with the hardness profile to see the combination of phases and relative volume fractions that correspond to peaks in hardness. Once the modelling capability of DICTRA is established then variations in composition,

tempering temperature and time can be considered to optimise the heat treatment for RQT701 type steels.

4. TEM analysis is necessary to confirm the suggested precipitate identification in the heat-treated samples, and would also be used to confirm any predictions from DICTRA and Thermo-Calc. TEM could also be used to determine the size (and morphology) of the different precipitate distributions, which could be used to determine their contributions to the hardness.

5. In addition to looking at a quenched microstructure of autotempered martensite, future work could look into the effects of tempering a mixed martensite and bainite microstructure. This is relevant to an industrial scenario where thick plate is quenched and a mixed microstructure might be expected towards the centre of the plate where the cooling rates are lower.

8. Bibliography

Abson D. J., Whiteman J. A. (1970) Precipitation from Iron-base Alloys Containing Cobalt. The Iron and Steel Institute, (208): 594-600

Askeland D. R., Phulé P. P. (2002) The Science and Engineering of Materials, 4th Edition, Thomson-Engineering, Australia.

Baker R. G., Nutting J. (1959) The Tempering of 2.25Cr – Mo Steel after Quenching and Normalising, Iron and Steel Institute, 192, pp. 257-268.

Bakhsheshi-Rad H. R., Monshi A., Monajatizadeh H., Idris M. H., Kadir M. R. A., Jafari H. (2011) Effect of Multi-step Tempering on Retained Austenite and Mechanical Properties of Low Alloy Steel. Iron and Steel Research International, 18 (12). pp. 49-56

Bhadeshia H.K.D.H. (2001) Design of Ferritic Creep-resistant Steel, ISIJ International, Vol. 41, No. 6, pp. 626-640

Bozorth R. M. (1993) Ferromagnetism, Wiley-IEEE Press. ISBN: 978-0780310322

Buschow J. K. H., Cahn R. W., Flemings M. C., Ilschner B., Kramer E. J., Mahajan S., Veyssière P. (2011) Encyclodepia of Materials: Science and Technology ISBN: 978-0-08-043152-9

Cohen M. (1962) The Strengthening of Steel. Trans. The Metallurgical Society TMS of AIME Vol. 224, pp. 638–657

Davis C. L., King J. E. (1993) Effect of Cooling Rate on Intercritically Reheated Microstructure and Toughness in High Strength Low Alloy Steel: Materials Science and Technology. 9,1, p. 8-15

Delagnes D., Pettinri-Sturmel F., Mathon M. H., Danoix F., Bellot C., Lamesle P., Grellier A. (2012) Cementite-free Martensiteic Steels: A New Route to Develop High Strength/high Toughness Grades by Modifying the Conventional Precipitation Sequence During Tempering. Acta Materialia 60. pp. 5877-5888

El-Rakayby A. M. (1986) A Study of the Microstructure and Wear of High Speed Steels. PhD Thesis, Department of Aeronautical and Mechanical Engineering, University of Salford, UK.

Fujita N. (2000) Modelling of Precipitation in Alloy Steels, PhD Thesis, University of Cambridge, UK.

Gladman T. (1997) The Physical Metallurgy of Microalloyed Steels. The Institute of Materials, London, UK.

Gomez M., Medina S. F. and Valles P. (2005) Determination of Driving and Pinning Forces for Static Recrystallization During Hot Rolling of a Niobium Microalloyed Steel, ISIJ International, Vol. 45, No. 11, pp. 1711-1720

Gorni A. A., (2011) Steel Forming and Heat Treating Handbook, São Vicente, Brazil.

Grange R. A., Hribal C. R., Porter L. F. (1977) Hardness of Tempered Martensite in Carbon and Low Alloy Steels, Metallurgical Transactions A, Volume 8A pp. 1776

Hall M. G., Kinsman K. R., Aaronson H. I. (1976) Surface Science, Metallurgical Transactions A 3A pp. 1320-1322

Hao X. University of Birmingham, Unpublished.

Hetzner D. W., Geertruyden W. V. (2008) Crystallography and Metallography of Carbides in High Alloy Steels, Materials Characterization, 59, pp. 825-841

Hodson S. M. (1989) MTDATA-Metallurgical and Thermochemical Databank, National Physical Laboratory. Teddington, UK.

Hollomon J. H., Jaffe L. D. (1945) Time-temperature Relations in Tempering Steel. Trans. Met. Soc. AIME, 162, pp. 223–249.

Honeycombe R. W. K., Bhadeshia H. K. D. H. (1995) Steels: Microstructure and Properties, 2nd edition, Edward Arnold, ISBN 0-340-58946-9

Honeycombe R. W. K., Bhadeshia H. K. D. H. (2006) Steels: Microstructure and Properties. 3rd edition. Oxford: Elsevier. ISBN: 978-0750680844

Hufenbach J., Giebeler L., Hoffmann M., Kohlar S., Kühn U., Gemming T., Oswald S., Eigenmann B., Eckert J. (2012) Effect of Short-term Tempering on Microstructure and Mechanical Properties of High-strength FeCrMoVC. Acta Materialia, 60, pp. 4468-4476

Hultgren A. (1947) Thermodynamic Properties of Metals. Trans. Amn. Soc. Metals, 39, 415.

Nobuyuki I., Yasunori H., Yoshikuni M., Yamamoto. (2006) Preparations of Carbon Nanofiber Emitters for Diode Type Field Emission Display with Organic Luminescence thin Films. Materials Science and Engineering: C, Vol. 27, Issues 5–8, pp. 1174-1180

Janjušević Z., Gulisija Z., Mihailovic M., Pataric A. (2009) The Investigation of Applicability of the Hollomon-jaffe Equation on Tempering the HSLA Steel. Chemical Industry & Chemical Engeneering Quarterly 15 (3) pp. 131-136

Janovec J., Svoboda M., Vyrostková A., Kroupa A. (2005) Time-temperature-precipitation Diagrams of Carbide Evolution in Low Alloy Steels. Materials Science and Engineering A 402, pp. 288-293

Jiang D. E., Carter E. A. (2003) Carbon Dissolution and Diffusion in Ferrite and Austenite from First Principles. Physical Review B 67, 214103

Kiatisaksri P., Meir S., Poncelow J., Madeni J. C., Hellner L. R. (2001) Assessment of Microstructure in Grade T22 CrMo Steel by Non-desctructive Tools. American Institute of Physics Conf. Proc. 1335, 1112; doi 10. 1063/1.3592060

Krauss G. (1999) Martensite in Steel: Strength and Structure, Materials Science and Engineering, A273-275, pp. 40-57

Krauss G. (2005) Steels, Processing, Structure and Performance, ASM International, Materials Park, OH 44073-0002

Kroupa A.,Vyrostkova A., Svoboda M., Janovec J. (1998) Carbide Reactions and Phase Equilibria in Low-alloy Cr-Mo-V Steels Tempered at 773-993 K. Part 2: Theoretical Calculations, Elsevier, Vol. 46, No 1, pp. 39-49

Kundu A. (2011) Grain Structure Development During Casting, Reheating and Deformation of Nb-microalloyed Steel, Thesis, University of Birmingham, UK.

Lagneborg R., Siwecki T., Zajac., Hutchinson B. (1999) The Role of Vanadium in Microalloyed Steels. Swedish Institute for Metals Research Stockholm Sweden. The Scandanavian Journal of Metallurgy.

Lement B. S., Averbach B. L., Cohen M. (1955) Further Study of Microstructural Changes on Tempering Iron Carbon Alloys. Trans. ASM. 41, pp. 219-319

Liu J., Strangwood M., Davis C. L., Peyton A. J. (2013) Magnetic Evaluation of Microstructure Changes in 9Cr-1Mo and 2.25Cr-1Mo Steels using Electromagnetic Sensors. Mat Trans, Vol. 44, Issue 13, pp 5897-5909, DOI: 10.1007/s11661-013-1938-x

Maalekian M. (2007) The Effects of Alloying Elements on Steels (I) Institute for Materials Technology, Welding Engineering, and Non-cutting and Shaping Processes. Christian Doppler Laboratory for Early Stages of Precipitation.

Maropolous S., Karagiannis S., Ridley N. (2008) The Effect of Austenitising Temperature on Prior Austenite Grain Size in a Low-alloy Steel. Material Science and Engineering A, Vol. 483–484, pp. 735–739

McMahon J. C. Jr. (1980) Solute Segregation and Intergranular Fracture in Steels: A Status Report. Materials Science and Engineering, Vol. 42, pp. 215-226

Miyamoto G., Oh J. C., Hono K. (2007) Effect of Partitioning of Mn and Si on the Growth Kinetics of Cementite in Tempered Fe-0.6 Mass % C Martensite. Acta Mater, 55 (15): 5027

Mohrbacher H. (2010) Principle Effects of Mo in HSLA Steels and Cross Effects of Microalloying Elements. International Seminar on Applications of Mo in Steels. June 27th - June 28th

Nooning R. G. Jr. (2002) Effect of Stabilizing Elements on the Precipitation Behaviour and Phase Stability of Type 409 Ferritic Stainless Steels. University of Pittsburgh. USA

Olefjord I. (1978) Temper Embrittlement. International Material Reviews, No. 4, Review 231.

Ooi S. W., Cho Y. R., Oh J. K., Bhadeshia H. K. D. H. (2009) Carbon Enrichment in Residual Austenite During Martensitic Transformation. Graduate Institute of Ferrous Technology pp. 790-784.

Payares-Asprino M C., Katsumoto H., Liu S. (2008) Effect of Martensite Start and Finish Temperature on Residual Stress Development in Structural Steel Welds. Welding Journal 279-s, ISSN: 0043-2296

Peng T., Chi Z., Zhi gang Y., Hiroyuki T. (2010) Evolution and Coarsening of Carbides in 2.25Cr-Mo Steel Weld Metal During High Temperature Tempering. Iron and Steel Research International. 17(5): pp. 74-78

Porter D. (2007) Multi-scale Modelling of Structural Materials. Multi-scale Materials Modelling, pp. 261-287

Porter D. A., and Easterling K. E. (2004) Phase Transformations in Metals and Alloys, Chapman & Hall, London, UK.

Roberts C. S., Averbach B. L., Cohen M. (1953) The Mechanism and Kinetics of the First Stage of Tempering. Trans. ASM. 45, pp. 576-604

Robson J. D. (1996) Modelling of Precipitation in Power Plant Steels: PhD. Thesis, University of Cambridge, UK.

Robson J. D., Bhadeshia H. K. D. H. (1996) Kinetics of Precipitation in Power Plant Steels. Calphad 20(4) pp.447-460

Robson J. D., Bhadeshia H. K. D. H. (1997a) Modelling Precipitation Sequences in Power Plant Steels Part 1 - Application of Kinetic Theory. Materials Science and Technology, 13, pp. 631–639

Robson J. D., Bhadeshia H. K. D. H. (1997b) Modelling Precipitation Sequences in Power Plant Steels Part 2 - Application of Kinetic Theory. Materials Science and Technology, 13, pp. 640–644

Rollason E. C. (1949) Metallurgy for Engineers, 2nd edition. Edward Arnold & Co.

Samuel F. H. (1985) Effect of Dual-phase Treatment and Tempering on the Microstructure and Mechanical Properties of a High Strength Low Alloy Steel, Materials Science and Engineering, Vol. 75 pp. 51-66

Servant C., Cizeron G. (1989) Investigation into the Structural Evolutions of a Low Alloy Steel during Tempering. Materials Science and Engineering, A117 pp. 175-189

Sherby O. D., Wadsworth J., Lesuer D. R., Syn C. K. (2008) Revisiting the Structure of Martensite in Iron-carbon Steels. Materials Transaction, Vol. 4, No. 9 pp. 2016-2027

Sinha A. K. (1989) Ferrous Physical Metallurgy, Chapter 4 Nucleation in Solids, Butterworths, pp. 127

Speich G. R. (1969) Tempering of Low-carbon Martensite. Trans. TMS-AIME. 245, 2553-64

Speich G. R., Leslie W. C. (1972) Tempering of steel. Metall. Trans. 3, 1043-54

Sun X., (2010) The Roles and Applications of Molybdenum Element in Low Alloy Steels. International Seminar on Applications of Mo in Steels. June 27th - June 28th.

Vyrostkova A., Kroupa A., Janovec J., Svoboda. (1998) Carbide Reactions and Phase Equilibria in Low Alloy Cr-Mo-V Steels Tempered at 773-993 K. Part 1: Experimental measurements, Acta Mater. Vol. 46. No. 1 pp. 31-38

Yan W., Zhu L., Sha W., Shan Y., Yang K. (2009) Change of Tensile Behaviour of a High-strength Low-alloy Steel with Tempering Temperature. Materials Science and Engineering A517 pp. 369-374

Young-Kook L., (1998) Unpublished, cited in: Processing Structure and Performance by Krauss G. (2005) ISBN: 0-87170-817-5.

Websites

www.brownmac.com/products/quenched-and-tempered-steel-plate/rqt-701. Accessed 27/11/13.

www.keytometals.com/Articles/Art146.htm accessed 27/11/13, updated 2010

www.matter.org.uk/steelmatter/metallurgy, accessed 27/11/13, updated 2000

9. Appendix: Electromagnetic Sensors

Previous research has indicated that EM sensors are sensitive to the microstructural changes that happen during tempering of power generation steels (J. Liu et al., 2013) and recent work at the University of Birmingham has shown in-situ measurements during tempering can be used to monitor the degree of tempering in a 4330V steel at 600 °C. (X. Hao, unpublished; Figure 30). The cylindrical EM sensor measures the inductance of a sample placed within it where the inductance is dependent on the size and geometry of the sample, the sample position in the sensor and the material properties of relative permeability and resistivity (a minor effect).

Figure 49 shows the inductance measured in the response to tempering RQT701 for several days, which had been hoped to be sufficient to assume microstructural stability. The initial sharp rise in inductance value is due to the sample heating up within the EM sensor, as there is a strong effect of temperature on the relative permeability (R. M. Bozorth, 1993). Once the sample has reached temperature (which occurs within the first 20 minutes of the heat treatment) any further change in inductance should be due to microstructural changes in the sample, as the sample position does not alter. Some oxidation occurs, but as this would effectively reduce the sample volume (albeit very slightly) a small decrease in inductance would be expected, which is not seen.

It can be seen from Figure 49 that the EM signal shows a higher inductance value for the samples tempered at the higher tempering temperature; this is likely to be due to the higher permeability of steel at higher temperatures (R. M. Bozorth, 1993), although there may also be an effect of sample position in the sensor. For all three samples it can be seen that the inductance value continues to rise with time after the sample has reached the tempering temperature. From previous results (J. Liu et al., 2013) this is consistent with a continuous increase in permeability due to a change in

microstructure by lath coarsening and precipitate coarsening. These results suggest that the tempering response in RQT701 is continuous with no stable microstructural state being reached during the test.

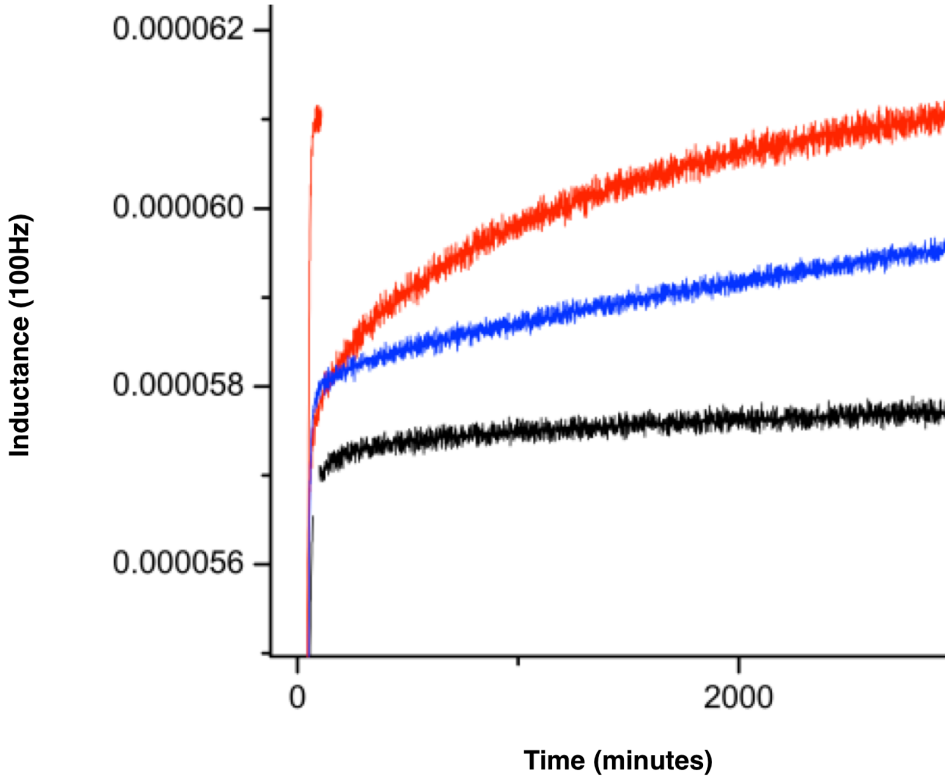

Figure 49: The change in inductance with time, measured for RQT701 tempered at 580 °C (black), 600 °C (blue) and 640 °C (red).

The results also indicate that the tempering response is more rapid when the temperature is increased to 640 °C, which is consistent with higher driving forces at higher temperatures. The hardness response during tempering, Figures 41 and 43, showed that there were two peaks; after 2 – 3 hours and after >27 hours (depending on the tempering temperature), due to the formation of

specific precipitate populations. No corresponding change in inductance was seen that could be matched to these hardness changes, although lath widths were not measured for the steels. It may be that the coarsening of laths is dominating the inductance response, whilst precipitate formation is having a dominant effect of hardness. However, without further experimental work this cannot be confirmed. In summary the results suggest that, whilst the tempering process results in a change in inductance, the inductance cannot be used to infer the types of precipitates present or hardness value.